Mixing and General Circulation Dynamics: Theory and Observations

by

Eli Tziperman

B.A., Physics and Mathematics
Hebrew University, Jerusalem, Israel
1982

Submitted in partial fulfillment of the
requirements of the degree of
Doctor Of Philosophy

at the

Massachusetts Institute of Technology

and the

Woods Hole Oceanographic Institution

February, 1987

Signature of the author _____

Joint Program in Oceanography,
Massachusetts Institute of Technology –
Woods Hole Oceanographic Institution, February 1987.

Certified by _____

Thesis supervisor

Accepted by _____

Chairman, Joint Committee for Physical Oceanography.
Massachusetts Institute of Technology –
Woods Hole Oceanographic Institution.

Mixing and General Circulation Dynamics:
Theory and Observations

by

Eli Tziperman

Submitted to the Massachusetts Institute of Technology – Woods Hole Oceanographic Institution Joint Program in January 1987 in partial fulfillment of the requirements for the degree of Doctor of Philosophy.

Abstract

This thesis studies the role of cross–isopycnal mixing in general circulation dynamics, from both the theoretical and observational points of view.

The first two chapters discuss some theoretical aspects of cross–isopycnal mixing in the oceans. In chapter one, an integral constraint relating the interior stratification and air-sea heat fluxes is derived, based on the condition that the total mass of water of given density is constant in a steady state ocean. Two simple models are then used to examine the way the numerically small mixing, together with air-sea fluxes, determines the average vertical density stratification of the oceans, and the deep buoyancy driven circulation.

In chapter two, a more complete model of a deep flow driven by cross isopycnal diffusion is presented, motivated by the Mediterranean outflow into the North Atlantic. Mixing in this model is responsible for the determination of the detailed structure of the flow and density field, while in the models of the first chapter it was allowed to determine only the average vertical density stratification.

In chapter three, a hydrographic data set from the Mediterranean sea is analyzed by inverse methods. The purpose is to examine the importance of mixing when trying to explain tracer distributions in the ocean. The time-mean circulation and the appropriate mixing coefficients are calculated from the hydrographic data.

We conclude that the numerically small cross isopycnal mixing processes are crucial to the dynamics, yet difficult to parameterize and measure using available hydrographic data.

Thesis supervisor: Carl Wunsch
Cecil and Ida Green Professor
of Physical Oceanography

Table of contents

Introduction

How the ocean mixes, and what effect the mixing has on the dynamics of the circulation, are among the major problems of physical oceanography. Understanding oceanic mixing is a precondition for trying to understand important processes such as the global CO_2 cycle, oceanic heat transport, dispersion of pollutants in the oceans, and climate change and evolution, to name a few.

The understanding, modeling and measuring of oceanic mixing faces many difficulties. Many physical processes are responsible for mixing in the ocean, from molecular diffusion and micro-scale turbulent motions, to mesoscale eddies and meanders. When referring to mixing, one often simply means all the processes that are not resolved by a given model. Even theoretical studies using very simplified parameterization of mixing lead to very difficult mathematical problems, while the obstacles in measuring the mixing effects are apparent from the diversity of the mixing processes.

It is our purpose in this work to deal with several aspects of oceanic mixing — more specifically cross–isopycnal mixing — from both the theoretical and the observational points of view.

In the context of theories of the oceanic general circulation, one usually examines an idealized smooth and steady ocean, modeling all time dependent small scale motions with eddy mixing coefficients. With the many simplifications normally used, such as geostrophic and hydrostatic momentum balance, the problem is still very complicated. The thermocline equations describing such steady large scale flows pose a difficult mathematical and conceptual problem, which has been occupying researchers for many years now. One expects mixing to be numerically smaller than other physical processes affecting the circulation, which makes it even more difficult to understand its importance in the dynamics.

In the first chapter of this work we model the effects of mixing on the large scale ocean circulation, beginning by deriving an integral relation between mixing in the

ocean interior, and air–sea fluxes. Then, two simple models are used to study the way the numerically small mixing processes determine the basic density stratification of the oceans. Cross–isopycnal mixing is shown to be important both for driving the deep flows, and for determining the average vertical stratification of the upper wind driven thermocline circulation. The work presented in this chapter can also be found in Tziperman (1986).

The emphasis in the first chapter is on the determination, by the cross–isopycnal mixing, of the basic stratification of the oceanic circulation. A more detailed analysis of the dynamics of buoyancy driven flows, forced by interior mixing, is presented in the second chapter. A layer model of a deep flow driven by cross–interfacial diffusion is presented, motivated by the deep outflow of Mediterranean water from the Gibraltar straits into the North Atlantic ocean. The assumed absence of wind forcing, and the simplification resulting from the layer formulation of the problem, allows a fairly detailed study of the dynamics of buoyancy driven flows. In particular, the importance of relating the mixing processes to the interior density stratification when modeling such flows is stressed.

Having discussed in the first two chapters the importance of cross–isopycnal mixing in the dynamics of the oceanic general circulation, the third chapter takes the observational point of view. More specifically, we discuss the problem of estimating the time–mean oceanic circulation from the available hydrographic data, which does not give an appropriate temporal and spatial sampling of the circulation. We also discuss the related problem of calculating mixing coefficients — parameterizing the time dependent eddy field — from hydrographic data. The discussion is based on the analysis, by inverse methods, of a hydrographic data set sampling a region of the eastern Mediterranean sea in both space and time. Absolute geostrophic velocities and mixing coefficients are calculated from the data using a finite difference inverse model.

We conclude by combining some of the more important results in the final chapter.

Chapter 1

On the role of interior mixing and air–sea fluxes in determining the stratification and circulation of the oceans

1. Introduction.

Theories of the oceanic general circulation are aimed at explaining the time–mean density and velocity fields in terms of the forcing by wind stress and heat fluxes at the upper surface of the ocean. However, the problem posed this way is very complicated, and researchers have usually tried to simplify the boundary conditions as well as the dynamics as much as possible. Among the first things to be sacrificed were the details of the thermodynamical processes. These simplifications allowed significant progress to be made, but also revealed several gaps in the theories that did not explicitly include the thermodynamics as part of the physics. These gaps hint that the density–changing processes, although weak in the ocean's interior, may nevertheless be a crucial part of the physics of the general circulation.

In this work we try to explore several areas of the theoretical study of the oceanic general circulation in which some understanding may be gained by including the physics of the density changing processes:

In *thermocline theories*, air–sea heat fluxes were usually not considered explicitly, and one specified the density at the base of the mixed layer in order to account for the effect of these fluxes. The role of diffusion in classical thermocline theories also seems to be unclear: In some similarity solutions (Needler, 1967) the diffusion contributed a constant deep upwelling of no major dynamical importance, while ideal fluid thermocline theories (Welander, 1971) had at least as much success in explaining the structure of the thermocline as the diffusive ones. (Reviews of these efforts and earlier ones can be found in Veronis (1969, 1981).)

This seeming unimportance of the diffusion, and its being smaller than the advection terms in the density equation, had led to two recent theories of the wind–driven thermocline circulation (Rhines and Young, 1982a, and Luyten, Pedlosky and Stommel, 1983), which are both density conserving. These models were able to reproduce the horizontal variations in the depth of the thermocline and to demonstrate the importance of several physical processes, but had to specify the basic vertical density stratification on the eastern boundary (in addition to the outcrop positions). In particular, the thickness of the lower layers in the ventilated thermocline model has to be specified on the eastern boundary, and the thickness of the upper layers vanishes there. When more physics is added to allow non–zero thickness for these layers on the eastern boundary, (Pedlosky, 1983), the stratification must still be specified there.

We show here that however small the diffusion is, it is still a crucial part of the thermocline dynamics, and has to be included in the physics in order to determine the basic stratification. Air–Sea heat fluxes must also be considered, and specifying the surface density does not account for their full effect on the interior circulation.

The physical principle guiding us throughout this investigation is simple: Air–Sea interaction may result in a net production of water of some density type which sinks and spreads in the ocean's interior. To keep the total mass of this density type constant, interior mixing must act to change the density of this water to other density ranges. The mixing effects are assumed to depend on the density stratification, so that the condition of constant mass of water of given density can be used to link the air–sea heat fluxes to the interior stratification!

The *mid–depth circulation* below the main thermocline is not very well understood observationally (see Reid, 1981, for a review), nor theoretically. It is probably not primarily wind-driven like the upper circulation, but buoyancy-driven by the mixing processes. Below, we construct a theory for this water range, in which the driving force

is the diffusive vertical velocity, and both wind and air–sea heat fluxes have indirect but important effects.

Finally, we note that the only model existing for the *bottom water circulation* is one for the vertically integrated transport (Stommel 1958, Stommel and Arons 1959a, 1959b), driven by a uniform upwelling at the top of the bottom water. Air–sea interaction enters only implicitly as a source of bottom water that replaces the upwelling water. By explicitly considering the air–sea fluxes and using the condition of constant mass of water of given density, we are able to develop a simple diffusive, continuous, nonlinear model of the bottom and lower mid-depth circulation, and to relate its stratification to the air–sea fluxes.

The development in the rest of this chapter is as follows: In section 2 we derive an integral constraint relating the air–sea fluxes to the interior stratification. This constraint is based on the condition of constant total mass of water of given density in a steady state ocean. In section 3 the constraint is applied to a continuous nonlinear diffusive model of the deep circulation below the influence of the wind driven circulation. The basic stratification of the model tends to *look like* an exponential profile, but the small deviations from exponential are crucial to the dynamics.

In section 4, which is independent of section 3, a three layer *diffusive* model of the deep, mid-depth and upper ocean is examined. The upper layer is a wind-driven two gyre ventilated thermocline, and the lower layers are driven by diffusive cross-interfacial velocities. Air–sea heat fluxes are specified as part of the thermal boundary conditions of the model, and the stratification on the eastern boundary is calculated in terms of these fluxes using the constraint from section 2. A two gyre mid-depth circulation is found, while the bottom circulation is similar to that of the Stommel-Arons model.

2. Derivation of a constraint on the basic stratification.

In this section we derive an integral relation between the air–sea fluxes of heat and fresh water and the interior stratification, in the presence of small scale mixing. The relation is based on the condition that the total mass of water of given density is constant in a steady state ocean. Before going into the details of the derivation, it is useful to examine the physics behind it, and in particular to see what "net production" means.

There are two processes acting to change the density of a given water particle in the ocean: air–sea exchanges that affect the surface water, and small scale mixing in the ocean interior. Consider now the schematic, zonally averaged picture in figure 1, and concentrate on the water between the two isopycnals ρ_1 and ρ_2. We first examine the effects of the air–sea fluxes. Suppose that the density surface ρ_1 outcrops where the ocean is losing heat to the atmosphere. As a result, some mass of water of density $\rho < \rho_1$ is cooled per unit time, and its density becomes $\rho_1 < \rho < \rho_2$. (We are not interested now in the question whether this water sinks or is advected horizontally to an area where the surface density is larger than ρ_1, but only in the density change itself.) Water of density $\rho_1 < \rho < \rho_2$ is also exposed to the atmosphere, and suppose it also loses heat to the atmosphere, but less than the water in the density range just smaller than ρ_1. As a result, a mass of water of density $\rho_1 < \rho < \rho_2$ is cooled and its density becomes $\rho > \rho_2$. But this time less water is involved in the process, because the mass of water whose density is changed is proportional to the heat loss suffered by this water. In the situation described here there is more water *entering* the density range $\rho_1 < \rho < \rho_2$ than *leaving* it, and therefore there is a *net production* of water of this density per unit time. Air–sea heat fluxes act in this case as a *source* of water of density between ρ_1 and ρ_2.

Next, consider the effects of small scale mixing. The mixing processes act to change the density of water particles, and therefore force cross-isopycnal velocities. These velocities depend on the interior stratification through the density equation $U \cdot \nabla \rho =$

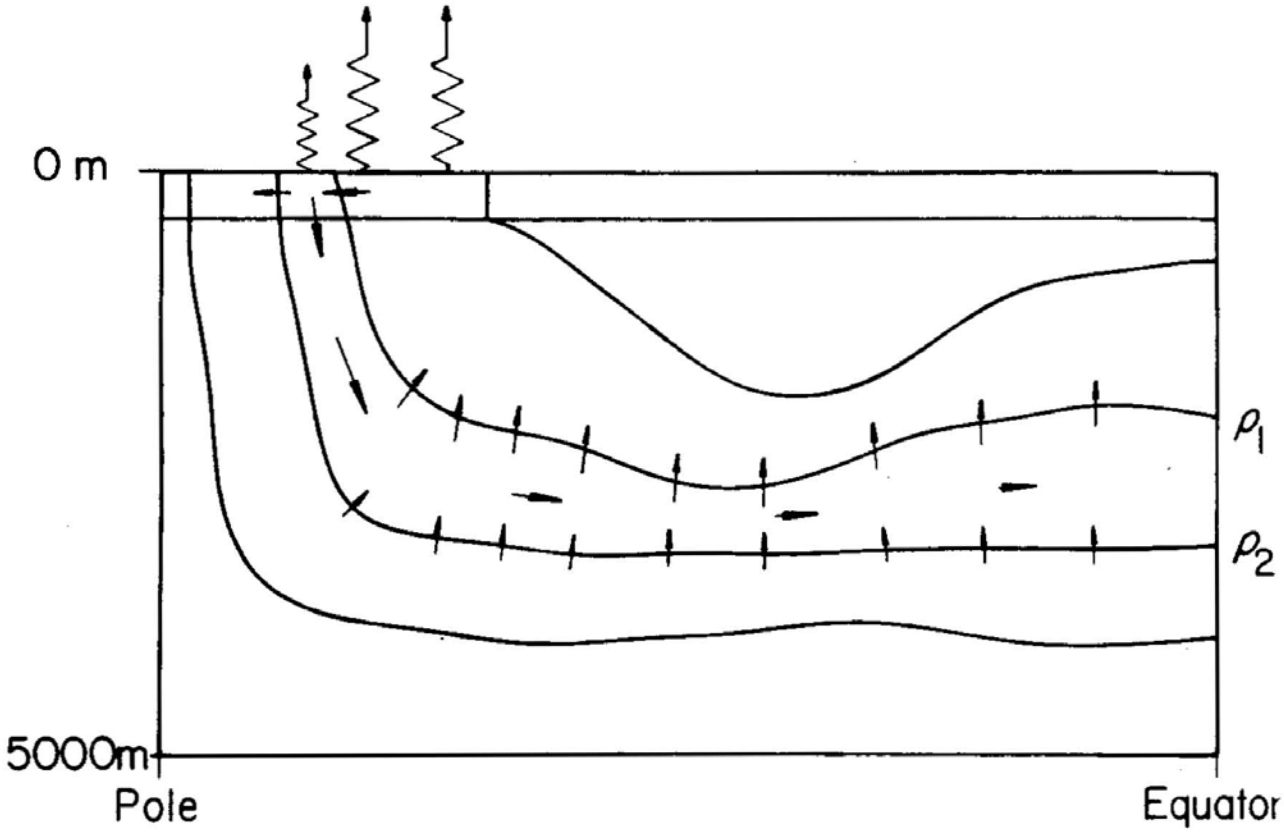

Figure 1. A schematic north–south vertical section showing the production of water of density between ρ_1 ,ρ_2 by air–sea heat fluxes, and dissipation of this water type by interior mixing.

$\nabla \cdot (\lambda \nabla \rho)$. Consider again the schematic picture in figure 1. Suppose that the interior stratification is such that there is net upwelling across the ρ_2 surface. This means that the mixing processes act to reduce the density of some mass of water heavier than ρ_2 and this mass upwells to the density range between ρ_1 and ρ_2. If there is also upwelling across the ρ_1 surface, but of larger magnitude, then more water leaves the density range $\rho_1 < \rho < \rho_2$ than enters it, and the interior mixing acts as a *sink* of this water type.

In a steady state the sinks and sources of any density type must balance to give *no net production.* This constraint of zero net production relates the air–sea fluxes to the interior stratification.

Two derivations of the constraint are given below. The first is more heuristic, the net production by each of the possible processes is derived separately, while ignoring the effects of the others. The second derivation is more formal, and includes all of the processes together, including the effects of seasonal variability of the air–sea interaction.

Small scale processes are modeled throughout this chapter in the simplest possible way, with a constant eddy-diffusivity coefficient in the density equation. Still, the procedures and physical principles we use do not depend on the particular parameterization chosen, and can be used with any other parameterization relating the small scale mixing to the mean fields. Given such a parameterization one can derive the constraint presented in this section, and then use it to find the effects of the mixing processes on the general circulation, as shown in the following sections. It is not clear to what extent the more specific results of the models developed below depend on the parameterization used.

A. An intuitive derivation:

In this sub-section, the expressions for the net production of water of given density by interior mixing, by air-sea heat fluxes, and by evaporation and precipitation are derived separately. This derivation should give an intuitive understanding of the physics involved, and will allow interpretation of the more formal results later in B.

(1) Production of water of given density by interior diffusion.

Ignoring air-sea fluxes, see figure 2. The mass flux across an isopycnal surface ρ is, for a Boussinesq fluid, the component of the velocity normal to a density surface, multiplied by a reference density ρ_0:

$$F(x,y,\rho) = \rho_0 U n \tag{2.1}$$

where n is a unit vector perpendicular to a surface of constant density.

Using $n = -\nabla\rho/|\nabla\rho|$, and the density equation

$$U \cdot \nabla\rho = u\rho_x + v\rho_y + w\rho_z = \lambda\nabla^2\rho \tag{2.2}$$

we get

$$F(x,y,\rho) = -\lambda\rho_0\nabla^2\rho/|\nabla\rho|,$$

and for almost horizontal density surfaces,

$$F(x,y,\rho) \approx -\lambda\rho_0\rho_{zz}/\rho_z. \tag{2.3}$$

The mass of water within the density range $(\rho, \rho + d\rho)$ that is produced per unit area, per unit time is the difference between the mass flux across the ρ–density surface and the $\rho + d\rho$ surface,

$$M_{\text{diffusion}}(x,y,\rho)d\rho = F(x,y,\rho+d\rho) - F(x,y,\rho),$$

so that

$$M_{\text{diffusion}}(x,y,\rho) = \frac{\partial F(x,y,\rho)}{\partial\rho}. \tag{2.4}$$

Using

$$\frac{\partial()}{\partial z} = (\frac{\partial z}{\partial\rho})^{-1}\frac{\partial}{\partial\rho},$$

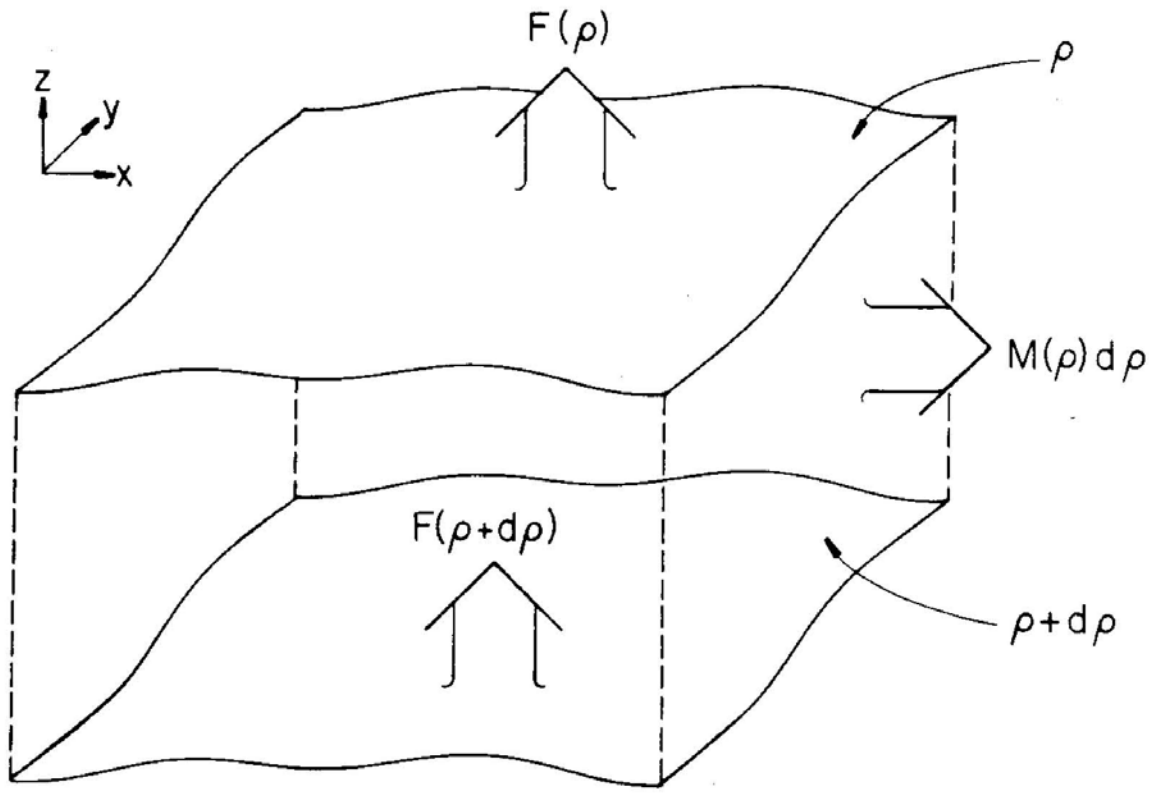

Figure 2. A perspective view of surface elements of two isopycnal surfaces, showing the local cross-isopycnal mass fluxes ($F(x, y, \rho)$) and the local production ($M(x, y, \rho)$) of water of density (ρ, $\rho + d\rho$) by the mixing processes.

the cross-isopycnal mass flux (2.1) can be written in (x, y, ρ) coordinates instead of (x, y, z) coordinates:

$$\begin{aligned} F(x,y,\rho) &\approx -\lambda\rho_0 \frac{\rho_{zz}}{\rho_z} \\ &= -\lambda\rho_0 \frac{\partial}{\partial\rho}\frac{1}{\partial z/\partial\rho} \end{aligned} \tag{2.5}$$

and we finally have

$$M_{\text{diffusion}}(x,y,\rho) = -\lambda\rho_0 \frac{\partial^2}{\partial\rho^2}\frac{1}{\partial z/\partial\rho}$$

or in the (x, y, z) coordinate system:

$$\begin{aligned} M_{\text{diffusion}}(x,y,\rho) &= -\lambda\rho_0 \frac{\partial}{\partial\rho}\frac{\nabla^2\rho}{|\nabla\rho|} \\ &= -\lambda\rho_0 \frac{1}{\rho_z}\frac{\partial}{\partial z}\frac{\nabla^2\rho}{|\nabla\rho|} \\ &\approx -\lambda\frac{\rho_0}{\rho_z}\frac{\partial^2 \log\rho_z}{\partial z^2} \end{aligned} \tag{2.6}$$

(2) Production of water of given density by air–sea heat fluxes.

Ignoring salinity variations of the surface water and effects of evaporation − precipitation, assuming $\rho = \rho_0 - \alpha(T - T_0)$, *see figure* 3. Suppose that the total amount of heat lost to the atmosphere by surface water of density ρ , per unit time, is $H(\rho)d\rho$. As a result, a volume dv_1 of water of (temperature, density)= (T, ρ) is cooled per unit time, to $(T - dT)$ and its density becomes $\rho + d\rho$. The volume dv_1 can be found by calculating the heat budget,

$$dv_1\rho C_p T + H(\rho)d\rho = dv_1(\rho + d\rho)C_p(T - dT). \tag{2.7}$$

The same time, a volume dv_2 of $(\rho - d\rho)$–water loses an amount of heat $H(\rho - d\rho)d\rho$ and becomes ρ–water. The net production of ρ–water is $M_{\text{heat}}(\rho)d\rho = \rho(dv_1 - dv_2)$. Substituting the values of dv_1 and dv_2

$$M_{\text{heat}}(\rho) = \frac{\alpha}{C_p}\frac{\partial H(\rho)}{\partial\rho}. \tag{2.8}$$

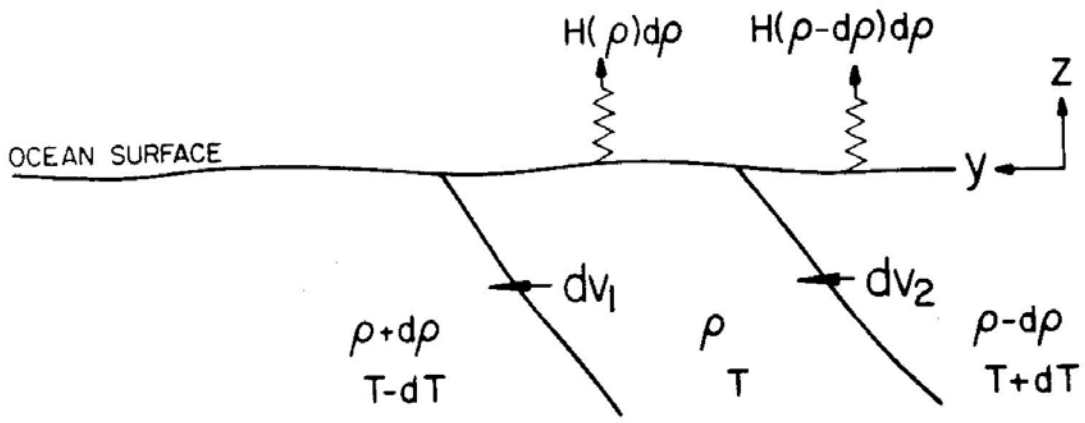

Figure 3. A schematic north-south vertical section through an outcropping region, showing the air–sea heat fluxes and the resulting cross-isopycnal mass fluxes.

(3) Production of water of given density by evaporation-precipitation.

Ignoring temperature variations of the surface water and effects of air-sea heat fluxes, assuming $\rho = \rho_0 + \beta(S - S_0)$, *see figure 4.* Let the evaporation−precipitation as a function of the surface water density be $Q(\rho)$. This means that all over the basin, a volume $Q(\rho)d\rho$ of fresh water is added per unit time to surface water of density ρ. As a result, a volume dv_1 of water of (salinity, density) $= (S, \rho)$ is joined by a volume $Q(\rho)d\rho$ of fresh water, and becomes a volume dv_1 of $(S - dS, \rho - d\rho)$–water. The volume elements dv_1, dv_1 can be found by calculating the mass and salt balances:

$$\text{salt:} \qquad \mathrm{dv}_1 \rho S = dv_1(\rho - d\rho)(S - dS), \tag{2.9}$$

$$\text{mass:} \qquad \mathrm{dv}_1 \rho = dv_1(\rho - d\rho) + Q(\rho)d\rho. \tag{2.10}$$

At the same time, a volume dv_2 of $(\rho + d\rho, S + dS)$–water is joined by a volume $Q(\rho + d\rho)d\rho$ of fresh water, and becomes a volume dv_2 of (ρ, S)–water. The net production of water of density ρ is

$$M_{\text{fresh water}}(\rho)d\rho = \rho(dv_2 - \mathrm{dv}_1). \tag{2.11}$$

By substituting the values of dv_1, dv_2 we have

$$\begin{aligned} M_{\text{fresh water}}(\rho) &= 2Q(\rho) + \beta S \frac{\partial Q(\rho)}{\partial \rho} \\ &= \partial \beta S Q(\rho)/\partial \rho + Q(\rho). \end{aligned} \tag{2.12}$$

Because the total production of water of density ρ should vanish, we can combine (2.6),(2.8) and (2.12) into

$$\frac{\partial}{\partial \rho} \iint \lambda \rho_0 \frac{\nabla^2 \rho}{|\nabla \rho|} = \frac{\partial \beta S Q}{\partial \rho} + Q(\rho) + \frac{\partial}{\partial \rho} \frac{\alpha}{C_p} H(\rho) \tag{2.13}$$

where the double integral is over the entire area of a density surface. The RHS of (2.13) is an expression for the mass of water of density ρ which is produced by the

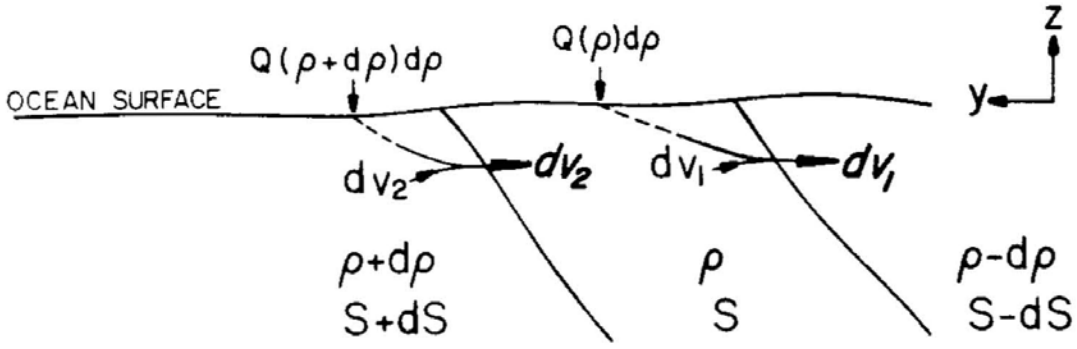

Figure 4. Same as figure 3, but with fresh water fluxes forcing the cross-isopycnal fluxes.

given air–sea fluxes of heat (H) and fresh water (Q). This expression does not change much when we allow for seasonal variability in the air–sea interaction (see (2.23) in B). The water mass production by the air–sea fluxes is balanced by the production by the mixing processes which, for our choice of the parameterization of the mixing processes, is given by the LHS. Equation (2.13) can be integrated over ρ from the highest surface density ρ_b to ρ , to give

$$\iint -\lambda\rho_0 \frac{\nabla^2\rho}{|\nabla\rho|} + \beta SQ + \frac{\alpha}{C_p} H(\rho) = -\int Q(\rho')d\rho'. \tag{2.14}$$

Each of the terms on the LHS is a contribution to the mass flux across the density surface ρ from one of the processes described in 1,2,3 above. The physical statement in (2.14) is that the total mass flux across the isopycnal surface ρ (the LHS) is equal to the flux of fresh water from the atmosphere into surface water of density greater than ρ (RHS). A similar result was discussed by Walin (1982) who considered the mass and heat balances for a volume of fluid bounded by an isothermal surface. He related the air–sea heat fluxes to interior cross-isothermal diffusive fluxes, and used this relation as an observational diagnostic tool to deduce the diffusive fluxes in the ocean interior.

B. A more formal derivation:

We now want to see if and how the results of the above heuristic derivation change when all the density-changing processes act together. We also allow seasonal time variations in the air–sea interaction and derive the time averaged constraint of zero net production. The results turn out to be essentially the same as in (A) above, and the reader may skip this sub-section on first reading.

The derivation is divided into three parts: We first derive the density and continuity equations in the presence of heat and fresh water sources. Then these equations are written in density coordinates, and relations are found between several quantities in (x, y, z) coordinates and in (x, y, ρ) coordinates. Finally the continuity equation is

integrated over an isopycnal surface and averaged in time to obtain the constraint of zero net production of water of given density.

In this derivation, the air–sea heat and fresh water fluxes are represented by distributed sources of heat ($\mathcal{H}(x,y,z,t)$) and fresh water ($\mathcal{Q}(x,y,z,t)$). (The sources are different from zero only near the surface.) The mass, heat, and salt budgets for a fixed volume of Boussinesq fluid are:

$$0 = -\iint d^2x\ \rho_0 U n + \iiint d^3x\ \mathcal{Q}(x,y,z,t)\rho_0, \tag{2.15}$$

$$\partial_t \iiint d^3x \rho_0 C_p T = -\iint d^2x \rho_0 C_p T U n + \iiint d^3x\ \mathcal{H}(x,y,z,t)\rho_0 + \iiint d^3x\ \mathcal{Q}(x,y,z,t)\rho_0 C_p T + \text{heat diffusion}, \tag{2.16}$$

$$\partial_t \iiint d^3x\ \rho_0 S = -\iint d^2x\ \rho_0 S U n + \text{salt diffusion}. \tag{2.17}$$

Using these relations and the equation of state $\rho = \rho_0 - \alpha(T - T_0) + \beta(S - S_0)$, we obtain the incompressibility equation

$$\nabla \cdot U = \mathcal{Q}(x,y,z,t), \tag{2.18}$$

and the density equation

$$\frac{\mathrm{d}\rho}{\mathrm{d}t} = \rho_t + U \cdot \nabla\rho = -\beta S(x,y,z,t)\mathcal{Q}(x,y,z,t) - \frac{\alpha}{C_p}\mathcal{H}(x,y,z,t) + \lambda\nabla^2\rho. \tag{2.19}$$

The gradient of the density field, represented in density coordinates, is

$$\nabla\rho = (\rho_x, \rho_y, \rho_z) = (\frac{\rho_0}{h})(z_x, z_y, 1) \tag{2.20}$$

and its Laplacian,

$$\nabla^2\rho = \frac{\rho_0}{h}\left(z_{xx} + z_{yy} + \left({z_x}^2 + {z_x}^2 + 1\right)\frac{\partial}{\partial\rho}\left[\frac{\rho_0}{h}\right]\right) \tag{2.21}$$

where

$$h \equiv -\rho_0\frac{\partial z}{\partial\rho}. \tag{2.22}$$

With these relations, we can rewrite the density equation (2.19) as

$$\frac{\mathrm{d}\rho}{\mathrm{d}t} = \dot{\rho} = -\beta S \mathcal{Q} - \frac{\alpha}{C_p}\mathcal{H} + \lambda \frac{\rho_0}{h}\left(z_{xx} + z_{yy} + \left({z_x}^2 + {z_x}^2 + 1 \right) \frac{\partial}{\partial \rho}\left[\frac{\rho_0}{h} \right] \right), \qquad (2.19a)$$

while the continuity equation (2.18) in density coordinates is

$$h_t + (uh)_x + (vh)_y + \frac{\partial h\dot{\rho}}{\partial \rho} = h\mathcal{Q}. \qquad (2.18a)$$

For the constraint of no net production of water of a given density, substitute (2.19a) in (2.18a), average the continuity equation (2.18a) over time, and integrate over the entire area of an isopycnal surface. Using the periodicity to eliminate the term

$$\iint dxdy \int h_t dt,$$

and noting that the along isopycnal transport $(uh)_x + (vh)_y$ vanishes when integrated over the entire density surface, we have

$$\begin{aligned} &\frac{\partial}{\partial \rho}\int dt \iint_{\rho=constant} dxdy\lambda \left(z_{xx} + z_{yy} + \left({z_x}^2 + {z_x}^2 + 1 \right) \frac{\partial}{\partial \rho}\left[\frac{\rho_0}{h} \right] \right) \\ &\quad - \frac{\partial}{\partial \rho}\int dt \iint_{\rho=constant} dxdy \frac{\alpha}{C_p} h\mathcal{H}(x,y,\rho,t) \\ &\quad - \frac{\partial}{\partial \rho}\int dt \iint_{\rho=constant} dxdy\beta S h\mathcal{Q}(x,y,\rho,t) = \int dt \iint dxdyh\mathcal{Q}(x,y,\rho,t). \end{aligned} \qquad (2.23)$$

To see that (2.23) is a generalization of (2.13), we now derive the relation between the distributed sources $\mathcal{Q}(x,y,z,t), \mathcal{H}(x,y,z,t)$, and the fluxes $\mathrm{H}(\rho), \mathrm{Q}(\rho)$ that were used in the heuristic derivation in A. The total heat gained by the ocean during one year in the derivation in (A) was (1 year) $\int H(\rho)d\rho$. In terms of the distributed sources it is $\int dt \iiint \mathcal{H}(x,y,z,t)\rho_0 d^3x$. Now,

$$\begin{aligned} (1 \text{ year}) \int H(\rho)d\rho &= \int dt \iiint \mathcal{H}(x,y,z,t)\rho_0 dxdydz \\ &= \int dt \iiint \mathcal{H}(x,y,\rho,t)\rho_0 dxdy \left(\frac{\partial z}{\partial \rho} \right) d\rho \\ &= \int d\rho \int dt \iint (-h)\mathcal{H}(x,y,\rho,t)dxdy, \end{aligned}$$

so that

$$H(\rho) = \frac{1}{(1 \text{ year})} \int dt \iint (-h) \mathcal{H}(x,y,z,t) dx dy. \tag{2.24}$$

And the same for the mass sources (evaporation-precipitation):

$$Q(\rho) = \frac{1}{(1 \text{ year})} \int dt \iint (-h) \mathcal{Q}(x,y,z,t) dx dy. \tag{2.25}$$

With the identities (2.24) and (2.25), the similarity between (2.23) and the result derived in a more heuristic way in (A) is clearly seen.

3. A continuous model of the deep and mid-depth circulation.

In section 2 we have not considered explicitly the dynamics of the circulation and the velocity field, but only assumed implicitly the existence of a velocity field connecting sources and sinks of a given density. In this section, a continuous model of the deep and mid-depth circulation below the influence of the wind driven circulation is described. The model is a simple application of the constraint derived in the previous section: A steady state density stratification is maintained by a balance between the production of water by air–sea heat fluxes and by interior small scale mixing.

Figure 5 is a schematic North–South vertical section, showing to what part of the oceanic circulation the model applies: The thermocline circulation (shown vertically hatched) is probably mostly wind–driven. The upper mid–depth water (diagonally hatched) is probably buoyancy driven, but is certainly influenced by the distortion of the isopycnals just above it by the thermocline circulation. These two upper regions and the interaction of the wind–driven circulation with the diffusive processes are not considered here. They are part of the model presented in section 4, which is independent of this one. The lower mid-depth and the bottom waters (unshaded in figure 5), where the isopycnals are nearly flat, are those addressed by the model in this section.

The basic dynamics of the model are geostrophic, hydrostatic and diffusive and it is nonlinear in the sense that there is no linearization about some specified basic

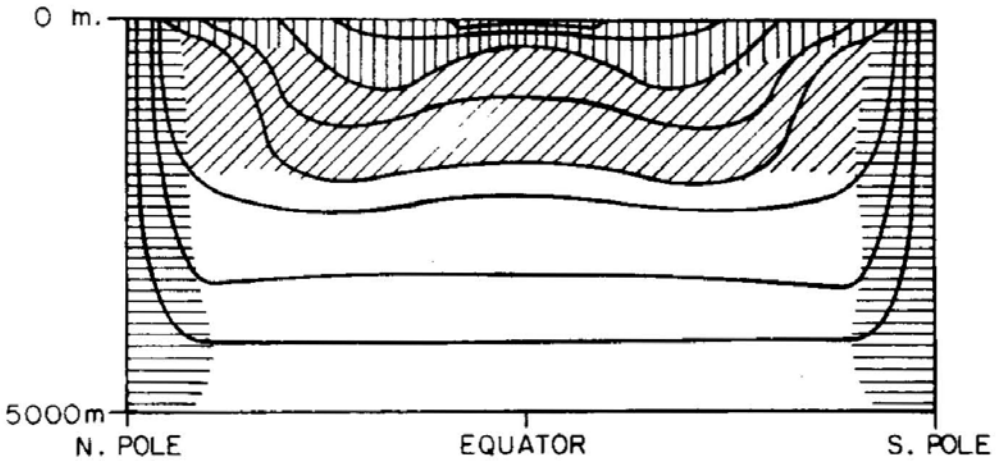

Figure 5. A north-south schematic vertical section, showing the regions of outcropping, of the upper circulation (shaded), and of the deeper circulation (unshaded) that is modeled in section 3.

stratification. Instead, the heating of the ocean by the atmosphere is specified as a function of the density of the surface water where the deep water is outcropping (horizontally hatched region in figure 5). Then the constraint which was derived in section 2 is used to calculate the stratification and the cross-isopycnal velocities in the interior. Finally, the geostrophic equations are used to calculate the deep horizontal velocity field.

We start by nondimensionalizing the equations, then a perturbation expansion in powers of the nondimensionalized diffusion coefficient is used to obtain the solution.

The equations are

$$\begin{aligned} fu &= -(1/\rho_0)p_y \\ fv &= (1/\rho_0)p_x \\ p_z &= -g\rho \\ u_x + v_y + w_z &= 0 \\ u\rho_x + v\rho_y + w\rho_z &= \lambda_* \nabla^2 \rho, \end{aligned} \tag{3.1}$$

where $f = 2\Omega \sin(\text{latitude})$ is the coriolis parameter, (x, y, z) and (u, v, w) are the (east, north, vertical) coordinates and velocity components, and we also use the notation $\beta = \mathrm{d}f/\mathrm{d}y$. p, ρ and ρ_0 are the pressure, density and a constant reference density.

The boundary conditions are:

* The air–sea heat fluxes as function of the surface density in areas where the deep and mid–depth water is outcropping are specified: $H(\rho)$.

* No zonal flow into the eastern boundary: $u(x_e, y) = 0$.

We introduce the scaling

$$\begin{aligned} x, y &\sim L, \qquad z \sim H \\ u, v &\sim V, \qquad w \sim W = VH/L \\ \rho &\sim B, \qquad p \sim P, \end{aligned} \tag{3.2}$$

and get the nondimensional equations

$$\begin{aligned} fu &= -p_y \\ fv &= p_x \\ p_z &= -\rho \\ u_x + v_y + w_z &= 0 \\ u\rho_x + v\rho_y + w\rho_z &= \lambda\nabla^2\rho, \end{aligned} \tag{3.3}$$

where

$$\begin{aligned} &f = \sin(y)/\sin(45^\circ); \qquad \lambda = \lambda_* L/VH^2; \qquad \delta = H/L \\ &\nabla^2 = \delta^2(\frac{\partial^2}{\partial x^2}, \frac{\partial^2}{\partial y^2}) + \frac{\partial^2}{\partial z^2}; \quad P = \rho_0 L 2\Omega \sin(45^\circ)V \\ &B = \rho_0 L 2\Omega \sin(45^\circ)V/Hg. \end{aligned} \tag{3.4}$$

Substituting reasonable values for the scales:

$$L = 3000\text{km}, \quad H = 1\text{km}, \quad V = 0.1\text{cm/sec}, \quad \lambda_* = 1\text{cm}^2/\text{sec}, \tag{3.5}$$

we obtain $\lambda = 0.3$, so that we can treat λ as a small parameter. Expanding the variables in a perturbation series

$$u = u_0 + \lambda u_1 + \lambda^2 u_2 + \ldots, v = \ldots, \tag{3.6}$$

the order one equations are

$$\begin{aligned} fu_0 &= -p_{0y} \\ fv_0 &= p_{0x} \\ p_{0z} &= -\rho_0 \\ u_{0x} + v_{0y} + w_{0z} &= 0 \\ u_0\rho_{0x} + v_0\rho_{0y} + w_0\rho_{0z} &= 0. \end{aligned} \tag{3.7}$$

Because to this order there are no cross-isopycnal fluxes, and because we are below the influence of the wind driven circulation, there is no forcing, and a solution is:

$$u_0 = v_0 = w_0 = 0, \qquad \rho_0 = \rho_0(z), \qquad p_0 = p_0(z). \tag{3.8}$$

To determine $p_0(z)$, $\rho_0(z)$ we must go to the $O(\lambda)$ equations and use the constraint from section 2. But before doing this, a comment on the $O(1)$ solution is needed:

It is clear that this solution of horizontal isopycnals cannot hold everywhere, because we expect the deep isopycnals to outcrop and to be influenced by the atmosphere in polar regions. Figure 5 shows schematically the large region (unshaded) in which the isopycnals are almost horizontal, and the small polar region where they are supposed to outcrop (horizontally hatched).

The $O(\lambda)$ equations are:

$$\begin{aligned} fu_1 &= -p_{1y} \\ fv_1 &= p_{1x} \\ p_{1z} &= -\rho_1 \\ u_{1x} + v_{1y} + w_{1z} &= 0 \\ w_1\rho_{0z} &= \rho_{0zz}. \end{aligned} \tag{3.9}$$

The last equation can be written as

$$w_1 = w_1(z) = \frac{\rho_{0zz}}{\rho_{0z}} = \frac{\partial}{\partial\rho_0}\frac{1}{\partial z/\partial\rho_0} = w_1(\rho_0), \tag{3.10}$$

where ρ_0 is the order one density field, and it is used as the vertical coordinate instead of z. Now, we saw in section 2 that if the effects of evaporation − precipitation in the outcropping region are ignored, then the net mass flux across an isopycnal surface due to air–sea heat exchanges and due to interior mixing is zero. Because the outcropping region is small, we assume that the total cross–isopycnal mass flux there *due to small scale mixing* is small compared to the cross–isopycnal fluxes integrated all over the density surface in the larger part of the ocean, where our $O(1)$ solution is valid. (We also ignore the boundary mixing, see comment in section 4.) These assumptions allow us to write the constraint of zero net mass flux across an isopycnal surface as

$$\iint dxdyU\cdot n \approx \iint dxdyW\lambda w_1(z) = \frac{\alpha}{C_p}H(\rho) \tag{3.11}$$

where $H(\rho)$ is the heat flux from surface water of density ρ to the atmosphere. Since w_1 is only a function of z, (or equivalently of ρ_0) we have

$$W\lambda w_1 \approx \frac{\alpha}{C_p Area} H(\rho). \tag{3.12}$$

Using (3.10), we obtain an equation for the horizontally uniform $O(1)$ density stratification. In dimensional form:

$$\lambda_* \frac{\partial}{\partial \rho} \frac{1}{\partial z/\partial \rho} \approx \frac{\alpha}{C_p Area} H(\rho). \tag{3.13}$$

and the solution for $z(\rho_0)$ is (C_1 and C_2 are two integration constants)

$$z(\rho_0) = \int^{\rho_0} d\rho' \left[\int^{\rho'} d\rho" \frac{\alpha}{\lambda_* C_p Area} H(\rho") + C_1 \right]^{-1} + C_2. \tag{3.14}$$

The solution (3.14) for $z(\rho_0)$ can be inverted to obtain $\rho_0(z)$. This procedure will be demonstrated by considering a specific heating function $H(\rho)$, but first it is possible to obtain the important $O(\lambda)$ and $O(\lambda^2)$ corrections to the velocity and density fields, and in particular the deviations from horizontally uniform stratification and upwelling.

Knowing $\rho_0(z)$ from (3.14), and $w_1(\rho_0)$ from (3.12), we can find $w_1(z)$. From the $O(\lambda)$ equations we have the other fields in terms of w_1

$$\begin{aligned}
u_1 &= \int_x^{x_e} \frac{1}{f} \frac{\partial}{\partial y} \left(\frac{f^2}{\beta} \right) \frac{\partial w_1}{\partial z} dx' \\
v_1 &= \frac{f}{\beta} \frac{\partial w_1}{\partial z} \\
p_1 &= \int_{x_e}^{x} \frac{f^2}{\beta} \frac{\partial w_1}{\partial z} dx' + G_1(z) \\
\rho_1 &= \int_x^{x_e} \frac{f^2}{\beta} \frac{\partial^2 w_1}{\partial z^2} dx' + \frac{\partial G_1(z)}{\partial z},
\end{aligned} \tag{3.15}$$

where $G_1(z)$ is a function of z only. To determine $G_1(z)$ we have to re-apply the constraint on the density field, this time with the $O(\lambda^2)$ corrections to the cross-isopycnal velocity and to the density field. But because G_1 is only a small correction to the

basic vertical stratification, and we are interested in the horizontal deviations from this uniform state, we may ignore $G_1(z)$.

To find the dynamically important corrections to the uniform upwelling w_1 , we consider the $O(\lambda^2)$ density equation:

$$(u_1\partial_x + v_1\partial_y w_1\partial_z)\rho_1 + w_2\rho_{0z} = \nabla^2\rho_1,$$

and we get w_2 in terms of the already known $O(\lambda)$ fields,

$$w_2(x,y,z) = (\nabla^2\rho_1 - U_1\cdot\nabla\rho_1)/\rho_{0z}. \tag{3.16}$$

An example with a specific heating function.

The zonally integrated heat fluxes from the ocean to the atmosphere as a function of latitude, have the schematic shape shown in figure 6.a . Because surface density is roughly monotonically increasing with latitude, we can assume that the heat fluxes as a function of the density of the surface water which is losing that heat, have the shape shown in figure 6.b . We are only interested now in $H(\rho)$ for the bottom and mid-depth densities, so that a reasonable choice for that density range is the one shown in figure 6.c .

A convenient analytic form is chosen for this heating:

$$H(\rho) = D\left[\cos\left(\frac{\rho-\rho_b}{\rho_b-\rho_s}\right) - \exp\left(\frac{\rho-\rho_b}{\Delta}\right)\right],$$

(ρ_s,Δ and D are constants, ρ_b is the bottom density), and is substituted in the solutions derived before for the density and velocity fields. Because w_1 is known from (3.12) as an explicit function of the basic density stratification ρ_0, it is convenient to evaluate the solutions (3.15) and (3.16) with ρ_0 as the vertical coordinate. This is done by using

$$\frac{\partial w}{\partial z} = \left(\frac{\partial z}{\partial \rho_0}\right)^{-1}\frac{\partial w}{\partial \rho_0}$$

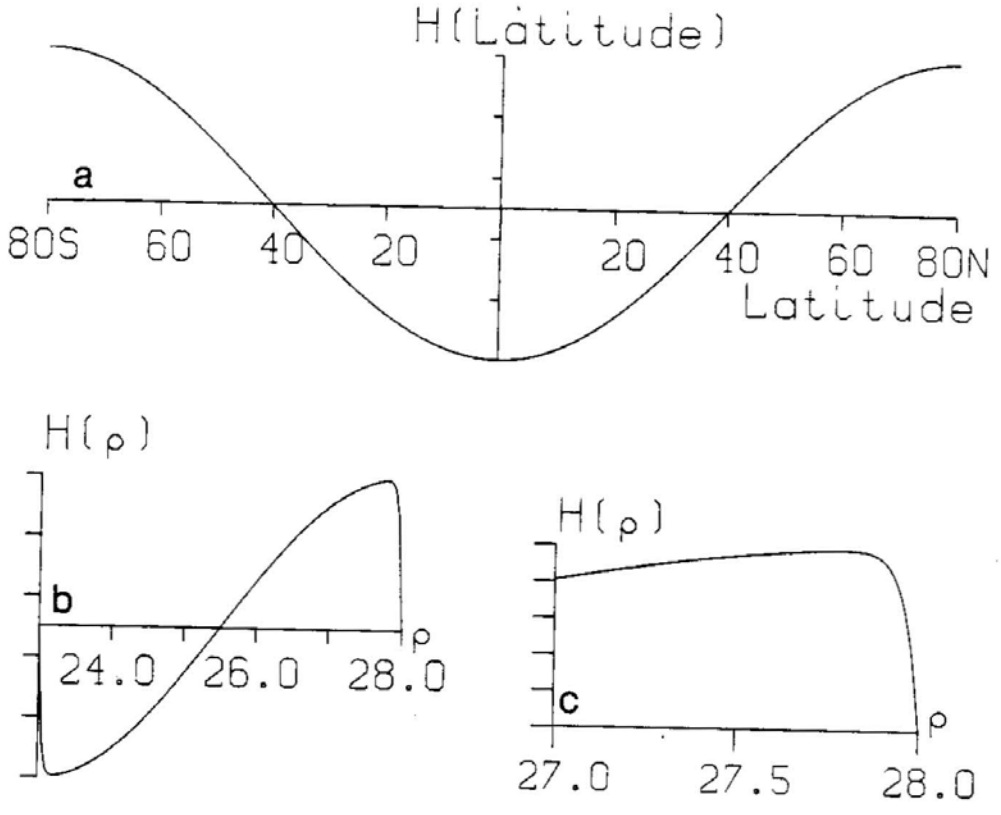

Figure 6. Schematic pictures of:

(a) Zonally averaged air–sea heat fluxes as function of latitude.

(b) Air–sea fluxes as function of the surface density.

(c) The heating (as function of the surface density in outcropping regions) used as forcing in the bottom and lower mid–depth circulation model in section 3.

with $\partial z/\partial \rho_0$ taken from (3.14). The explicit analytic solutions (3.15) and (3.16) in terms of the specific heating are quite long expressions, and were found by using the MACSYMA symbolic-manipulation computer program (Mathlab Group MIT, 1983).

A few words should be said about the boundary conditions for the density and vertical velocity profiles in figure 7. The constants C_1 and C_2 in (3.14) were chosen to satisfy $z(\rho = 1.027) = -2km$, $z(\rho = 1.028) = -5km$. The vertical velocity is zero at the bottom (by (3.12)) because the air–sea heat fluxes vanish for the highest surface density, ρ_b, which is also the density at the bottom of the model (figure 6.c). If $H(\rho)$ were not zero for $\rho = \rho_b$, then a finite mass $\frac{\alpha}{C_p} H(\rho_b)$ of a ***single*** density $\rho = \rho_b$ would form at the surface. This would mean a completely homogeneous unstratified layer at the bottom of our model, where the physics we use does not apply.

Figure 7 shows the solutions for the basic density stratification $\rho_0(z)$ and for the lowest order upwelling velocity $w_1(z)$. Note that the solution for $\rho_0(z)$ resembles an exponential profile, which is (Munk, 1966) a solution of $w\rho_z = \lambda \rho_{zz}$, with a constant upwelling velocity w. But w in our solution is a strongly varying function of depth! The apparent insensitivity of the exponential profile to variations in the vertical velocity is a result of the smoothing effect of the vertical diffusion. Two integrations are needed to solve the vertical density balance $w\rho_z = \lambda \rho_{zz}$ for ρ in terms of w, so that even a relatively large variation in $w(z)$ is smoothed and is not seen in $\rho(z)$. The tendency towards exponential density profile will still be present when λ is varying with depth. If $\lambda = \lambda_0 f(z)$, we can write the vertical density balance as $[w(z)/f(z)]\rho_z = \lambda_0 \rho_{zz}$, and $\rho(z)$ would again tend to look like an exponential profile for different forms of $w(z)$ and $f(z)$. This insensitivity is unfortunate when we want to calculate $w(z)$ from observations of $\rho(z)$. It is probably unsafe to calculate $w(z)$ by substituting $\rho(z) = \exp(z/H)$ in $w\rho_z = \lambda \rho_{zz}$ with a constant λ (Munk, 1966), or even with a more realistic structure for $\lambda(z)$ (Gargett, 1984). A very small deviation of the actual density profile

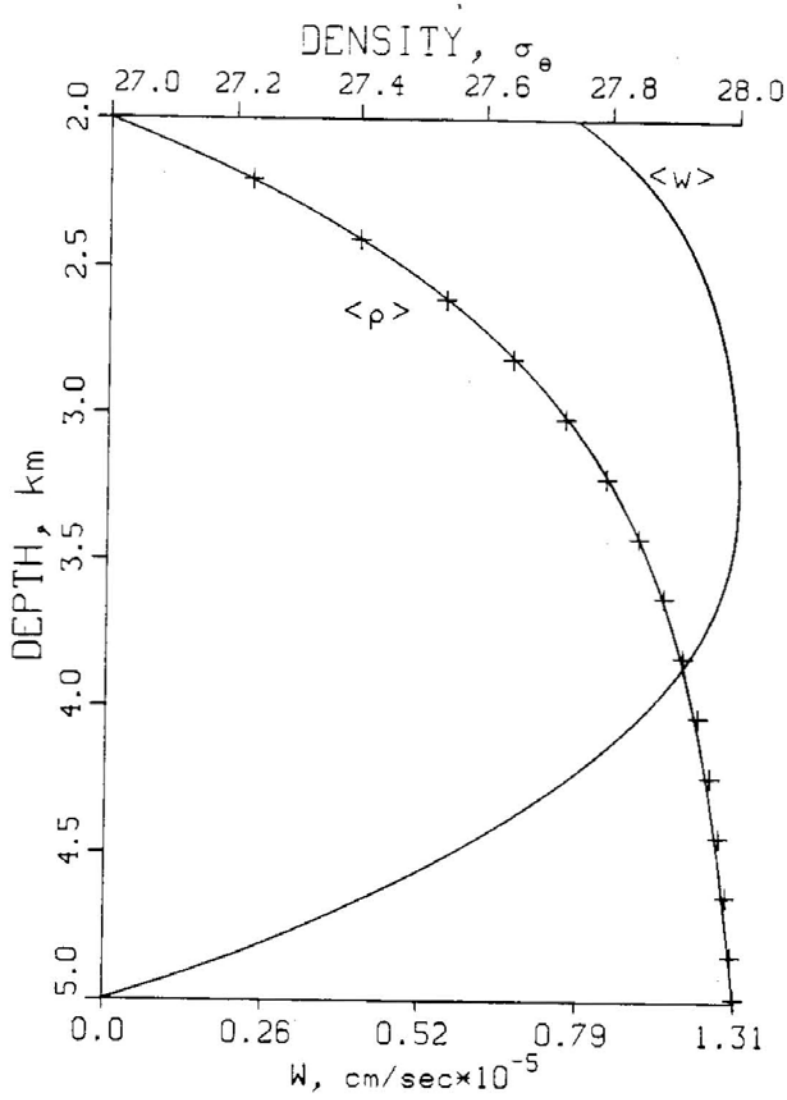

Figure 7. An example of the bottom and mid-depth circulation model of section 3: The solution for the basic density profile $\rho_0(z)$ (full line) together with a matched exponential profile (crosses), and the vertical velocity $w_1(z)$ for the same solution.

from an exponential shape, perhaps even below the noise level, may lead to a large change in the calculated structure of $w(z)$.

The variation in $w_1(z)$ is responsible for driving the horizontal circulation in the solution showed here, through the linear vorticity equation $\beta v = f w_z$. The bottom water circulation, which occupies the upper density range where $H(\rho)$ is rapidly decreasing, is driven poleward in the interior by an upward increasing $w(z)$. The mid-depth circulation in this example is driven *equatorward* in the interior by an upward decreasing upwelling, as determined by the structure of $H(\rho)$ for the mid-depth densities.

Figures 8.a-c show the deviations of the pressure, density and upwelling from the horizontally uniform lowest order fields, at a depth of the bottom water circulation. The density field has the expected gyre shape, with the strongest signal at the northwest corner. This shape is induced by the deep circulation itself, through the distortion of the isopycnals by the velocity field. Note that boundary currents are needed to close the circulation and to connect the interior flows to the outcropping region.

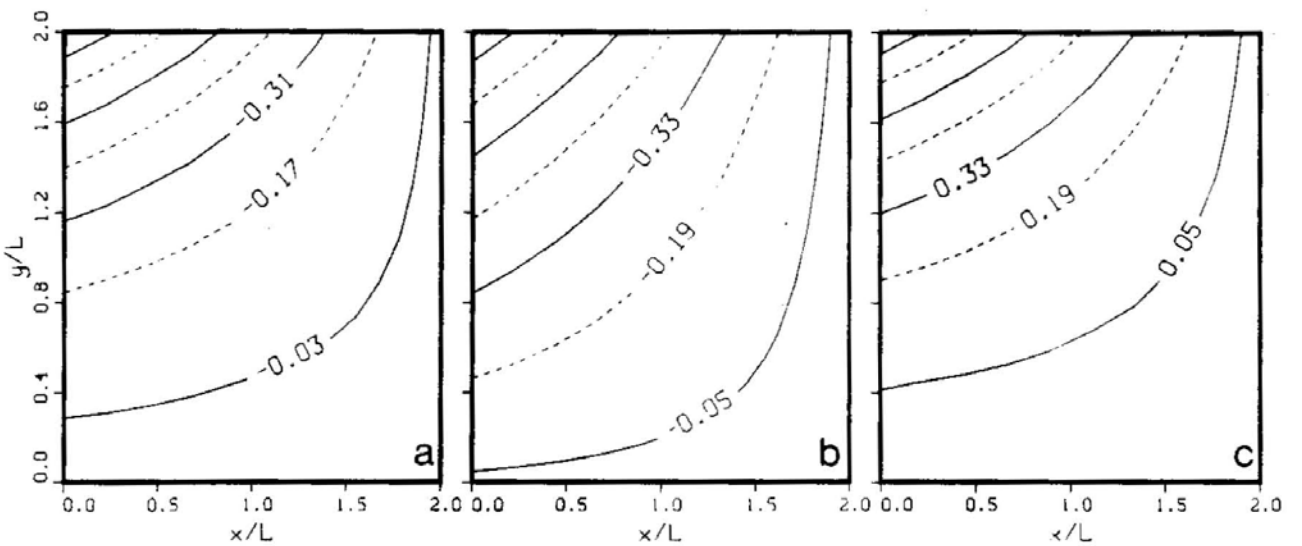

Figure 8. Corrections to the horizontally uniform basic stratification, pressure field and upwelling velocity, on a constant depth surface at a depth of the bottom circulation. (all non dimensional, see 3.2, 3.4 .)

4. The interaction of the wind driven circulation with thermal processes.

In this section some aspects of the interaction of the wind driven circulation with the cross-isopycnal processes are investigated using a simple layer-model. We demonstrate how the principle of no net production of water of given density can be used to determine the basic stratification (stratification on the eastern boundary) of the wind driven circulation. We also discuss the way the wind and the buoyancy forcings combine to determine the circulation of the mid-depth water just below the main thermocline, and we try to obtain some insight into the problem of formulating the right thermal boundary conditions for the thermocline problem.

First, in A, a parameterization of density diffusion in layer models is derived, and then, in B, a simple 3-layer diffusive model of the wind and thermohaline oceanic circulation is described. The reader is advised to start by reading the model description in B, and to refer to A for the details of the parameterization only when it is actually used in the model.

A. *A parameterization of density diffusion in layer models.* The parameterization we suggest here is based on the similarity between layer models and density coordinates, and is actually a finite difference approximation to the equations in density coordinates. It enables one to enjoy the mathematical simplification of layers vs. continuous stratification, while not ignoring the cross–isopycnal processes. The equations reduce to the usual equations for an immiscible layer model if the coefficient of diffusion is set to zero. The diffusive processes are modeled as before with a constant eddy coefficient in the density equation.

In order to establish some necessary notation, consider a continuously stratified ocean which is to be modeled by a finite number of discrete layers of uniform density: Suppose we choose to represent the density range between the two densities ρ_a and ρ_b by the nth layer. Then the density of this layer is $\rho_n = (\rho_a + \rho_b)/2$, its thickness is

$h_n(x,y) = z(x,y,\rho_a) - z(x,y,\rho_b)$, where z is the height of a density surface, and we define $\Delta_n\rho$ to be the density range represented by this layer: $\Delta_n\rho = \rho_a - \rho_b$.

With this notation we can now proceed to calculate the velocity across an interface between two layers. In continuous stratification, the cross isopycnal velocity in the direction normal to a constant density surface is $(U \cdot \hat{n})\hat{n}$, where $\hat{n}$ is the unit vector normal to a density surface: $\hat{n} = \nabla\rho/|\nabla\rho|$.

Using the density equation (2.2), we have

$$U \cdot \hat{n} = \frac{U \cdot \nabla\rho}{|\nabla\rho|} = \lambda\frac{\nabla^2\rho}{|\nabla\rho|} \tag{4.1}$$

If the density surfaces are horizontal or very nearly so, then

$$\hat{n} \approx \hat{k}, \quad (U \cdot \hat{n})\hat{n} \approx \hat{k}\lambda\rho_{zz}/\rho_z, \tag{4.2}$$

where $\hat{k}$ is a unit vector in the vertical (z) direction. Writing this in density coordinates, we have

$$(U \cdot \hat{n})\hat{n} \approx \hat{k}\lambda\frac{\partial}{\partial\rho}\left(\frac{\partial z}{\partial\rho}\right)^{-1}. \tag{4.3}$$

Now, $\partial z/\partial\rho$ can be approximated for the nth layer in a layer model by $\Delta z/\Delta\rho = h_n/\Delta_n\rho$ and the derivative w.r.t. ρ of some quantity B evaluated at the interface between the $n, n+1$ layers, can be replaced by

$$\frac{\partial B}{\partial\rho} \approx \frac{(B_{n+1} - B_n)}{\rho_{n+1} - \rho_n}, \tag{4.4}$$

where B_n is the value of B in the nth layer. Combining (4.3) and (4.4) we have

$$\text{the cross interfacial velocity} \equiv w_n^* \approx \lambda\frac{\Delta_{n+1}\rho/h_{n+1} - \Delta_n\rho/h_n}{\rho_{n+1} - \rho_n}. \tag{4.5}$$

(This expression is all we need for the layer model presented in B) The approximation in (4.2) is not necessary, and the parameterization can be extended to non–horizontal isopycnals. It is also possible to extend the parameterization to the case of outcropping

layers, while avoiding the singularity in $\Delta_n\rho/h_n$ where $h_n \to 0$ in the outcropping region.

As another example of the parameterization, we briefly derive the gyre-scale potential vorticity equation for layer models, including the diffusive effects. In a continuously stratified ocean, for planetary scale motions, small Rossby number and in the presence of vertical diffusion, the potential vorticity equation is: (Pedlosky, 1979)

$$U \cdot \nabla(f\rho_z) = (u\partial_x + v\partial_y + w\partial_z)(f\rho_z) = \lambda \frac{\partial^2 f\rho_z}{\partial z^2} \tag{4.6}$$

In density coordinates this is

$$(u\partial_x + v\partial_y)\frac{f}{h}|_{\rho=constant} = \frac{\lambda\rho}{h^2}\frac{\partial^2 \frac{f}{h}}{\partial z^2} \tag{4.6}$$

where $h = -\rho\partial z/\partial\rho$. For the nth layer h can be approximated by

$$h \approx h_n \frac{\rho_n}{\Delta_n\rho} \approx h_n \frac{\rho_0}{\Delta_n\rho},$$

and (4.7) becomes

$$(u_n\partial_x + v_n\partial_y)\frac{f}{h_n} = \frac{\lambda f}{{h_n}^2}\left[\frac{\Delta_{n+1}\rho/h_{n+1} - \Delta_n\rho/h_n}{\rho_{n+1} - \rho_n} - \frac{\Delta_n\rho/h_n - \Delta_{n-1}\rho/h_{n-1}}{\rho_n - \rho_{n-1}}\right]. \tag{4.8}$$

Note that when $\lambda = 0$, (4.8) reduces to the usual potential vorticity equation in layer models for this type of motions.

B. The model. The three layer model we use is shown schematically in figure 9. The upper layer represents the wind driven circulation above the main thermocline (vertically hatched in figure 5), and is driven by a wind stress curl that forces a two-gyre circulation. The second layer represents the upper mid-depth water, below the main thermocline and above about two kilometers depth (diagonally hatched in figure 5). This layer is buoyancy-driven, by the cross isopycnal velocities due to the mixing processes. The wind affects this circulation by changing the local vertical stratification

(and therefore the local diffusive vertical velocities), through the changes in the depth of the main thermocline. The air–sea fluxes affect the circulation in this layer not by direct cooling or heating, but through the production of water which sinks and joins the mid-depth water. The bottom layer represents the vertically integrated transport of the lower mid-depth and bottom circulations (unshaded in figure 5), that were described in more details in the continuous model of section 3. The circulation in this layer is similar to that of the Stommel-Arons model.

The deeper layers do not outcrop within the two gyres, but it is assumed that they do outcrop somewhere, and interact with the atmosphere. (This restriction is not necessary, and is made only to keep the model as simple as possible.) This outcropping region is not explicitly a part of the model; we only specify the air–sea fluxes there as a function of the surface density, and assume that water which is produced by these fluxes is carried towards the ocean interior. One can think of the Norwegian sea as an example of such a polar outcropping region, as shown by the broken lines in figure 9, but the outcropping region, where the production of water types is taking place, is not necessarily northward of the sub-polar gyre. The outcrop may be in the western boundary region or within the gyres, if we allow outcropping there.

The model equations for the nth layer are (see (3.1)):

$$\begin{aligned} f u_n &= -\frac{1}{\rho_0} p_{ny} \\ f v_n &= \frac{1}{\rho_0} p_{nx} \\ p_{nz} &= -g\rho_n \end{aligned} \tag{4.9}$$

$$u_{nx} + v_{ny} + w_{nz} = 0.$$

The boundary conditions are:

* The wind-forced Ekman pumping at the base of the mixed layer, $w_e(x, y)$, is given.
* The air–sea heat flux as function of the surface density in the outcropping region, $H(\rho)$, is assumed known.

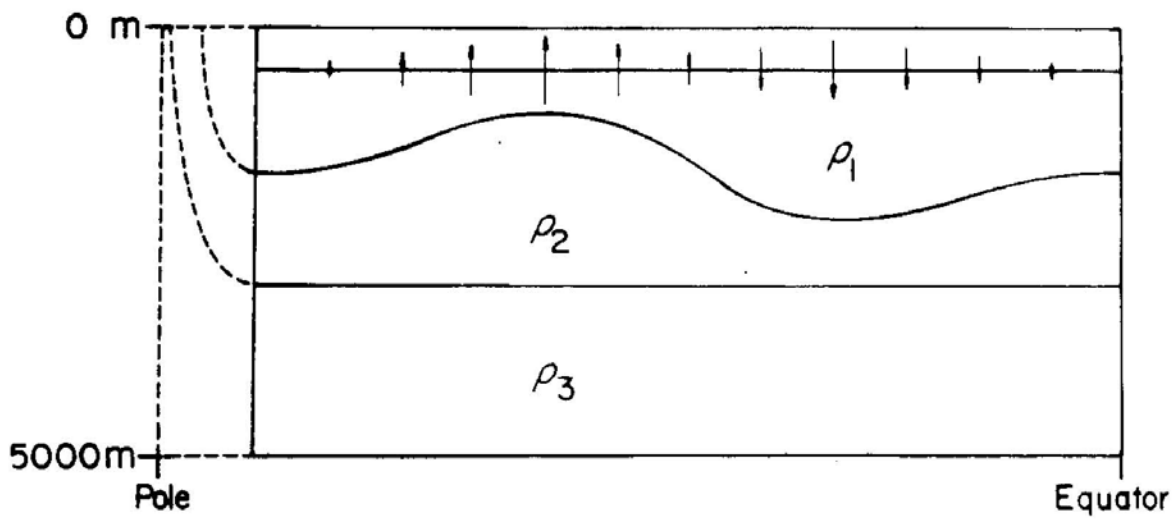

Figure 9. The three layer model described in section 4.

* No zonal flow into the eastern boundary: $u(x_e, y) = 0$.

Vertical diffusion is permitted, and we will use the parameterization derived in (A) to calculate the small cross-interfacial velocities resulting from this diffusion. To solve for the layer thicknesses and velocities, an approach similar to that of section 3 is used. Assume that the diffusive effects are small, so that to lowest order density is conserved, and the two deeper layers are motionless. (By assumption, the wind driven circulation is confined to the upper layer, and the other layers are driven only by the cross-isopycnal velocities.) With these assumptions the upper layer is a one layer ventilated thermocline, (Luyten, Pedlosky and Stommel, 1983) with thickness given by

$$h_1(x,y) = ({D_0}^2(x,y) + {H_1}^2)^{\frac{1}{2}} \tag{4.10}$$

where

$$\begin{aligned} {D_0}^2(x,y) &= -\frac{2f^2}{\beta\gamma}\int_x^{x_e} w_e(x',y)dx', \\ \gamma &= g\frac{\rho_2 - \rho_1}{\rho_0}; \qquad H_1 = h_1(x_e,y) = constant. \end{aligned} \tag{4.11}$$

For the 2nd and 3rd layers:

$$\begin{aligned} h_2(x,y) &= (H_1 + H_2) - h_1(x,y) \\ h_3(x,y) &= H_3, \end{aligned} \tag{4.12}$$

where, again $H_n = h_n(x_e, y) =$ constant.

To find the basic stratification parameters H_1 ,H_2 and H_3, and the buoyancy driven circulation in the deeper layers, we *must* consider the thermal boundary conditions and the diffusive processes. Given the air–sea heat fluxes as function of the density of the surface water that is losing/gaining this heat, $H(\rho)$, we first calculate the net production of water of given density (see (2.8)),

$$M(\rho) = \frac{\alpha}{C_p}\frac{\partial H}{\partial \rho}.$$

The net production of water of the density ranges represented by layers 2 and 3 is

$$M_{n,\text{heat fluxes}} = \int_{\rho_n - \frac{1}{2}\Delta_n\rho}^{\rho_n + \frac{1}{2}\Delta_n\rho} M(\rho)d\rho = \frac{\alpha}{C_p} H(\rho)|_{\rho_n - \frac{1}{2}\Delta_n\rho}^{\rho_n + \frac{1}{2}\Delta_n\rho} \quad n = 2, 3. \tag{4.13}$$

In terms of layers, $M_{n,\text{heat fluxes}}$ is the the mass of water of density ρ_n which enters the nth layer, per unit time, after being formed at the surface.

Next, the net production/dissipation of water types represented by the nth layer by the diffusive processes, is found in terms of the stratification parameters H_n. This production is simply equal to the difference between the total cross isopycnal mass flux into and out of the nth layer:

$$M_{n,\text{diffusion}} = \iint dxdy(w_n^* - w_{n+1}^*), \tag{4.14}$$

where w_n^* is the local velocity across the interface of the $n, n+1$ layers. Using the parameterization (4.5) for w_n^*, we have,

$$M_{n,\text{diffusion}} = \lambda \iint dxdy \left[\frac{\Delta_{n+1}\rho/h_{n+1} - \Delta_n\rho/h_n}{\rho_{n+1} - \rho_n} - \frac{\Delta_n\rho/h_n - \Delta_{n-1}\rho/h_{n-1}}{\rho_n - \rho_{n-1}} \right] \tag{4.15}$$

and in particular,

$$M_{2,\text{diffusion}} = \lambda \iint dxdy \left[\frac{\Delta_3\rho/h_3 - \Delta_2\rho/h_2}{\rho_3 - \rho_2} - \frac{\Delta_2\rho/h_2 - \Delta_1\rho/h_1}{\rho_2 - \rho_1} \right] \tag{4.16a}$$

$$M_{3,\text{diffusion}} = \lambda \iint dxdy \left[\frac{\Delta_3\rho/h_3 - \Delta_2\rho/h_2}{\rho_3 - \rho_2} \right] \tag{4.16b}$$

For the total mass of fluid represented by the nth layer to remain constant, we must have

$$M_{n,\text{diffusion}} + M_{n,\text{heat fluxes}} = 0. \tag{4.17}$$

The production $M_{n,\text{diffusion}}$ depends on the eastern boundary stratification parameters through (4.15) and (4.10-12), so that we can now write three equations for the three unknowns H_1 ,H_2 and H_3:

$$\begin{aligned} H_1 + H_2 + H_3 &= H = 5km \quad (= \text{total ocean's depth}) \\ M_{2,\text{diffusion}} + M_{2,\text{heat fluxes}} &= 0 \\ M_{3,\text{diffusion}} + M_{3,\text{heat fluxes}} &= 0 \end{aligned} \tag{4.18}$$

and we can solve for the stratification in terms of the air–sea fluxes as represented by the M_ns . Before showing a few examples with specific M_ns, we calculate the buoyancy driven circulation in layers 2 and 3.

With H_1, H_2 and H_3 now known, we can find the local values of the vertical velocities across the interfaces, and then use

$$\beta h_n v_n = f(w_n^* - w_{n+1}^*) \qquad n = 2,3 \tag{4.19}$$

to find the horizontal velocities in these layers:

$$\begin{aligned} h_2 v_2 &= \frac{f}{\beta}(w_2^* - w_3^*) \\ h_3 v_3 &= \frac{f}{\beta} w_3^*. \end{aligned} \tag{4.20}$$

A short comment on the role of western boundary currents is relevant here: Much of the heat loss from the ocean to the atmosphere probably occurs in the western boundary currents of the wind driven circulation (Bunker, 1976), and this is considered implicitly above as part of the specified heat flux $H(\rho)$. We did not, however, consider the effect of boundary mixing (Wunsch, 1970). If it is believed to be non–negligible (although the area involved is small), it can be incorporated into (4.17) by specifying $M_{n,\text{boundary mixing}}$ (or calculating it by matching boundary currents to the model), and then constraining the interior by

$$M_{n,\text{diffusion}} + M_{n,\text{heat fluxes}} + M_{n,\text{boundary mixing}} = 0,$$

Table 1: Parameters used in the examples of section 4.

Ekman pumping: $w_e(x,y) = -10^{-4}$; $\sin(\pi y/3000km)$ cm/sec

Densities and density ranges of the layers (see section 4A):

$\rho_1 = 1.02575$ $\quad \Delta_1\rho = -0.00250$

$\rho_2 = 1.02740$ $\quad \Delta_2\rho = -0.00080$

$\rho_3 = 1.02786$ $\quad \Delta_3\rho = -0.00012$

Summary of the results: $(1Sv. = 10^6 m^3/sec.)$

$M_{2,\text{heat fluxes}}$	$M_{3,\text{heat fluxes}}$	H_1	H_2	H_3	See figures
0Sv.	5Sv.	770m	950m	3280m	10.a–c
-1Sv.	5Sv.	880m	950m	3170m	11.a–c
1Sv.	5Sv.	700m	950m	3350m	12.a–c

instead of by (4.17).

Examples and discussion.

In the following examples we specify $M_{n,\text{diffusion}}$ and $M_{n,\text{heat fluxes}}$, and determine the stratification parameters H_1 ,H_2 ,H_3 , and buoyancy-driven circulation in layers 2 and 3. This is done by integrating (4.16a,b) numerically for different values of H_n, until the values satisfying (4.18) are found. Three different cases are examined, and the results are shown in figures 10-12, and are summarized in Table 1.

Consider first the case shown in figure 10. The circulation in the bottom layer (figure 10.c) is basically the same as in the Stommel-Arons model, except that the vertical velocity at the top of this layer is not uniform and is determined as part of the solution instead of being specified.

The circulation in layer 2 (figure 10.b) shows some interesting features. In this example $M_{2,\text{heat fluxes}}$ is zero, so that the total upwelling across the interface between layers 2,3 is equal to the total upwelling across the interface between layers 1,2. Still, locally, the difference $w_2^* - w_3^*$ does not vanish everywhere. The horizontal variations in the depths of layers 1 and 2 (figure 10.a) induce variations in w_2^* and w_3^*. These variations tend to make the difference $w_2^* - w_3^*$ positive under the sub-polar gyre, and

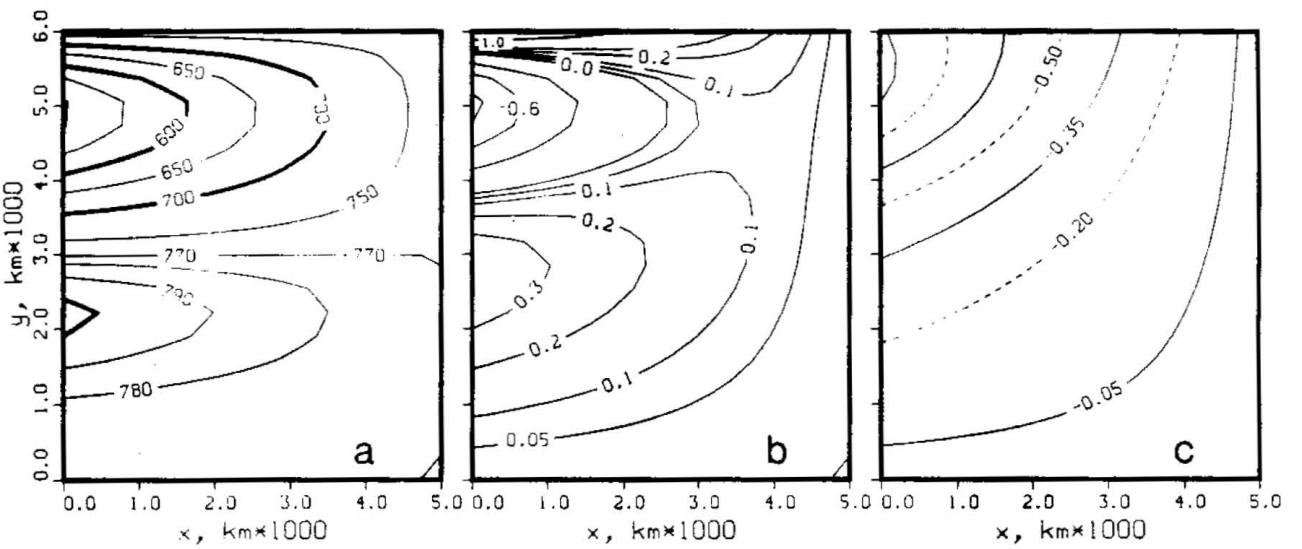

Figure 10. Results of the layer model of section (4.B), for the thermal boundary conditions: $M_2 = 0Sv$, $M_3 = 5Sv$:

(a) The thickness of layer 1, in meters.

(b) Transport stream function($\Psi_n = \int_{x_e}^{x}[v_n h_n]dx$) for layer 2, normalized by its maximum absolute value$|\Psi_2|_{max} = 1.28 \times 10^6 m^3/sec.$

(c) As (b), for layer 3. $|\Psi_3|_{max} = 6.55 \times 10^6 m^3/sec.$

negative under the sub-tropical gyre, therefore driving the mid-depth circulation in the same direction as that of the wind driven circulation! Note that we do not impose heating of layer 2 in the sub-tropical gyre and cooling in the subpolar gyre, and that there is not any momentum transfer from the upper layer to the middle one. The circulation in layer 2 is driven only by the diffusive processes, and the only effect of the upper wind driven circulation on the second layer is through the variations in the thickness of layer 1.

Unfortunately, it is not possible to deduce the buoyancy driven corrections to the velocities in the upper layer because we do not know the diffusive corrections to the vertical velocity at the top of this layer. It is not clear how to model the diffusion between the upper layer and the Ekman layer on top of it, but we can increase the resolution of the wind driven circulation by adding more layers, and then it will be possible to find the diffusive effects on each of the layers except for the uppermost one.

In the second example considered here (figures 11.a-c) $M_{2,\text{heat fluxes}} = -1$ Sverdrup, so that there is a net vortex compression in the middle layer: $\iint (w_2^* - w_3^*) dx dy < 0$. This tends to induce a southward flow in layer 2 (see (4.20)), but the structure of the flow is still dominated by the variations in the thickness of the upper layer.

In the last example (figures 12.a-c) $M_{2,\text{heat fluxes}} = +1$ Sverdrup, so that there is a net vortex stretching in layer 2. This enforces the northward flow under the wind driven subpolar gyre, and weakens the southward flow under the subtropical gyre. The circulation in layer 2 is still similar to the two-gyre wind driven circulation in layer 1.

The above examples demonstrate the physics of the mid-depth circulation: It is driven by the cross isopycnal diffusive velocities, and is affected by the air–sea heat fluxes through the formation of water masses, and by the wind driven circulation that causes the variations in the depth of the main thermocline. The two gyre mid-depth circulation seems to be quite robust to changes in the amount of water injected into it from the outcropping region. It is not clear how a more realistic parameterization

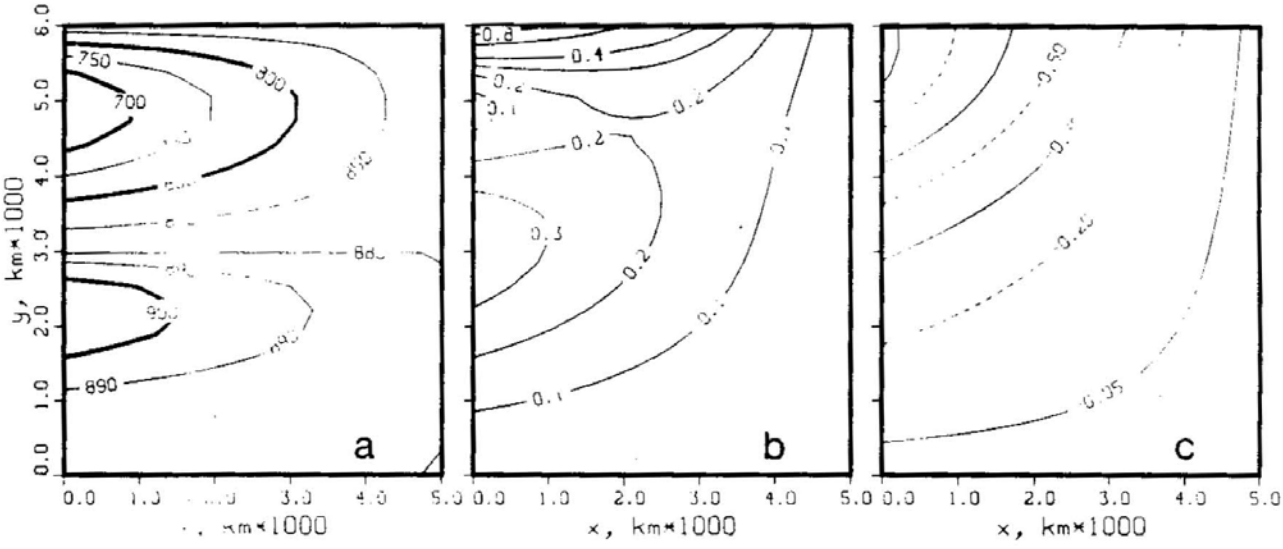

Figure 11. Same as figure 10, with: $M_2 = -1Sv$, $M_3 = 5Sv$. $|\Psi_2|_{max} = 2.34 \times 10^6 m^3/sec$, $|\Psi_3|_{max} = 5.32 \times 10^6 m^3/sec$.

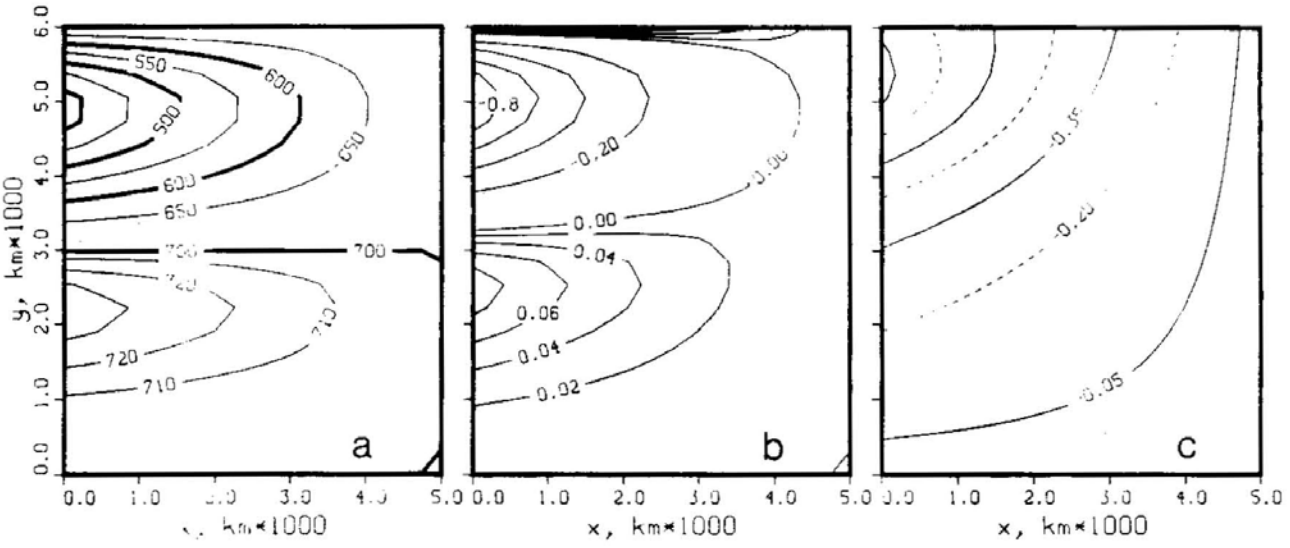

Figure 12. Same as figure 10, with: $M_2 = +1Sv$, $M_3 = 5Sv$. $|\Psi_2|_{max} = 2.71 \times 10^6 m^3/sec$, $|\Psi_3|_{max} = 7.82 \times 10^6 m^3/sec$.

of the mixing processes will affect it. What we want to emphasize here, however, is not the specific result of two-gyre mid-depth circulation, but the mechanisms by which heat fluxes and wind affect this circulation.

Perhaps the most important conclusion of this section concerns the formulation of the correct thermal boundary conditions for the thermocline problem: The usual approach is to replace the physical boundary conditions of heat fluxes with a specification of the density at the base of the mixed layer. It should be clear from the model here, that the heat fluxes have another, independent effect - the production of water masses. Information on this formation (or equivalently, on the air–sea heat fluxes) is necessary for the determination of the basic stratification and the buoyancy driven flows, and has to be specified as part of the thermal boundary conditions. The only way to avoid having to specify both surface density and heat fluxes is to include the physics of the mixed layer within the model.

5. Conclusions.

We have tried to examine the importance of the thermodynamical processes to the dynamics of the general circulation. Two simple models were presented and used to understand the role of interior small scale mixing and of air–sea exchanges: A continuous model of the deep circulation and a three layer model of the deep and wind driven circulations. The results seem to lead to two main conclusions:

(1) The mixing processes are essential not only for driving the deep thermohaline circulation, but also for determining the basic vertical density stratification of the wind driven circulation.

(2) The air–sea heat fluxes affect the interior circulation in two ways. They determine the surface density (together with the surface circulation), and they produce masses of water of different densities which determine the basic interior stratification together with the mixing processes. As a result, one has to specify the heat fluxes *in addition* to specifying the surface density, as the thermal boundary conditions for the thermocline problem. These boundary conditions account for the full effects of the heat fluxes on the interior *without* explicitly considering the mixed layer physics, and allow one to determine the basic stratification of the circulation, as shown in the previous sections.

Recent studies (Rhines and Young 1982b, Pedlosky and Young 1983) have demonstrated the importance of the small frictional dissipation due to the meso-scale eddies to the dynamics of the wind driven circulation. Together with the results here, it seems that the physics of the general circulation, and of the thermocline problem in particular, is more intricate than anticipated from simple scaling arguments. Both friction and mixing (diffusion) are small, but their effects are crucial.

Chapter 2

The Mediterranean outflow as an example of a deep buoyancy – driven flow

1. Introduction

The models presented in chapter 1 demonstrate the importance of interior mixing processes for determining the basic vertical stratification of the oceans. The dynamics of the circulation driven by the mixing, however, is restricted and is dominated by other effects in these models. In the deep circulation model of section (1.3) the $O(1)$ stratification is horizontally uniform, while in the layer model of section (1.4) the horizontal density structure is determined by the wind forcing only. The horizontal variations in the stratification affect the vertical (cross–isopycnal) velocity through the density equation, and the vertical velocity, in turn, forces the horizontal circulation, through the vorticity balance. The buoyancy driven horizontal circulation in the above models is therefore somewhat passive, being forced by a stratification whose horizontal structure it cannot affect.

The purpose of this chapter is to present a more complete model of a deep buoyancy driven flow. In this model, the buoyancy driven circulation determines the horizontal as well as the vertical density structure. The circulation therefore sets its own path, and is not passively forced by externally determined horizontal density structure. The model enables us to examine the detailed dynamics of the buoyancy driven flows, which was impossible with the previous restricted models.

The physical problem modeled is of a mid–depth inflow from the eastern boundary, and the resulting large scale interior circulation. The dynamics are geostrophic, hydrostatic, mass conserving and diffusive. The problem is motivated by the Mediterranean outflow, although the emphasis is on demonstrating the general physical principles governing deep buoyancy driven flows rather than on realistically modeling the

Mediterranean outflow. The model does suggest, however, a possible mechanism for the spreading of the Mediterranean water, and makes clear what parameters one needs to calculate from the data to better understand such a circulation.

In the present model, mixing, advection, basic vertical density stratification and horizontal density structure are all coupled. Previous efforts to model the interior buoyancy driven circulation have usually dropped one or more of these ingredients by specifying it, and proceeded to solve for the rest.

Olson (1985) used a density equation of the form $d\rho/dt = G$ where G is the density flux (due to mixing) convergence. The horizontal structure of G was related to the heating or cooling at the surface by the atmosphere, while the vertical structure of G was specified and assumed not to depend on the stratification. Rhines (1985), Pedlosky (1986) and Luyten and Stommel (1986) all specified the cross–isopycnal interior velocity field, and calculated the resulting horizontal circulation patterns, in order to study the effects of buoyancy forcing on the wind driven circulation. Arhan (1986) used the same approach as Luyten and Stommel to model the effects of double diffusion on the dynamics of the Mediterranean outflow, by specifying the cross-interfacial velocity in the interior.

Specifying the interior cross–isopycnal velocities or relating it directly to atmospheric heating does simplify the problem, but causes some problems as well. One does not expect the direct atmospheric heating to penetrate beyond the depth of the mixed layer and directly affect the deep flows, while observations indicate that interior mixing depends on the interior stratification through a relation like $\mathbf{u}\cdot\nabla\rho = [\kappa(z)\rho_z]_z$ (Gargett, 1984). It is probably necessary, therefore, to have a parameterization of mixing which depends on the stratification when modeling buoyancy driven flows below the surface waters. From a theoretical point of view, specifying the buoyancy forcing rather than

letting the model determine it from the stratification means that the model cannot explain the basic vertical stratification. Also, as discussed above, the model loses a degree of freedom when the horizontal circulation is not allowed to affect its own forcing.

Other approaches to modeling buoyancy driven flows include linearization of the equations about some mean specified state (e.g. Gill, 1985), and similarity solution for the diffusive thermocline equations (Veronis, 1969 or more recently Young and Ierley, 1986). In both cases the mathematical simplification involved enables one to obtain continuous solutions to the problem, but the physics suffers limitations. These models include a diffusion term in the density equation, and therefore allow the model to determine the forcing of the horizontal circulation. But the average vertical stratification is still specified in the linearized case, and the similarity solutions are very restricted by the assumed similarity form.

In the following sections the layer model we use is formulated (section 2), and then a series of problems of increasing complexity is solved. First, in section 3, the ideal case (no diffusion) is solved. Then the diffusive case with the vertical density equation $w\rho_z = \lambda_v \rho_{zz}$ only (sections 4, 5), and finally the effects of horizontal advection of density are included (section 6). The relation of the results to different observations is discussed in section 7.

2. The model

The layer model used is shown in figure 1. The inflow from the eastern boundary is confined to a limited latitude band, $y_1 < y < y_2$, in one layer (layer 0) only. It is assumed to be below the wind-driven circulation, and above the bottom water. No transport of water across the basin boundaries (e.g. cross-equatorial flow) is allowed. To keep the total amount of water in layer 0 constant, the water entering layer 0 from the eastern boundary has to leave this layer through interior cross-interfacial fluxes. These fluxes are analogous to cross-isopycnal fluxes in a continuously stratified model, and are present in the model because we allow for diffusion of heat across the interfaces between layers.

The vertical circulation in the model can be described schematically as follows. Deep water masses are formed at some polar basin, sink to the bottom, and spread in the ocean interior. This water then upwells through cross-isopycnal velocities balanced by diffusion, and appears in the model as an upwelling across the lower interfaces of the model. At the depth of layer 0, this upwelling is joined by the water coming from the eastern boundary, making the total upwelling at the top of layer 0 larger than that at the bottom. This larger upwelling leaves the upper layers of the model; some of it flows into the marginal sea to reappear later as the inflow from the eastern boundary; a larger portion flows poleward, where it loses heat and sinks to the bottom. Western boundary currents are needed to close the interior horizontal circulation and to connect the interior with the region of bottom water formation.

The dynamics we use are geostrophic, hydrostatic and diffusive. The equations for

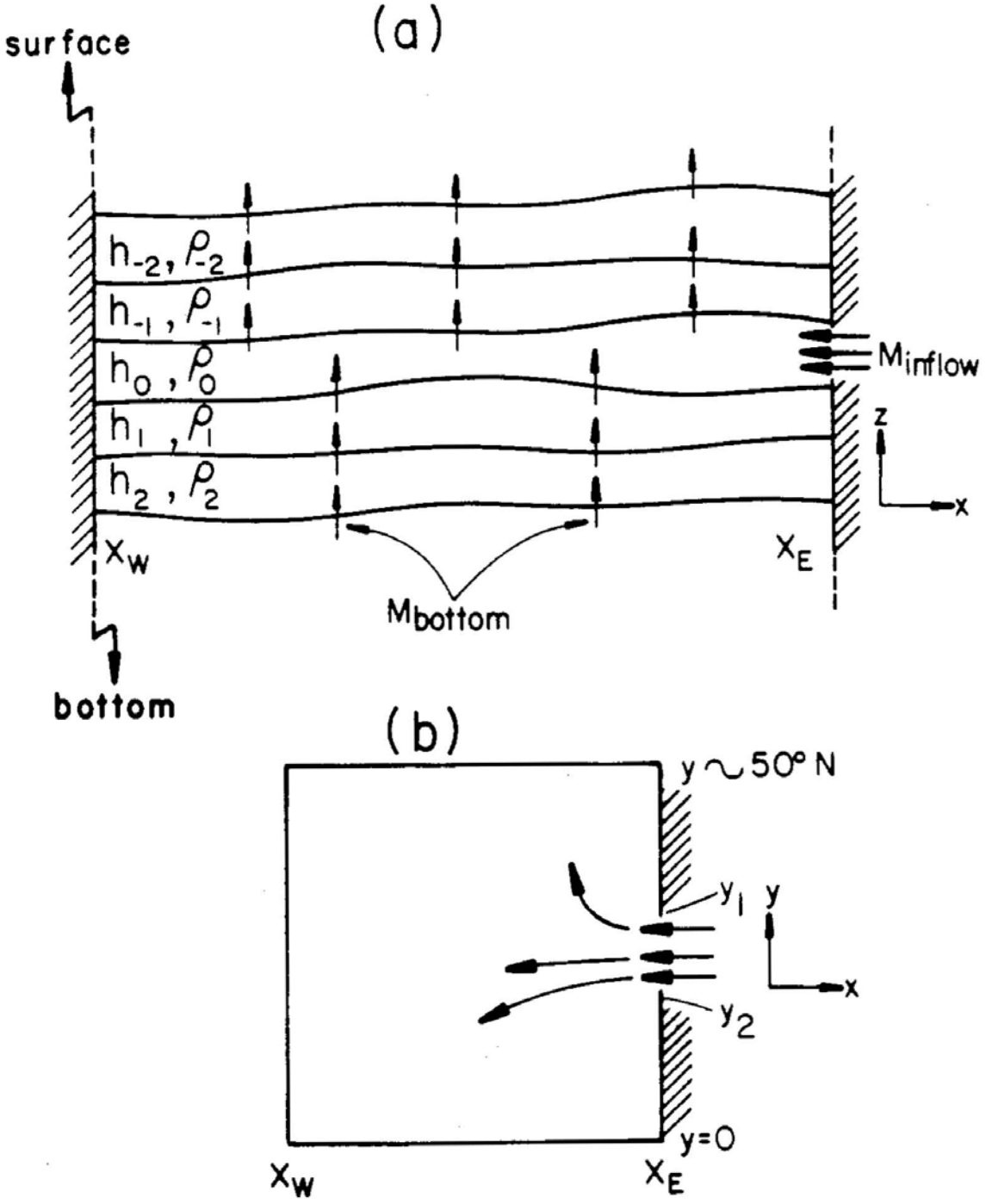

Figure 1: A schematic picture of the inflow and layers from above, and in a zonal section.

the nth layer are

$$\begin{aligned} fu_n &= -\frac{1}{\rho_0} p_{ny} \\ fv_n &= \frac{1}{\rho_0} p_{nx} \\ p_{nz} &= -g\rho_n \\ u_{nx} + v_{ny} + w_{nz} &= 0, \end{aligned} \tag{2.1}$$

where $x = R\phi\cos\theta$, $dy = Rd\theta$, (ϕ, θ) are the longitude and latitude, and R is the radius of the earth. $f(y) = 2\Omega\sin\theta$ is the Coriolis acceleration, and we also use $\beta(y) = df/dy$. The β plane approximation is not made, and both f and β are functions of latitude. The density equation is

$$u\rho_x + v\rho_y + w\rho_z = \lambda_H \nabla_H^2 \rho + \lambda_V \frac{\partial^2 \rho}{\partial z^2}, \tag{2.2}$$

and we will express it later in terms of the layer thicknesses instead of continuous stratification. There are two observations we can make to simplify the problem:

First, following Warren (1977), we use a simple scaling argument to show that the dominant balance in the density equation for the mid–depth circulation is simply

$$w\rho_z = \lambda_V \frac{\partial^2 \rho}{\partial z^2}. \tag{2.3}$$

Let $\Delta_H \rho$ and $\Delta_V \rho$ be the variations of the density on the horizontal (L) and vertical (D) scales of motion respectively. For the mid–depth circulation, where the density surfaces are nearly flat, the ratio $\epsilon \equiv \Delta_H \rho / \Delta_V \rho$ is a small parameter (about 0.2). Nondimensionalizing the density equation (2.2), using the scales $(u, v) \sim U$, $w \sim UD/L$, we find the non dimensional density equation

$$\epsilon(u\rho_x + v\rho_y) + w\rho_z = \left(\frac{\lambda_V}{WD}\right) \frac{\partial^2 \rho}{\partial z^2} + \epsilon \left(\frac{\lambda_H}{UL}\right) \nabla_H^2 \rho. \tag{2.4}$$

With

$$W = 10^{-5} cm/sec \qquad D = 1km \qquad L = 5000km$$

$$\lambda_H = 5 \times 10^6 cm^2 sec^{-1} \qquad \lambda_V = 1 cm^2 sec^{-1},$$

it is clear that the leading order balance in (2.4) is the vertical density equation (2.3). Using the parameterization of diffusion in layer models, we can write (2.3) in terms of layers' thickness:

$$w_n = \lambda_v \frac{\Delta_{n+1}\rho/h_{n+1} - \Delta_n \rho/h_n}{\rho_{n+1} - \rho_n}, \tag{2.5}$$

where w_n is the vertical velocity across the interface of layers n, $n+1$. In section (6) we use a perturbation expansion in powers of ϵ and examine the effects of the horizontal diffusion and advection which are ignored now. In the same section ϵ is also expressed in terms of the forcing (inflow) parameters, and the explicit conditions that make it small are made clear. It turns out that ϵ is small when the transport of the inflow is weak.

To further simplify the problem, we note that the horizontal velocity fields above and below the inflow ought to decay away from layer 0. For layers far enough from layer 0, the cross–interfacial upwelling and the layer thicknesses become uniform in (x, y), and the horizontal velocities vanish. To see why this is correct, consider the forcing of each of the layers. We have already mentioned that the total upwelling at the top of layer 0 is larger than that at the bottom of this layer. This makes $w_{0,top} - w_{0,bottom}$ (or w_{0z}) positive, therefore forcing a northward flow in the interior through $\beta v = f w_z$. The circulation in layer 0 is a combination of the westward flow entering from the eastern boundary, and the northward flow induced by $w_z > 0$. The motion in layer 0 induces variations in the thickness of that layer and of adjacent ones.

Consider next the situation in layers -1 and $+1$. Because there is no inflow into these layers, the horizontally averaged $w_{n,top} - w_{n,bottom}$ vanishes. Still, the variations in the thickness of these layers due to the motion in layer 0 induce local variations in $w_{n,top} - w_{n,bottom}$ through the density equation (2.5). Consequently, these layers are moving. Because the direct forcing due to the inflow and to the requirement that $\iint_{whole\ basin}(w_{n,top} - w_{n,bottom})dxdy > 0$ are missing now, the circulation in layers $+1,-1$ and the variations in their thickness are weaker than for layer 0. Considering

layers which are even further away from the inflow, we see that their circulation is even weaker, and their thickness becomes uniform in (x, y).

We assume below that the horizontal velocities vanish in layers far enough above and below the inflow. This assumption will enable us to solve for the circulation in the layers assumed moving. In the following sections we first solve the simplest problem of only one moving layer (layer 0), and later the case of three moving layers $(-1, 0, +1)$. In the solution to the three moving layer model (section 5) the circulation above and below the inflow is weaker than that at the inflow depth. This is consistent with the above argument about the decay of the solution away from the inflow.

But first, it is useful to examine the solution to the problem when we ignore the diffusive effects and assume that density is conserved. This will give us some idea of the possible importance of the diffusion in this problem.

3. The non diffusive case.

Let us assume that the diffusive effects in the ocean interior are very weak, so that we can set the diffusion coefficient λ_V to zero, and use the ideal fluid geostrophic equations. It is known (Rhines and Young, 1982b) that the solution to these equations is not unique. In the case considered here, there are many possible solutions consistent with a given specified inflow into layer 0. The circulation we find will depend, for example, on the specified transport from the western boundary current into the layers above and below the inflow.

We now examine the simplest problem, where there is no inflow from the western boundary current into layers above and below layer 0. Only layer 0 is moving, and we can solve for its thickness and velocity for a given inflow from the eastern boundary.

From the hydrostatic equation (2.1c) we have

$$\frac{1}{\rho_0}\nabla_H p_{n+1} = \frac{1}{\rho_0}\nabla_H p_n + \gamma_n \nabla_H z_n(x, y), \tag{3.1}$$

where $\gamma_n \equiv g(\rho_{n+1} - \rho_n)/\rho_0$, and $z_n(x,y)$ is the height of the interface between the n and $n+1$ layers. Because layers above and below layer 0 are at rest, $\nabla_H p_n = 0$ for $n \neq 0$. Using (3.1) we find

$$\begin{aligned} \frac{1}{\rho_0}\nabla_H p_0 &= -\gamma_0 \nabla_H z_0(x,y) \\ &= -\gamma_0 \nabla_H h_1(x,y), \end{aligned} \tag{3.2}$$

and

$$\nabla_H z_n = 0 \qquad n \neq -1, 0. \tag{3.3}$$

This last equation means that all interfaces are flat except for those enclosing layer 0. Using (3.1) we also find

$$0 = \frac{1}{\rho_0}\nabla_H p_1 = \gamma_1 \nabla_H h_0 + (\gamma_0 + \gamma_1)\nabla_H h_1$$

or

$$\begin{aligned} \gamma_1 h_0(x,y) + (\gamma_0 + \gamma_1) h_1(x,y) &= \text{constant} \\ &= \gamma_1 h_0(x_e,y) + (\gamma_0 + \gamma_1) h_1(x_e,y) \\ &= \gamma_1 H_0 + (\gamma_0 + \gamma_1) H_1, \end{aligned} \tag{3.4}$$

where $H_n \equiv h_n(x_e, y_1)$ is the thickness of the nth layer on the eastern boundary, south of the inflow. From (2.1) and (3.4) we derive the vorticity equation

$$\beta v_0 h_0 = -\beta \frac{\gamma_0}{f} h_{1x} h_0 = f(w_{0,top} - w_{0,bottom}). \tag{3.5}$$

The vertical velocities are zero for the resting layers -1, $+1$, and therefore also at the interfaces of layer 0. The forcing on the rhs of (3.5) vanishes therefore, and the circulation in layer 0 is simply a zonal flow

$$\begin{aligned} &u_0(x,y) = u_0(x_e,y), \qquad v_0(x,y) = 0, \qquad w_0(x,y) = 0, \\ &h_n(x,y) = h_n(x_e,y), \qquad n = -1, 0, +1. \end{aligned}$$

The thickness on the eastern boundary is determined from the specified inflow. Let the inflow velocity be

$$u_0(x_e, y) = \begin{cases} U_0 f_0/f & y_1 < y < y_2; \\ 0 & \text{elsewhere,} \end{cases}$$

where $f_0 = f(\frac{y_1+y_2}{2})$ and $U_0 = \text{constant}$. Using $fu_0 = \gamma_0 h_{1y}$ and (3.4), we find

$$\begin{aligned} h_1(x_e, y) &= H_1 + \frac{U_0 f_0}{\gamma_0}(y - y_1) \\ h_0(x_e, y) &= H_0 - f_0 U_0 \left(\frac{1}{\gamma_{-1}} + \frac{1}{\gamma_0}\right)(y - y_1) \\ h_{-1}(x_e, y) &= (H_1 + H_0 + H_{-1}) - (h_0(x_e, y) + h_1(x_e, y)), \end{aligned} \tag{3.8}$$

where, again,

$$H_n \equiv h_n(x_e, y_1).$$

Note that we have to specify the thickness of all layers on the eastern boundary, south of the inflow.

We now proceed to the diffusive case, with several questions in mind: Can the addition of diffusion to the physics resolve the non uniqueness problem? Can one find the H_ns as part of the solution? How does the circulation change in the presence of diffusion, and does the diffusive solution reduce to the above ideal fluid solution as we let $\lambda_\nu \to 0$?

4. The diffusive case: one moving layer

As explained in section 2, we expect the horizontal velocity and pressure gradients to weaken with increasing distance from layer 0. We now assume that the pressure gradients in layers -1, $+1$ are already very small, and can be taken to be zero. The actual pressure gradients in layers -1 and $+1$ are not exactly zero, and they affect the circulation in layer 0 [through (3.1)]. The solution we derive below for the circulation in layer 0 is valid as long as $|\nabla_H p_{\pm 1}| \ll |\nabla_H p_0|$. Physically, the decay of the horizontal velocity fields should be determined by the model itself. We are forced to truncate the solution somewhat arbitrarily because of the technical difficulty of solving for a large number of moving layers. The truncation is justified if the addition of more moving layers does not drastically change the circulation found when these layers were assumed at rest. In the next section we truncate the solution further away from the inflow, and assume that layers -2, $+2$ are at rest, while layers -1, 0 and $+1$ are moving. We will see there that the circulation in layer 0 does not change much when we explicitly allow for motion in layers ± 1.

The assumption of only one moving layer has a different physical content in the diffusive and ideal cases. In the ideal case of the previous section the total three dimensional velocity field vanishes for the layers assumed at rest. Here, in the presence of diffusion, only the horizontal velocities vanish for these layers, while the vertical velocity is independent of depth, but is not necessarily zero. The solution for the resting layers is analogous to an exponential density profile in the continuous diffusive case: $\rho = \exp[z\lambda_v/\bar{w}]$, $\bar{w}$ =constant, $u = v = 0$.

With only layer 0 moving, we need to solve for the thickness of three layers: -1, 0 and $+1$. By (3.3), the thickness of all other layers is uniform in (x, y). Taking w from the density equation (2.5), the vorticity equation (3.5) is

$$-\beta\gamma_0 h_{1x} h_0 = f^2\lambda_v \left(\frac{\Delta_0\rho/h_0 - \Delta_{-1}\rho/h_{-1}}{\rho_0 - \rho_{-1}} - \frac{\Delta_1\rho/h_1 - \Delta_0\rho/h_0}{\rho_1 - \rho_0} \right). \qquad (4.1)$$

From (3.3) and (3.4) we have

$$h_{-1}(x,y) + h_0(x,y) + h_1(x,y) = \text{constant} = H_{-1} + H_0 + H_1, \tag{4.2}$$

$$\gamma_1 h_0(x,y) + (\gamma_0 + \gamma_1) h_1(x,y) = \gamma_1 H_0 + (\gamma_0 + \gamma_1) H_1. \tag{4.3}$$

We now have three equations for the three unknowns h_1, h_0 and h_{-1}. Using (4.2) and (4.3) to express h_0 and h_{-1} in terms of h_1, and then substituting them into (4.1) we find a single equation for $h_1(x,y)$ of the form

$$\frac{\partial h_1}{\partial x} = \mathcal{F}\left[h_1(x,y), H_n, f(y)\right] \tag{4.4}$$

The thickness of layer 1 is found by integrating this equation from the eastern boundary, where $h_1(x_e,y)$ is given by the boundary condition (3.8). The thickness of the other two layers is then found from (4.2) and (4.3).

The solution we found for the h_n is not the end of the way. The boundary condition (3.8) used to find $h_n(x,y)$ is given in terms of $H_n = h_n(x_e,y_1)$, which had to be specified. But with diffusion included in the physics, we expect to be able to determine the basic stratification of the model, as represented by the H_n. The H_n are found by requiring the solution to satisfy the integral constraints on the cross–interfacial fluxes.

The circulation in layer 0 depends on the values of the vertical velocities at the top and bottom interfaces of this layer through $\beta v_0 h_0 = f(w_{-1} - w_0)$. To have the correct circulation in layer 0, we must make sure the vertical velocities at its interfaces are correct. Because we have assumed the horizontal velocities to vanish for all other layers, we do not need to worry about the value of w at other interfaces. This leaves us with two constraints on the vertical velocities $w_0(x,y)$ and $w_{-1}(x,y)$. To find what the constraints that we need to apply to w_{-1} and w_0 are, consider figure 2. The schematic figure shows that the total mass flux through the lower interface of layer 0 is equal to the amount of bottom water formed per unit time. The total flux through the upper interface of layer 0 is equal to that through the lower interface of that layer plus the

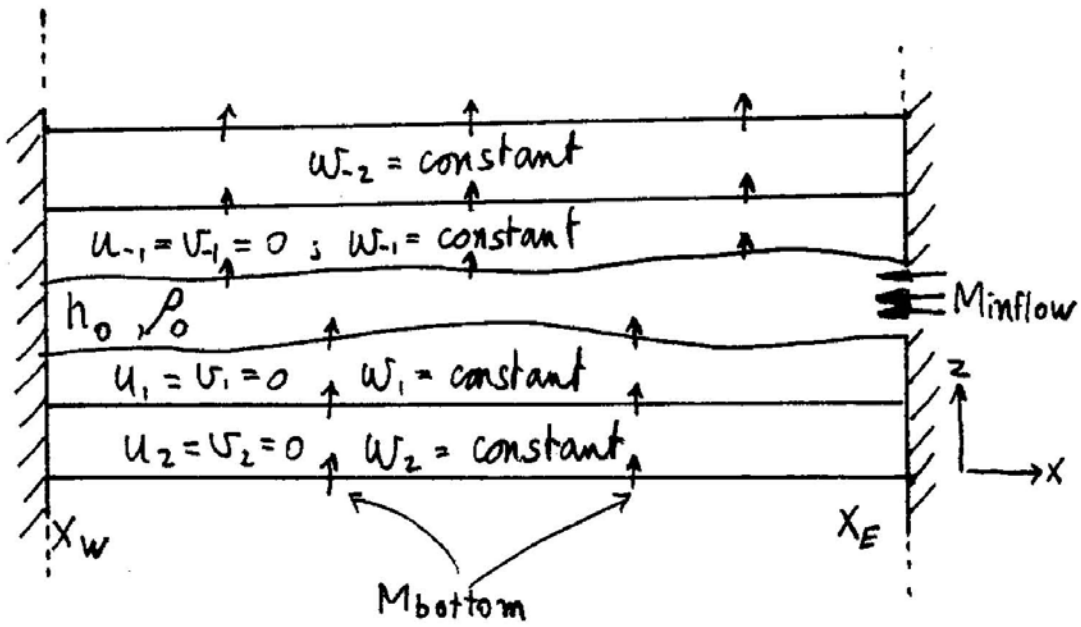

Figure 2: A schematic picture of the solution for the one moving layer case, showing the varying thickness of layers $-1, 0$ and 1, the flat interfaces elsewhere, and the upwelling across the different interfaces.

inflow from the eastern boundary. Once we specify the transport of the inflow, and the amount of bottom water formation, we can write the two constraints as

$$\iint w_0(x,y)\,dxdy = \iint \lambda_r \left(\frac{\Delta_1\rho/h_1 - \Delta_0\rho/h_0}{\rho_1 - \rho_0} \right) dxdy = M_{bottom}, \tag{4.5}$$

$$\iint w_{-1}(x,y)\,dxdy = \iint \lambda_r \left(\frac{\Delta_0\rho/h_0 - \Delta_{-1}\rho/h_{-1}}{\rho_0 - \rho_{-1}} \right) dxdy = M_{bottom} + M_{inflow} \tag{4.6}$$

The double integral in (4.5) and (4.6) is over the entire area of the interior of the basin. The transport of the inflow from the eastern boundary is

$$\begin{aligned} M_{inflow} &= \int_{y_1}^{y_2} u_0(x_e,y) h_0(x_e,y)\,dy \\ &= \int \left[U_0 \frac{f_0}{f} \right] \left[H_0 - f_0 U_0 \left(\frac{1}{\gamma_{-1}} + \frac{1}{\gamma_0} \right) (y - y_1) \right] dy. \end{aligned} \tag{4.7}$$

Specifying $u_0(x_e,y)$ and M_{inflow}, the transport of the inflow, is equivalent by (4.7) to specifying H_0. Equations (4.5) and (4.6) can then be used to solve for the remaining stratification parameters H_{-1} and H_1 using the following procedure. For given values of the the H_n we can calculate the thickness of the layers $h_n(x,y)$ everywhere by integrating (4.4) from the eastern boundary. The lhs of the constraints (4.5), (4.6) can then be evaluated, and used to define a function of the stratification parameters

$$\begin{aligned} \mathcal{G}(H_{-1},H_1) = &\left(\iint w_0(x,y)\,dxdy - M_{bottom} \right)^2 \\ &+ \left(\iint w_{-1}(x,y)\,dxdy - (M_{bottom} + M_{inflow}) \right)^2. \end{aligned} \tag{4.8}$$

The absolute minimum of this function, when $\mathcal{G} = 0$, corresponds to the H_n that satisfy the constraints (4.5) and (4.6). A quasi–Newton routine was used to find the minimum of $\mathcal{G}$, and therefore complete the solution for the stratification and circulation in the model. Equation (4.8) is obviously highly nonlinear in the parameters H_{-1}, H_1, and we have found no mathematical proof for the uniqueness of the solution obtained for these parameters from (4.8). The physics of the problem, and some experimentation with the routine used to solve for H_n indicate that the solution *is* unique.

Results, discussion.

Figure 3 shows the geostrophic pressure in layer 0, and $w_{0,top} - w_{0,bottom}$, for the parameters $M_{bottom} = 2.5$Sv, $U_0 = 0.2$cm/sec, $M_{inflow} = 0.3$Sv, $\lambda_v = 1$ cm^2/sec. The difference $w_{0,top} - w_{0,bottom}$, integrated all over the basin, is positive and equal to the transport of the inflow. This ensures that the total mass in layer 0 is constant, although water is entering it from x_e and leaving through cross–interfacial upwelling. The positive $w_{0,top} - w_{0,bottom}$ induces a northward velocity through the vorticity equation (3.5), therefore turning the inflow northward, as seen in figure 3. This northward flow is forced by the cross interfacial velocities which are present due to the vertical mixing. It does not exist in the ideal fluid case presented in the previous section.

After turning northward, the flow becomes narrower as it flows northward. This is entirely due to the variation of the Coriolis parameters f and β with latitude. The northward velocity is given by $v = (f/\beta)w_z$. On $x = x_e$ the stratification is a function of z only, because of the boundary condition $u(x_e, y, z) = 0$ in combination with the thermal wind relation. The density equation then implies that $w = w(z)$ on x_e, so that near the eastern boundary the northward velocity v varies in y like f/β. Consequently, v increases with latitude and the flow becomes faster and therefore narrower. Figure 4 shows the β–plane case, where f is taken constant except when differentiated and β is constant. In this case there is no change in the width of the flow after it turns northward.

Examining figure 3, we note that the inflow flows westward only about a third of the basin width before turning northward. One would like to know what determines this distance, and whether it can get so small that we effectively have a narrow eastern boundary current, with friction or nonlinearity dominating the dynamics and where the physics of the model is no longer valid. Figure 5 shows that the distance over which the inflow turns northward (L_N) does not depend on the transport of the inflow, but it does depend both on the magnitude of the diffusion coefficient, and on the latitude

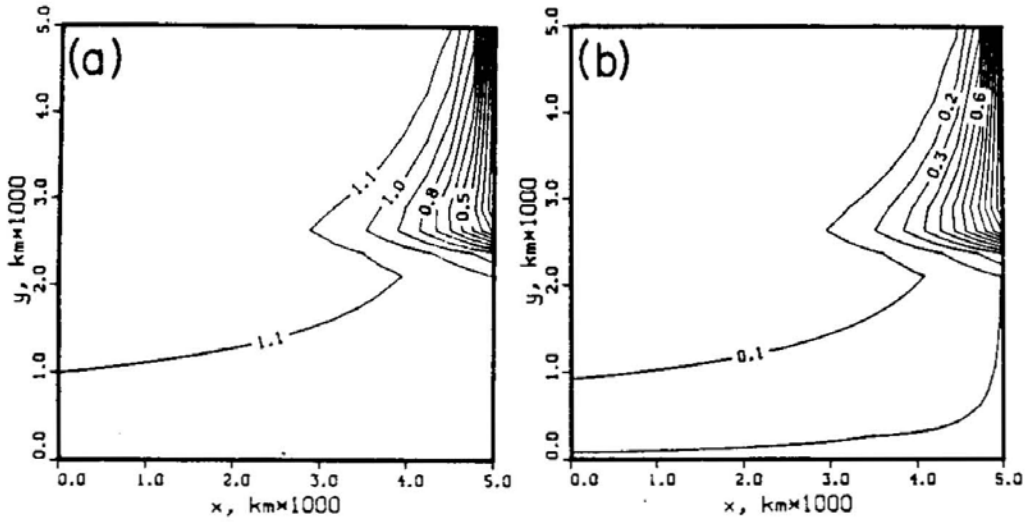

Figure 3: The solution for one moving layer: pressure in layer 0 (a), and $w_{0,top} - w_{0,bottom}$ (b).

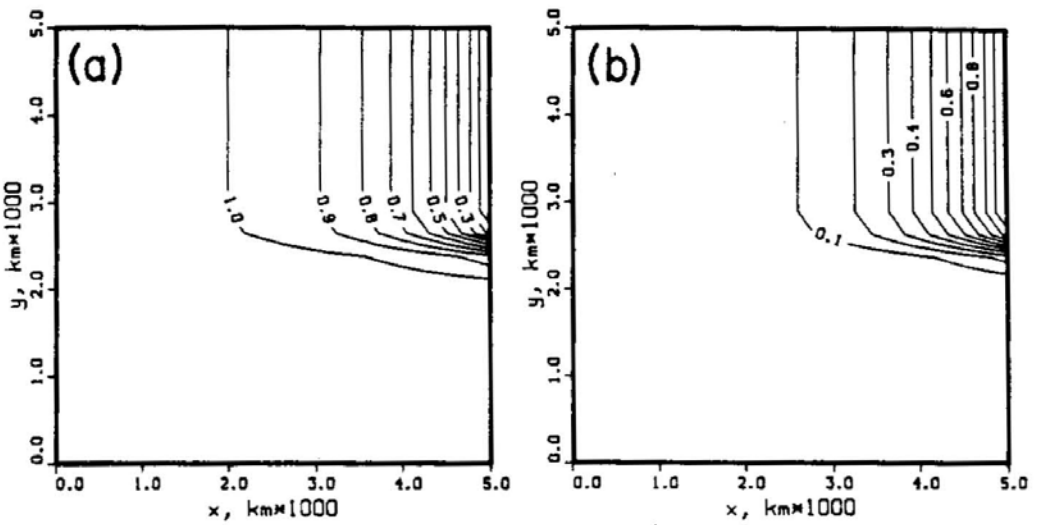

Figure 4: Same as figure 3, except that β–plane approximation is made. β is taken constant, and $f = f_0$ except when differentiated.

of the inflow. The physical processes that determine L_N are discussed below from two points of view.

(a) Linearized steady scaling: Let us define

$$\Delta w \equiv w_{0,top} - w_{0,bottom}|_{x_e, y \geq y_2} \tag{4.9}$$

we then have from the vorticity equation

$$V \equiv v(x_e, y, z) \approx \frac{f}{H_0 \beta} \Delta w \tag{4.10}$$

If L_N is the east–west distance over which the *total* transport of the inflow turns northward, then

$$M_{inflow} \approx L_N H_0 V. \tag{4.11}$$

Combining (4.10) and (4.11),

$$L_N = \frac{M_{inflow} \beta}{f \Delta w}. \tag{4.12}$$

Next, let us express Δw in terms of the diffusion parameter and the transport of the inflow. Using (2.5) we find

$$\Delta w = \lambda_v \left(\frac{\Delta_0 \rho / h_0 - \Delta_{-1} \rho / h_{-1}}{\rho_0 - \rho_{-1}} - \frac{\Delta_1 \rho / h_1 - \Delta_0 \rho / h_0}{\rho_1 - \rho_0} \right). \tag{4.13}$$

Assuming now that all the $\Delta_n \rho$ are equal, so that $\rho_{n+1} - \rho_n = \Delta_n \rho =$ constant, and linearizing (4.13) about the basic stratification

$$h_n(x, y) \equiv h_n(x_e, y_1) + \eta_n(x, y) = H_n + \eta_n(x, y), \qquad \eta_n \ll H_n,$$

we have

$$\Delta w \approx -\lambda_v \left(\frac{1}{H_{-1}} - \frac{2}{H_0} + \frac{1}{H_1} \right) + \lambda_v \left(\frac{\eta_{-1}}{H_{-1}^2} - \frac{2\eta_0}{H_0^2} + \frac{\eta_1}{H_1^2} \right) \tag{4.14}$$

The first term on the RHS is just $w_{0,top} - w_{0,bottom}$ at (x_e, y_1), and figure 3 shows that this can be taken as zero. This is equivalent to saying that the stratification south of

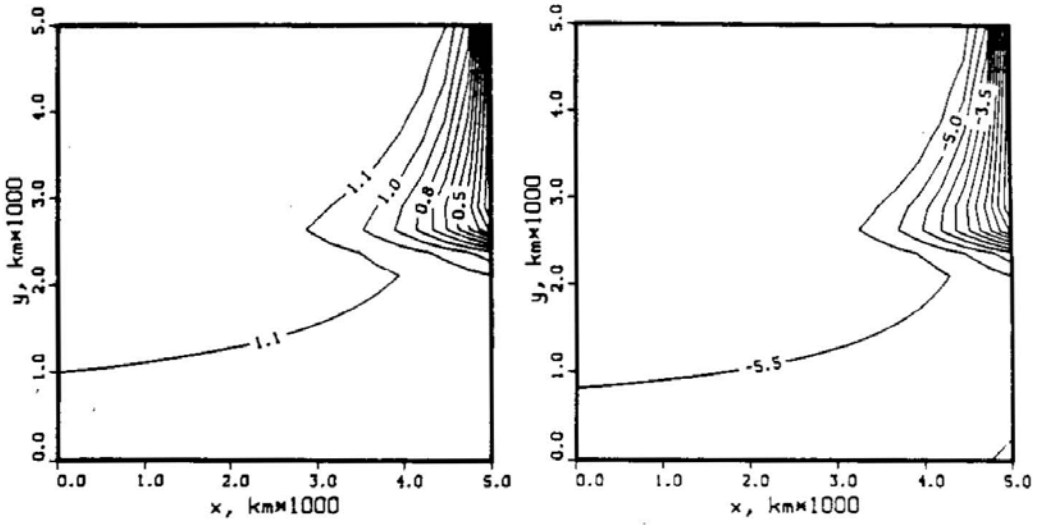

Figure 5: The dependence on the initial east–west extent of the inflow on different parameters: (a) on the inflow transport; solution is shown for M_{inflow}, $M_{inflow} \times 5$, $M_{inflow}/4$, where M_{inflow} is the value used for the solution of figure 3.

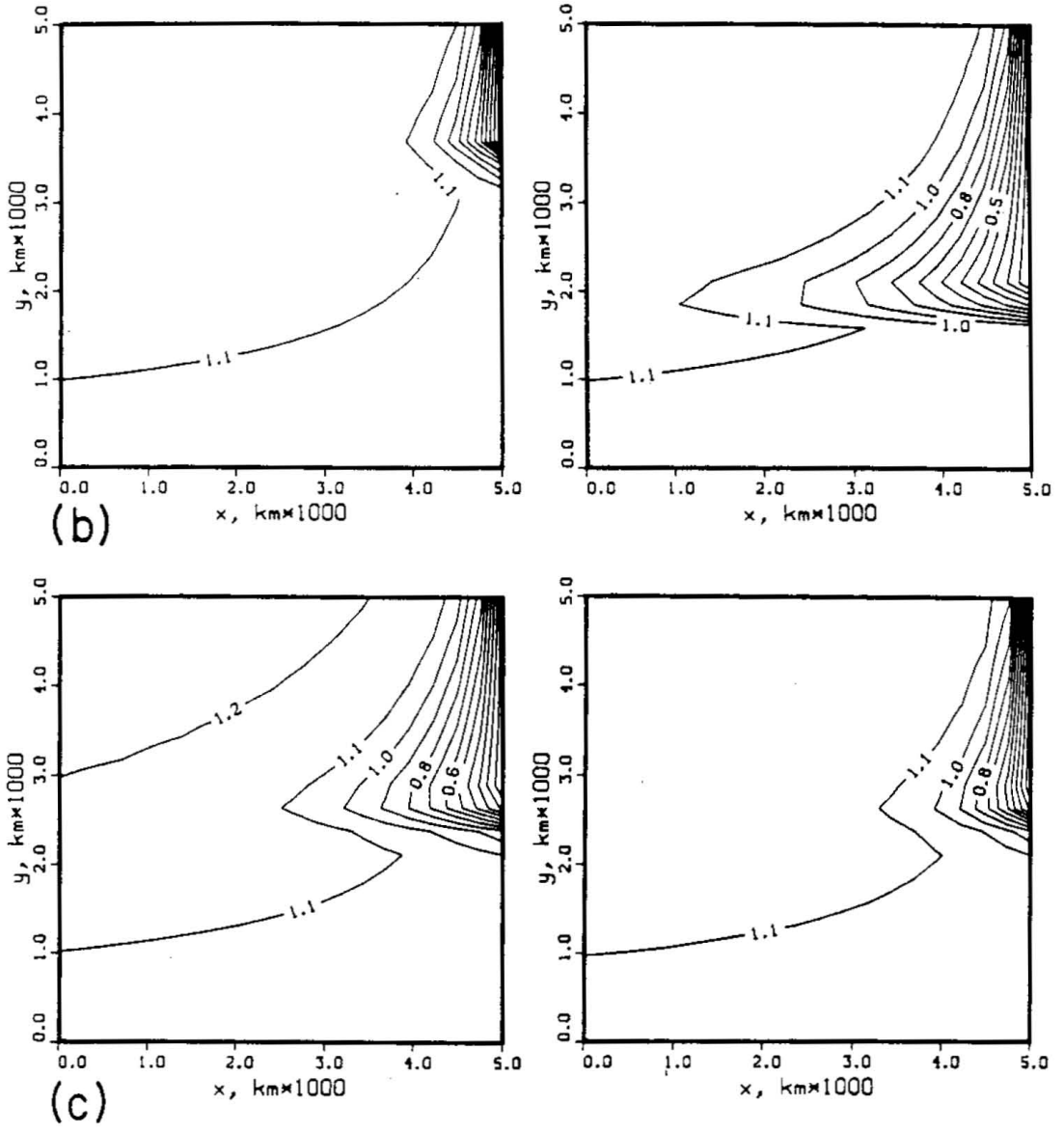

Figure 5: continued. (b) dependence on the latitude of the inflow. (c) on the vertical diffusivity coefficient. Left: $\lambda_\nu = 1.5$. Right: $\lambda_\nu = 0.75$.

the inflow is exponential, and $w(z)$ is constant there. The eastern boundary condition for h_n, (3.8), written in terms of the η_n is

$$\eta_1 = \frac{U_0 f_0}{\gamma_0}(y_2 - y_1) = \frac{M_{inflow} f_0}{\gamma_0 H_0}, \qquad \eta_0 = -2\eta_1, \qquad \eta_{-1} = -(\eta_0 + \eta_1) = \eta_1. \tag{4.15}$$

Using these η_n in (4.14), and substituting the resulting Δw in the expression (4.12) for L_N, we have

$$L_N = \frac{\beta}{\left[\frac{1}{H_0^2}\left(\frac{1}{H_{-1}^2} + \frac{4}{H_0^2} + \frac{1}{H_1^2}\right)\right]\left(f^2/\frac{\gamma_0}{H_0}\right)\lambda_v}. \tag{4.16}$$

Note that there is no dependency on the inflow transport, which can now be interpreted as follows. The larger is the transport, the larger is the deviation of the stratification north of the inflow from exponential profile. This deviation results (through the density equation) in increasing variation in w across the thickness of layer 0, therefore forcing a larger northward velocity (through the vorticity equation). Because the northward velocity increases with increasing transport of the inflow, the distance over which the total inflow is turned northward does not depend on the magnitude of the transport. The expression (4.16) also has the correct dependence on the latitude of the inflow and the diffusivity, as seen in figure 5.

(b) L_N from Rossby-wave argument: It is possible to derive an expression for L_N by considering a linearized time dependent problem. The argument is similar to that used to explain the existence of the western boundary current in terms of Rossby waves (Pedlosky, 1979). In the WBC case, the balance is between eastward propagation of short Rossby waves, and their dissipation (and trapping) by horizontal friction. Here we have westward propagating long Rossby waves, which are dissipated and trapped near the eastern boundary by the vertical density diffusion.

Consider a continuously stratified ocean, and linearize the equations of motion about a basic state of rest and a linear vertical density profile $\bar{\rho}(z)$. The linearized

equations for the small perturbations about the basic state are

$$\begin{aligned} fu &= -\frac{1}{\rho_0} p_y \\ fv &= \frac{1}{\rho_0} p_x \\ p_z &= -g\rho \\ \rho_t + w\bar{\rho}_z &= \lambda_v \rho_{zz} \\ u_x + v_y + w_z &= 0. \end{aligned} \tag{4.17}$$

From (4.17) we can derive a single equation for $\rho(x, y, z, t)$

$$\rho_{zzt} + \frac{-\beta}{f^2 / \left(\frac{g}{\rho_0}\bar{\rho}_z\right)} \rho_x = \lambda_v \rho_{zzzz}. \tag{4.18}$$

Substituting a wave solution

$$\rho = e^{ikx+imz-i\sigma t}, \tag{4.19}$$

we find the dispersion relation

$$\sigma = \frac{-\beta k}{m^2 \left(\frac{f^2}{N^2}\right)} - im^2\lambda_v. \tag{4.20}$$

The real part of σ is the frequency of a westward propagating long Rossby wave. The imaginary part is the decay due to the vertical diffusion. A wave generated at the eastern boundary will travel westward at a speed $C_{g,x} = -\beta / \left(m^2 \frac{f^2}{N^2}\right)$, with its amplitude decaying with the e–folding diffusion time

$$t_d = (m^2\lambda_v)^{-1}. \tag{4.21}$$

The distance such a wave travels westward is

$$L_N = |C_{g,x}| t_d = \frac{\beta}{m^4 (f^2/N^2)\lambda_v}. \tag{4.22}$$

This is basically the same expression for L_N derived in (4.16) using steady state scaling. We can now tell the significance of the expression with the H_n in (4.16), which is

replaced here by the factor m^4. It simply expresses the fact that an inflow of smaller vertical scale will have a smaller L_N because it will be dissipated faster by the vertical diffusion. We would like to note now that the relatively narrow northward flow in layer 0 implies a return southward flow near the eastern boundary in the layers above and below the inflow. This point will be discussed in detail in the following section, where the circulation in layers above and below the inflow is calculated by the model.

Having understood what determines the east–west width of the flow, L_N, we now need to make sure that it does not get too small, and violate the basic assumption of geostrophy. The Rossby and Ekman numbers based on the length scale L_N are

$$\begin{aligned} Ro &= \frac{\text{Nonlinear terms}}{\text{Coriolis acceleration}} = \frac{V^2/L_N}{fV} = \frac{V}{fL_N}, \\ E &= \frac{\text{Horizontal friction}}{\text{Coriolis acceleration}} = \frac{A_H V/L_N^2}{fV} = \frac{A_H}{fL_N^2}. \end{aligned} \tag{4.23}$$

For $L_N \approx 2000$km, $A_H = 10^7 \text{cm}^2/\text{sec}$, $y_2 - y_1 = 400$km, inflow velocity $U_0 = 0.2$cm/sec, and using the northward velocity scale

$$V \approx U_0 \frac{L_N}{y_2 - y_1}. \tag{4.24}$$

we find

$$Ro = 5 \times 10^{-5} \ll 1,$$

$$E = 3 \times 10^{-6} \ll 1,$$

so that the flow is in geostrophic balance to a good approximation. (For the linear vorticity equation to be valid, one also needs to make sure that $U/\beta L^2 \ll 1$, and this can be shown to hold for the above parameters.) It is also useful to express Ro and E in terms of the external parameters and forcing. This enables one to see what range of diffusion coefficient or inflow velocity are consistent with the model assumptions. Substituting L_N from (4.22) into (4.23), we have

$$\begin{aligned} Ro|_{y_2} &= \frac{V}{fL_N} = \frac{U_0}{f(y_2 - y_1)} \\ E|_{y_2} &= \frac{f_0^3 A_H \lambda_V^2 m^8}{\beta_0^2 N^4}. \end{aligned} \tag{4.25}$$

The subscript 0 refers to values of parameters at the inflow region. These two nondimensional numbers are based on the velocity and the width of the flow just after it turns northward, at $y = y_2$. North of that point, V increases like f/β, and the width of the flow decreases as β/f. The Rossby and Ekman numbers are then

$$\begin{aligned} Ro|_{y \geq y_2} &= Ro|_{y=y_2} \left(\frac{\beta/f}{\beta_0/f_0} \right)^2 \\ E|_{y \geq y_2} &= E|_{y=y_2} \left(\frac{\beta/f}{\beta_0/f_0} \right)^2 . \end{aligned} \tag{4.26}$$

From (4.25) and (4.26) we see that the *horizontal* friction may become dominant ($E \approx 1$) when the *vertical* diffusion is large enough to decrease the width of the flow significantly. The dependence on $(\beta/f)^2$ in (4.26) may make the nonlinear and frictional terms large for points far enough to the north, where the flow becomes narrow, as seen in figure 3.

It is instructive now to compare the diffusive solution found above to the ideal fluid case examined in section 3. The circulation is obviously different, due to the meridional flow forced by the vertical diffusion, as opposed to the purely zonal flow in the ideal fluid case. Another difference, perhaps more fundamental, is in the number of boundary conditions that may be applied, and the amount of information that can be extracted from the model as part of the solution. The addition of vertical diffusion to the dynamics enables one to add boundary conditions on the upwelling across the layer interfaces, and in return to calculate the average vertical stratification, as represented by the H_n. Note that we *cannot* specify the upwelling *locally*, but only in an integral sense, by specifying the total upwelling across a given interface. The local variations in the cross–interfacial velocity are determined by the model itself.

Let us examine now the limit $\lambda_v \to 0$. As λ_v becomea smaller, the interior is not diffusive enough to support the specified amount of cross–interfacial flux, and as a result the integral constraints (4.5) and (4.6) cannot be satisfied by physically reasonable

values of the H_n. To see how this happens, let us ignore for a moment the horizontal variations in the density stratification. In the continuous case, with $w(z)$ =constant, the solution to $w\rho_z = \lambda_v \rho_{zz}$ is $\rho(z) = \exp(wz/\lambda_v)$. The depth scale of the stratification is $D = \lambda_v/w$. In the layer formulation, the above density equation is replaced by (2.5). Assuming again a horizontally uniform stratification, we can write (2.5) in terms of H_n, the stratification on the eastern boundary

$$w_n \sim \lambda_v \frac{\Delta_{n+1}\rho/H_{n+1} - \Delta_n\rho/H_n}{\rho_{n+1} - \rho_n}.$$

Let now $|\Delta_{n+1}\rho| = |\Delta_n\rho| = |\rho_{n+1} - \rho_n|$ (note that $\Delta_n\rho < 0$ by definition, see chapter 1, section 4a), and consider the vertical velocity across the interface between layers 0 and 1

$$w_0 \sim \lambda_v \left(\frac{1}{H_0} - \frac{1}{H_1}\right)$$

or

$$H_1 \sim \left(\frac{1}{H_0} - \frac{w_0}{\lambda_v}\right)^{-1}.$$

As we let λ_v vanish, H_1 becomes larger. (A similar argument shows that $H_{-1} \to 0$ as $\lambda_v \to 0$.) In the limit when $D^{-1} = w_0/\lambda_v \to 1/H_0$, we find that $H_1 \to \infty$, so that when the depth scale of the density field is smaller than the specified thickness of layer 0, the layer formulation breaks down because the layers cannot resolve the vertical density profile.

For the parameter range examined here, this happens for $\lambda_v \leq 0.5\text{cm}^2/\text{sec}$. But even without the above problem with the H_n, resulting from the limitation of the layer formulation, it is clear that as $\lambda_v \to 0$, the stratification becomes non realistic. One must then specify the eastern boundary stratification, and drop the additional boundary conditions (4.5), (4.6). Then, with the H_n fixed and specified, as λ_v gets even smaller, the circulation reduces to a zonal flow, as shown in figure 6. One assumes that mixing in the western boundary current takes care of the integral constraints on

the total mass in each layer, by allowing large enough cross interfacial fluxes there. It is also possible that the inflow leaves layer 0 across the basin boundaries (e.g. across the equator).

There are several conclusions of a more general character concerning diffusion–driven flows which may be drawn from this model. It has already been emphasized above that finding the basic vertical stratification is a necessary part of the solution when diffusion is included in the physics. Arbitrarily specifying the basic stratification in a diffusive model will result in the wrong circulation as well as incorrect total upwelling across interfaces. Clearly, because the vertical velocity (and therefore the horizontal velocity) depends on the stratification through the density equation, one must know the correct stratification to calculate the correct velocity field.

Another conclusion concerns the modeling of cross–isopycnal velocity in interior buoyancy driven flows. The distribution of the cross isopycnal velocity in models of buoyancy driven flows is often specified and the resulting horizontal circulation is then examined. Although this approach simplifies matters, it is not complete nor physically correct. Figures 3b and 4b show that when the vertical velocity is allowed to be determined by the model, its distribution is shaped by *and* influences the horizontal circulation. For a consistent picture of the interior circulation, the cross–isopycnal velocity must be balanced by some mixing (diffusion). Any parameterization of mixing in terms of average stratification links the cross–isopycnal velocity to the stratification, and necessarily couples the horizontal and vertical velocity fields, as demonstrated by the model examined above.

Note especially the difference between the results here, and in a Stommel-Arons type model, where the mass source at the eastern boundary is balanced by a uniform upwelling. With $\Delta w = w_{0,top} - w_{0,bottom}$ assumed uniform in (x, y), one expects the inflow to shoot to the western boundary, and then flow as a broad, basin scale,

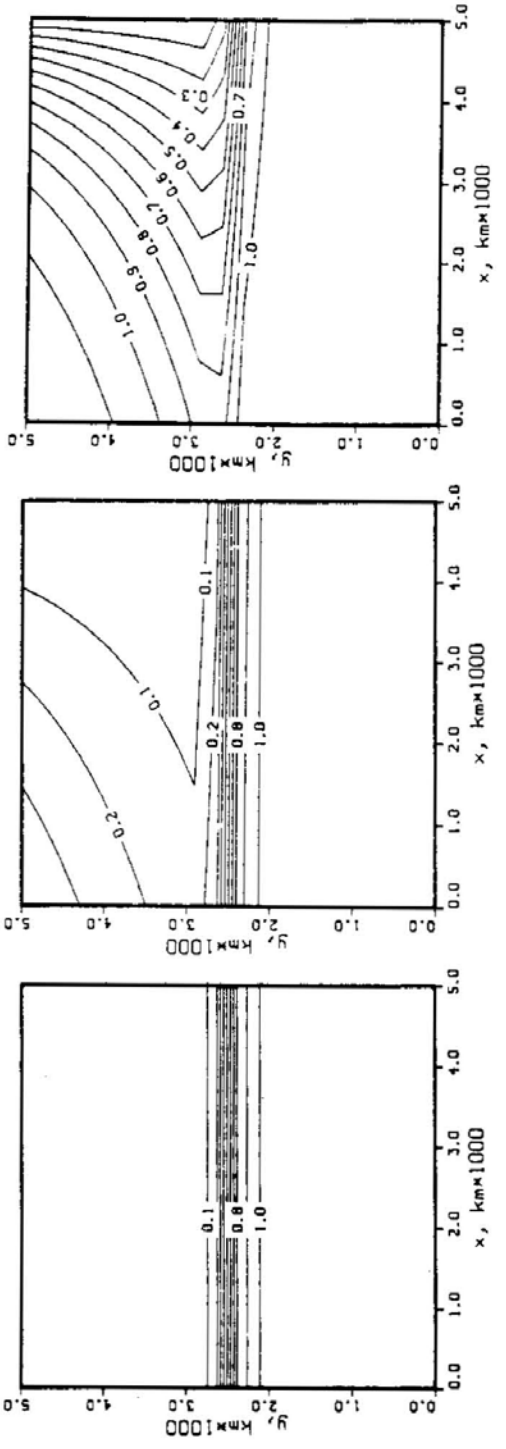

Figure 6: The solution for the pressure in layer 0 as the diffusivity λ_v becomes small. solutions are shown for $\lambda_v = 0.2,\ 0.02,\ 0.0002\text{cm}^2/\text{sec}$.

northward circulation governed by $\beta v h_0 = f \Delta w$. But the above model shows that if the interior diffusion is large enough to support upwelling that balances the inflow:

$$\iint_{entire\ basin} w_{0,top} - w_{0,bottom} dx\, dy = M_{inflow},$$

then it is also strong enough to turn the entire inflow northward before it reaches the western boundary. The relation to models with uniform upwelling is further discussed in the end of section 5, in connection with the calculation of the circulation in layers $-1, 1$.

Finally, the model lets us examine the behavior of potential vorticity in diffusive flows. Potential vorticity ($f\rho_z$ or $f/h_n(x,y)$ for the dynamics used here) has proved to be a useful diagnostic tool for distinguishing between different possible physical processes driving large–scale flows [Luyten et al. (1983), Rhines and Young (1982)]. In the present model the thickness of the layers, $h_n(x,y)$ is determined solely by the diffusive flow. This gives us an opportunity to compare iso-lines of potential vorticity and geostrophic pressure in a purely diffusive flow. [Such a comparison would not be meaningful in the model of section (1.4), where the wind driven circulation determined the horizontal structure of h_n, and the diffusion set only the basic vertical stratification.] Figure 7 shows the potential vorticity and "perturbation" potential vorticity ($f/h_n - f/H_n$), for the moving 0th layer. Potential vorticity contours follow latitude circles closely, and are very different from the stream lines of horizontal velocity (figure 3a). This is what one expects to find for a very diffusive flow, as in the present model. The "perturbation" potential vorticity, on the other hand, does resemble the pressure contours to some extent.

Another way to characterize diffusive and ideal flows is to examine the relation between the potential vorticity, q, density, ρ, and the Bernoulli function, B. For ideal fluid one has $B = B(q,\rho)$ (Welander, 1971), so that a scatter plot of B and q on a density surface should indicate a clear functional relation between them. In a layer

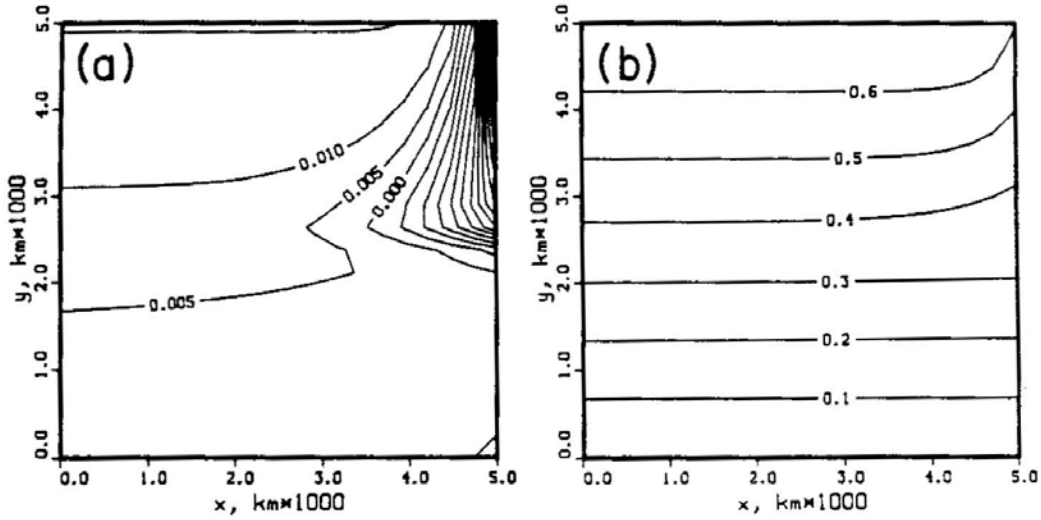

Figure 7: Potential vorticity f/h_n (b) and perturbation potential vorticity $\frac{f}{h_n} - \frac{f}{H_n}$ (a) for the one moving layer case.

model the Bernoulli function for the nth layer is $B_n = p_n + gz\rho_n$ and is independent of z within each layer. Figures 8a,b show scatter plots of B_n vs. $q_n = f/h_n$ for layer 0 in the ideal and diffusive solutions presented in sections 3 and 4. There is a well defined B_n–q_n relation is the ideal case, but as expected, not for the diffusive case.

5. The diffusive case: three moving layers

In the previous section we assumed that the layers above and below the inflow are at rest, and solved for the circulation in layer 0. We now allow for motion in layers -1, 0 and 1, and assume that all other layers are at rest. The physical problem remains the same, (see figure 1) and the solution in this section may be viewed as a better approximation to the full untruncated problem, than that in the previous section.

In return for having to deal with a somewhat more complicated algebra, we hope to achieve several goals. By comparing the circulation in layer 0 in this section and in the previous one, we will try to justify the truncation of the problem to a (small) finite number of moving layers. We will also see how the injection of water into layer 0 affects the circulation above and below it. The problem is very similar to the one considered in section 4, so we only briefly derive the solution.

The equations of motion are given by (2.1), and we use the vertical diffusion equation (2.5). The horizontal velocities (u_n, v_n) are assumed to vanish for $|n| \geq 2$. Using (3.1) we find

$$\nabla_H z_n(x,y) = 0, \qquad n \neq -2,-1,0,1 \tag{5.1}$$

so that only layers $-2,-1,0,1$ and 2 have varying thickness, which we need to solve

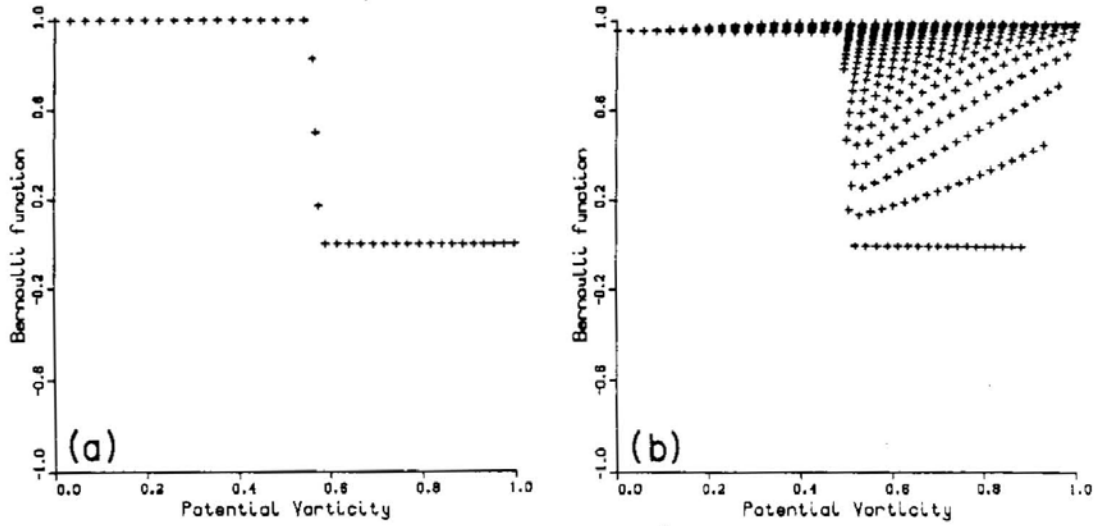

Figure 8: Scatter plot of Bernoulli function vs. potential vorticity (a) for the ideal case of section 3, (b) for the diffusive solution of figure 3.

for. From (3.1) we also find

$$\begin{aligned}
\frac{1}{\rho_0}\nabla_H p_{-2} = 0 = &-\gamma_{-2}\nabla_H(h_2+h_1+h_0+h_{-1}) - \gamma_{-1}\nabla_H(h_2+h_1+h_0) \\
&- \gamma_0\nabla_H(h_2+h_1) - \gamma_1\nabla_H h_2 \\
\frac{1}{\rho_0}\nabla_H p_{-1} = &-\gamma_{-2}\nabla_H h_{-2} \\
\frac{1}{\rho_0}\nabla_H p_0 = &-\gamma_1\nabla_H h_2 - \gamma_0\nabla_H(h_2+h_1) \\
\frac{1}{\rho_0}\nabla_H p_1 = &-\gamma_1\nabla_H h_2
\end{aligned} \tag{5.2}$$

The vorticity equation for the moving layers is

$$\beta v_n(x,y)h_n(x,y) = f\left[w_{n-1}(x,y) - w_n(x,y)\right] \qquad n = -1,0,1 \tag{5.3}$$

Using (2.1) and (5.2) we can write (5.3) as

$$\frac{\partial h_2}{\partial x} = -\frac{f^2}{\beta\gamma_1}(w_0 - w_1)\frac{1}{h_1} \tag{5.4.a}$$

$$\frac{\partial h_1}{\partial x} = -\frac{f^2}{\beta\gamma_0}(w_{-1} - w_0)\frac{1}{h_0} - \left(\frac{\gamma_1}{\gamma_0}+1\right)\frac{\partial h_2}{\partial x} \tag{5.4.b}$$

$$\frac{\partial h_{-2}}{\partial x} = -\frac{f^2}{\beta\gamma_{-2}}(w_{-2} - w_{-1})\frac{1}{h_{-1}} \tag{5.4.c}$$

The vertical velocities can be written in terms of the h_n using the density equation (2.5). Two more equations can be derived from (5.1) and (5.2a),

$$\begin{aligned}
p_{-2} = &-\gamma_{-2}(h_2+h_1+h_0+h_{-1}) - \gamma_{-1}(h_2+h_1+h_0) \\
&- \gamma_0(h_2+h_1) - \gamma_1 h_2 = \text{constant} \\
= &-\gamma_{-2}(H_2+H_1+H_0+H_{-1}) - \gamma_{-1}(H_2+H_1+H_0) \\
&- \gamma_0(H_2+H_1) - \gamma_1 H_2,
\end{aligned} \tag{5.4.d}$$

$$\sum_{n=-2}^{2} h_n(x,y) = \text{constant} = H_{-2}+H_{-1}+H_0+H_1+H_2. \tag{5.4.e}$$

Using (5.4.d,e) to express $h_0(x,y)$ and $h_{-1}(x,y)$ in terms of h_{-2}, h_1, h_2 and the H_n, and substituting them into (5.4.a,c), we have three coupled first order ODE's for h_{-2},

h_1 and h_2. These equations can be integrated from the eastern boundary, where the h_n are given by the boundary condition (3.8), with the two additional conditions

$$h_n(x_e, y) = H_n \qquad n = 2, -2 \tag{5.5}$$

where, as before

$$H_n \equiv h_n(x_e, y_1).$$

To complete the solution, we need to find the four stratification parameters H_{-2}, H_{-1}, H_1 and H_2, by applying the constraints on the cross-interfacial velocities (H_0 is specified as in the previous section). With only layers -1, 0 and 1 moving, we need to find the vertical velocities only at the interfaces of these layers. This gives us four constraints:

$$\iint w_n(x, y)\, dxdy = \begin{cases} M_{bottom} & n = -1, 0; \\ M_{bottom} + M_{inflow} & n = 1, 2. \end{cases} \tag{5.6}$$

The fifth equation for the H_n is given by specifying the transport of the inflow, as in (4.7).

Results

Figure 9 shows the pressure in layers $-1, 0, +1$. Note that although we did not require so *a priori* the circulation in layers $-1, 1$ is weaker than that of layer 0, as was assumed in the preceding section. This justifies (or at least is consistent with) the truncation of the model to a finite number of moving layers, in order to get an approximate solution for the circulation in the layers assumed moving. In the full problem, however, the vertical extent of the circulation must be determined by the dynamics.

The circulation in layer 0 has the same characteristics as in the more truncated model of section 4. The main difference between the results of the two models, as seen in figures 3a and 9a, is the westward distance L_N traveled by the inflow before

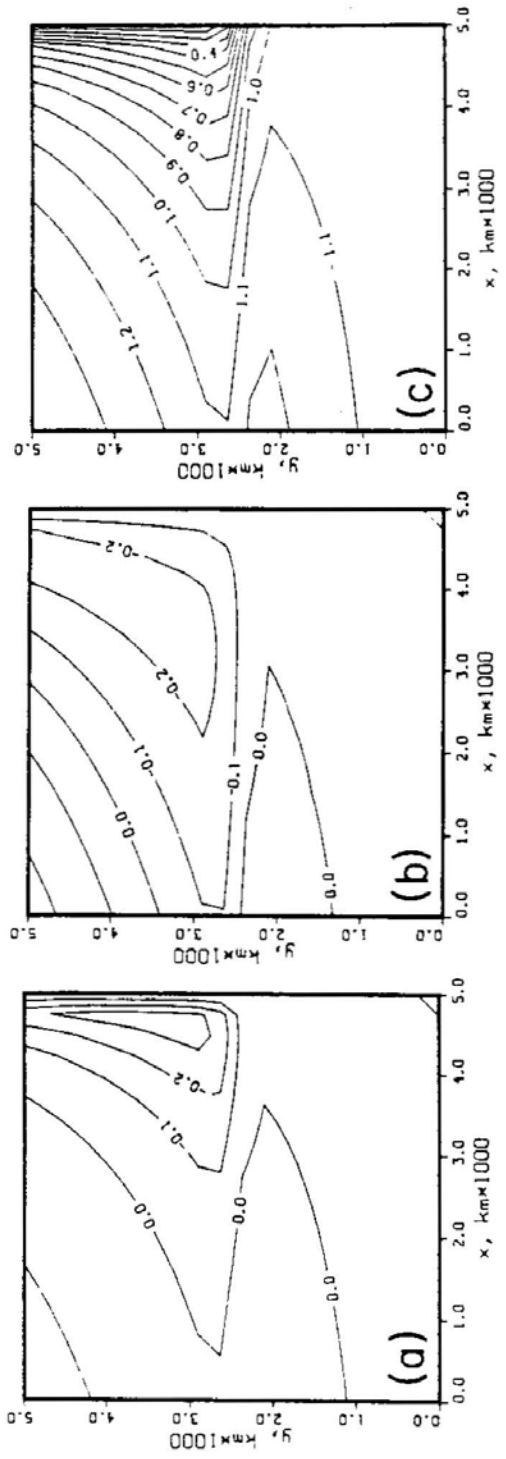

Figure 9: Pressure in layers $1, -1, 0$ (from left to right) for the three moving layer solution of section 5.

it turns northward. This difference can be explained by expression (4.22) for L_N, as derived from the Rossby wave argument. We have seen that the distance traveled by a westward going Rossby wave, before it is dissipated by the vertical mixing depends on the vertical wave number (m) of the wave. Waves of higher vertical wave number are dissipated faster and reach a shorter distance westward. The truncation to one moving layer in section 4 is equivalent, in a sense, to limiting the scales to high wave numbers. We should expect, therefore, to find a smaller L_N in the more truncated problem.

To understand the circulation found for the layers above and below the inflow, we need to consider the vertically integrated circulation forced by the inflow. We have assumed that far above and below layer 0 the vertical velocity is uniform in (x, y), and the horizontal circulation vanishes. The vertical velocity at layers far enough above the inflow is therefore

$$w_{\text{top}} = (M_{bottom} + M_{inflow})/\text{area} = \text{constant},$$

and far below the inflow

$$w_{\text{bottom}} = M_{bottom}/\text{area} = \text{constant}.$$

Integrating the vorticity equation over all the layers in between, we find the total northward transport forced by the inflow

$$\beta \sum v_n h_n = f(w_{\text{top}} - w_{\text{bottom}}) = f M_{inflow}.$$

The transport stream function for this flow is shown in figure 10a. Comparing figure 10a and the circulation in layer 0 (figure 9a), we see that the vertically integrated circulation (figure 10a) does not turn northward near the eastern boundary as found for layer 0. Instead, most of the inflow flows westward to the western boundary current region, and then returns to the interior and flows northward, filling the basin width as in the Stommel–Arons model.

The difference between the vertically integrated signal and the circulation in layer 0 means that somewhere above and below the inflow there must be a southward circulation near the eastern boundary, canceling the signal of the narrow northward flow in layer 0. Examining now the solution for layers $+1, -1$ (figure 9), we see that there is such a return flow in both layers near the eastern boundary. Figure 10b shows the transport stream function for the three layers together, and one can see how the transport in layers $+1, -1$ modifies that of layer 0, so that the total horizontal circulation in the three layers is very close to that of figure 10a. The small differences between figures 10a,b are taken care of by the weak circulation ignored by the present model in layers above layer -1 and below layer $+1$.

6. Effects of horizontal advection and diffusion

So far we have ignored the horizontal advection and diffusion terms in the density equation, based on the assumption that isopycnal surfaces are nearly horizontal ($\epsilon = \Delta_H \rho / \Delta_V \rho \ll 1$). In this section the conditions for these terms to be small are derived by expressing ϵ in terms of the forcing parameters. Then the effects of the horizontal advection and diffusion are incorporated into the model using a perturbation expansion in powers of ϵ.

The scale for the horizontal variation in density, $\Delta_H \rho$, may be taken to be equal to the variation of the density across the inflow on the eastern boundary. The thermal wind relation in the inflow region, $f u_z = (g/\rho_0)\rho_y$, gives the scaling relation

$$\frac{f U_0}{H_0} = \frac{g \Delta_H \rho}{\rho_0 (y_2 - y_1)},$$

or

$$\Delta_H \rho = \frac{[U_0 (y_2 - y_1) H_0] \ \rho_0 f}{g H_0^2} = M_{inflow} \frac{\rho_0 f}{g H_0^2}. \tag{6.1}$$

This gives

$$\epsilon = \frac{\rho_0 f_0 M_{inflow}}{H_0^2 g \Delta_V \rho}, \tag{6.2}$$

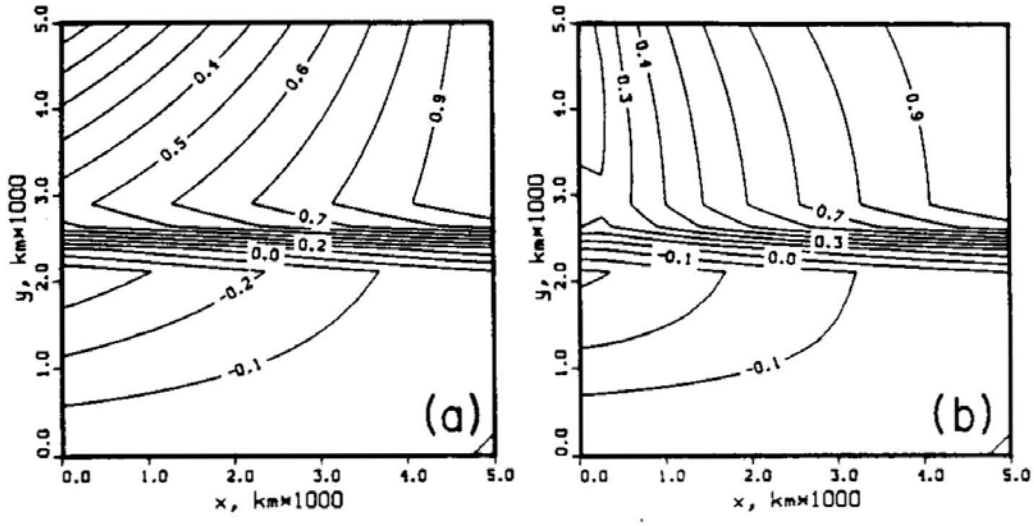

Figure 10: comparing the vertically integrated circulation forced by the inflow (a) and the combined transport of layers $-1, 0, 1$ calculated by the three layers model (b). See text.

where $\Delta_v \rho = \Delta_0 \rho$ is the density range represented by layer 0. As long as the transport of the inflow, M_{inflow}, is relatively weak, ϵ is small and the density equation is (2.3) to a good approximation. With the parameters used to obtain the solution in figure 3

$$\begin{aligned} &\rho_0 = 1, \qquad f_0 = f(\frac{y_1 + y_2}{2}) = 7 \times 10^{-5}\text{sec}^{-1}, \qquad H_0 = 350m \\ &M_{inflow} = 0.3\text{Sv}, \qquad \Delta_v \rho = 0.0002\text{gr/cm}^3, \end{aligned} \tag{6.3}$$

we find $\epsilon \approx 6 \times 10^{-2} \ll 1$.

Although small, the $O(\epsilon)$ deviations from the vertical density equation (2.3) will affect the solutions for the thickness and circulation derived above. For $\epsilon \ll 1$, it is possible to calculate the corrections due to horizontal advection and diffusion by expanding all variables in powers of ϵ

$$\begin{aligned} u_n &= u_n^{(0)} + \epsilon u_n^{(1)} + O(\epsilon^2) \\ h_n &= h_n^{(0)} + \epsilon d_n + O(\epsilon^2). \end{aligned} \tag{6.4}$$

But before writing the $O(1)$ and $O(\epsilon)$ equations and going through the details of the solution, we need to consider carefully the boundary conditions to be applied at each order. To lowest order, the problem is equivalent to that discussed in sections 4 and 5, with $w\rho_z = \lambda_v \rho_{zz}$ as the density equation. We already know that as part of the thermal boundary conditions for that problem one needs to make sure that the total mass in each of the layers remains constant in spite of cross interfacial mass fluxes, and injection from the eastern boundary. The requirement of constant total mass is satisfied, as we have seen, by using the integral constraints (4.5,4.6) or (5.6) to calculate the eastern boundary stratification. With no horizontal diffusion of heat, the condition of constant total amount of *heat* in each layer is automatically satisfied by the constraints on the total *mass*. This equivalence between heat and mass is due to the fact that heat can enter the system only where mass can — through injection from the eastern boundary, or through vertical advection/diffusion across interfaces. When horizontal diffusion is present, however, heat may diffuse from side boundaries even where the condition of

no normal mass flux is satisfied by the velocity field. As a result, when adding the $O(\epsilon)$ horizontal advection and diffusion, one is forced to modify the $O(1)$ solution so that there is no heat flux from side boundaries. This requires boundary layers of width $\propto \epsilon$, in which the isopycnals approach the boundary in a 90° angle. These boundary layers should not affect the $O(1)$ interior stratification which is determined by the constraints on the total mass in each layer.

To summarize, adding the weak $O(\epsilon)$ horizontal diffusion we expect $O(\epsilon)$ modifications to the interior density and velocity fields, and perhaps an $O(1)$ modification to these fields in narrow boundary layers near horizontal boundaries. Adding the numerically small horizontal diffusive effects may also cause an $O(1)$ change to *interior* fields in some cases, but we will postpone discussing this till later.

Consider now the problem of 3 moving layers, as discussed in section 5, but with the full density equation (2.2) instead of the vertical one (2.3). Substituting the perturbation expansion in equations (2.1, 2.2) the $O(1)$ equations are

$$\begin{aligned} f u_n^{(0)} &= -\frac{1}{\rho_0} p_{ny}^{(0)} \\ f v_n^{(0)} &= \frac{1}{\rho_0} p_{nx}^{(0)} \\ p_{nz}^{(0)} &= -g\rho_n \\ u_{nx}^{(0)} + v_{ny}^{(0)} + w_{nz}^{(0)} &= 0. \\ w^{(0)} \rho_z^{(0)} &= \lambda_v \rho_{zz}^{(0)} \end{aligned} \tag{6.5}$$

These are the equations used in section 5, and we can proceed and calculate the $O(1)$ thickness fields in terms of the H_n, and then to calculate the H_n by applying the constraints (5.6). In this section we are interested in the corrections due to horizontal

advection and diffusion, and for these we need to consider the $O(\epsilon)$ equations

$$\begin{aligned}
f u_n^{(1)} &= -\frac{1}{\rho_0} p_{ny}^{(1)} \\
f v_n^{(1)} &= \frac{1}{\rho_0} p_{nx}^{(1)} \\
p_{nz}^{(1)} &= -g\rho_n \\
u_{nx}^{(1)} &+ v_{ny}^{(1)} + w_{nz}^{(1)} = 0. \\
w^{(1)} &= \lambda_V \left(\frac{\rho_{zz}}{\rho_z}\right)^{(1)} + \left[-u^{(0)}\rho_x^{(0)} - v^{(0)}\rho_y^{(0)} + \lambda_H \nabla_H{}^2 \rho^{(0)}\right] \frac{1}{\rho_z^{(0)}}
\end{aligned} \tag{6.6}$$

We now want to derive an equation for the $O(\epsilon)$ thickness corrections, d_n, and we start with the $O(\epsilon)$ vorticity equation, derived from (5.3) and (6.4)

$$\beta \left[v_n^{(0)} d_n + v_n^{(1)} h_n^{(0)}\right] = f \left[w_{n-1}^{(1)}(x,y) - w_n^{(1)}(x,y)\right]. \tag{6.7}$$

In density coordinates, $w^{(1)}$ from (6.6) can be written as

$$\begin{aligned}
w^{(1)} = \lambda_V &\left[\frac{\partial}{\partial\rho}\frac{1}{z_\rho}\right]^{(1)} + u^{(0)} z_x^{(0)} + v^{(0)} z_y^{(0)} \\
&+ \lambda_H \left[z_{xx}^{(0)} + z_{yy}^{(0)} + \frac{\partial}{\partial\rho}\frac{(z_x^{(0)})^2 + (z_y^{(0)})^2}{z_\rho^{(0)}}\right],
\end{aligned} \tag{6.8}$$

which can then be written in discrete layer form

$$\begin{aligned}
w_n^{(1)} = \lambda_V (\rho_{n+1} - \rho_n)^{-1} &\left[\frac{\Delta_{n+1}\rho}{h_{n+1}^{(0)} + \epsilon d_{n+1}} - \frac{\Delta_n \rho}{h_n^{(0)} + \epsilon d_n}\right]^{(1)} \\
&+ u_n^{(0)} z_{n,x}^{(0)} + v_n^{(0)} z_{n,y}^{(0)} + \lambda_H Z_n(z_{n,xx}^{(0)}, z_{n,yy}^{(0)}, \ldots)
\end{aligned} \tag{6.9}$$

$w_n^{(1)}$ is the $O(\epsilon)$ correction to the vertical velocity across the interface between the $n, n+1$ layers, and $z_n^{(0)}$ is the $O(1)$ height of this interface. The term Z_n includes all the horizontal diffusion terms. Expanding the first term on the rhs of the last equation we have

$$\begin{aligned}
w_n^{(1)} = \lambda_V (\rho_{n+1} - \rho_n)^{-1} &\left[\frac{-\Delta_{n+1}\rho}{[h_{n+1}^{(0)}]^2} d_{n+1} - \frac{-\Delta_n \rho}{[h_n^{(0)}]^2} d_n\right] \\
&+ u_n^{(0)} z_{n,x}^{(0)} + v_n^{(0)} z_{n,y}^{(0)} + \lambda_H Z_n(z_{n,xx}^{(0)}, z_{n,yy}^{(0)}, \ldots)
\end{aligned} \tag{6.10}$$

To obtain an equation for the d_n from (6.7), we still need to express the $O(\epsilon)$ velocity $v_n^{(1)}$ in terms of d_n. The hydrostatic equation applies to the $O(\epsilon)$ fields, and, by assumption, the horizontal pressure gradients vanish for layers other than $+1, 0, -1$. We can therefore express the $O(\epsilon)$ pressure in terms of the $O(\epsilon)$ thicknesses d_n, as in (5.2), with d_n replacing h_n, and $p^{(1)}$ replacing p_n. Such a relation can be used together with the geostrophic equations (6.6) to express $v_n^{(1)}$ in terms of $\partial d_n/\partial x$. Substituting (6.10) and $v_n^{(1)}$ into (6.7) one gets a coupled set of first order differential equations for the d_n, in the form

$$\frac{\partial}{\partial x} d_n(x,y) = \mathcal{F}_n(h_m, d_m). \tag{6.11}$$

These equations can now be integrated from the eastern boundary to give the corrections to the layer thickness everywhere. At the eastern boundary $d_n(x_e, y) = 0$ because the total thickness there, $h_n + \epsilon d_n$ is given by the boundary condition (3.8), and is satisfied by the $O(1)$ thickens h_n.

As was mentioned before, the perturbation expansion may break down under certain circumstances. Before examining specific solutions to (6.11), let us see when is the expansion valid. Because we did not include any physics capable of smoothing the lowest order solution, the $O(1)$ thickness of the layers may, in principle, have discontinuous (x, y) derivatives. Looking at (6.10) we see that the horizontal diffusion term $\lambda_H \mathcal{Z}_n(z^{(0)}_{n,xx}, z^{(0)}_{n,yy}, ...)$ in the $O(\epsilon)$ vertical velocity may become infinite at points where $z^{(0)}_{n,x}$ $z^{(0)}_{n,y}$ are discontinuous. To avoid this problem, and the complications resulting from the $O(\epsilon)$ boundary layers near horizontal boundaries mentioned before, we simply assume that the horizontal diffusion is very weak even compared with the horizontal advection, and we solve for the second order effects due to the horizontal advection only.

Figure 11 shows the solution to (6.11) for $\lambda_H = 0$, with the rest of the parameters as in the $O(1)$ solution of section 5. The effect of the $O(\epsilon)$ horizontal advection in the density equation is to move the stream lines in the direction of the $O(1)$ flow. In

regions of westward $O(1)$ flow the total $O(1) + O(\epsilon)$ flow extends further westward. North of this region, where the $O(1)$ flow is in the northeast direction, stream lines of the $O(1) + O(\epsilon)$ circulation are pushed eastward. The results can be interpreted in terms of Rossby waves, extending the arguments of section 4 to include the effects of advection on the propagation of the waves. Here the waves are advected by the flow, in addition to propagating westward, so that they reach points more or less further westward, depending on the direction of the advecting flow, before being dissipated by the vertical diffusion.

7. Relation to observations.

a. *The Mediterranean outflow:* The most obvious feature of the solutions presented in the previous sections is the turning northward of the flow entering from the eastern boundary (figures 3,9). Arhan (1986) presented and analyzed observations indicating that the Mediterranean outflow turns northward after entering the eastern North Atlantic. In particular, he showed dynamic height maps at the depth of the Mediterranean outflow from Maillard (1986), and salinity maps from Käse, Zenk and Armi (1986), all indicating that the Mediterranean outflow turns northward before getting to about 30° west. His analysis seems to show a northward flow of the upper Mediterranean water, and a south-west flow of the lower Mediterranean water. He tries to explain both these features by cross–isopycnal velocities resulting from double diffusive mixing activity in the Mediterranean tongue region. The resemblance of the above observations and present model results is appealing, but one needs to carefully examine the sensitivity to the model's assumptions before inferring that the dynamics used in the model applies to the Mediterranean outflow.

An important assumption made here is that all the mass entering some density range (layer) from the eastern boundary, must leave this density range through interior cross–isopycnal velocities. This assumption is the basis for the application of the

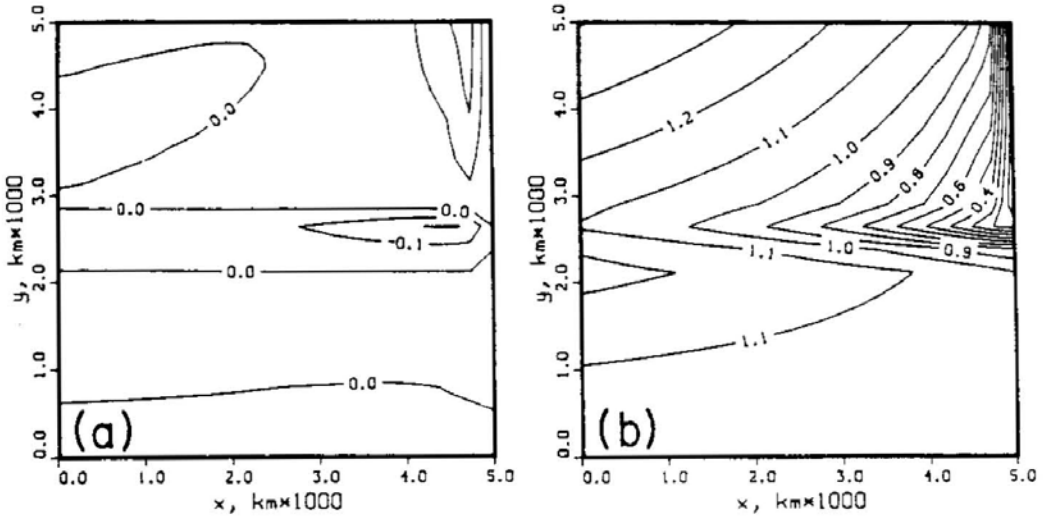

Figure 11: Effects of horizontal advection terms in the density equation: (a) $O(\epsilon)$ and (b) $O(1) + O(\epsilon)$ pressure from the solution of section 6. The $O(1)$ solution is as in figure 9.

integral constraint (4.5, 4.6) of constant total mass of given density. There are two possible problems with this assumption. First, if the interior mixing is too weak, the interior cannot support large enough cross–isopycnal mass flux, and the integral constraint based on this assumption cannot be used. This case was discussed in section 4, where the ideal limit of the diffusive solution was analyzed. Another possibility is that the diffusion (mixing) is large enough, but some of the inflow into a given layer leaves this layer across the gyre boundaries (across the equator in the western boundary current region, for example), instead of through interior cross interfacial velocities. Figure 12 shows the circulation in the one moving layer case of section 4, when none of the inflow mass is absorbed by the interior cross–isopycnal velocities. The integral constraint applied in this case is

$$\iint w_{0,top} dx\, dy = \iint w_{0,bottom} dx\, dy = M_{bottom} \tag{7.1}$$

instead of (4.5, 4.6). The averaged vortex stretching in this case in zero

$$\iint (w_{0,top} - w_{0,bottom}) dx\, dy = 0, \tag{7.2}$$

and the vorticity equation $\beta v_0 h_0 = f(w_{0,top} - w_{0,bottom})$ implies a southward as well as a northward circulation in the interior. In the β plane case, with f and β constant, the inflow is equally split into southward and northward parts (figure 12b). When the β plane approximation is not made, and both f and β are functions of latitude, this symmetry is broken (figure 12a), and the southward flow is much weaker.

This significant difference between the β plane case and the variable f and β case is a result of the integral constraints (4.5) and (4.6), and demonstrates the importance of calculating the correct basic stratification as part of the solution. In the β plane case, a given difference $\Delta w = w_{0,top} - w_{0,bottom}$ forces the same meridional circulation everywhere. The condition (7.2) results, therefore, in a symmetric vertical velocity distribution, and horizontal velocity field (figure 12b). Note that because the vertical

velocity field is coupled to the horizontal velocity field through the vorticity equation and the stratification, contours of Δw look like the stream lines of the horizontal flow.

When f and β are functions of y, there can be no flow across the equator, where $f = 0$, and stream lines of the southward flow must hit the western boundary before they reach $y = 0$. The constraint (7.2) is satisfied in this case by balancing a large region of small and negative Δw with a smaller region of large and positive Δw. This vertical velocity distribution forces, in turn, a weak southward flow and a stronger northward flow, as seen in figure 12a.

One may conclude that even when not all the inflow is absorbed by the interior cross–isopycnal velocities, it will still tend to flow northward as seen for the Mediterranean outflow.

Another assumption made in the model is of a constant diffusion coefficient in the density equation. Although a more realistic parameterization should probably have a depth-varying mixing coefficient (Gargett, 1984), this should not change the horizontal circulation we find here very much. As long as $\iint (w_{0,top} - w_{0,bottom}) = M_{inflow} > 0$, the vorticity balance implies a northward flow, and this does not depend on the parameterization of the mixing. A variable diffusion coefficient means that the vertical velocities are balanced by the mixing in a different manner, the basic stratification may change, and the westward penetration distance of the inflow may be different. But the average structure of the vertical velocity field, the basic vorticity balance, and therefore the northward flow, will not change significantly.

A final assumption we discuss in relation to observations is that the density surfaces are nearly horizontal ($\epsilon = \Delta_H \rho / \Delta_V \rho \ll 1$). When leaving the straits of Gibraltar, the Mediterranean water is heavier than the bottom water of the north Atlantic. There is, as a result, a large horizontal density variation $\Delta_H \rho$ there. This $\Delta_H \rho$ is not, however, the one used for the scaling arguments of sections 2 and 6. The heavy Mediterranean water flows along the shelf, entrains lighter surrounding water, increases in volume and

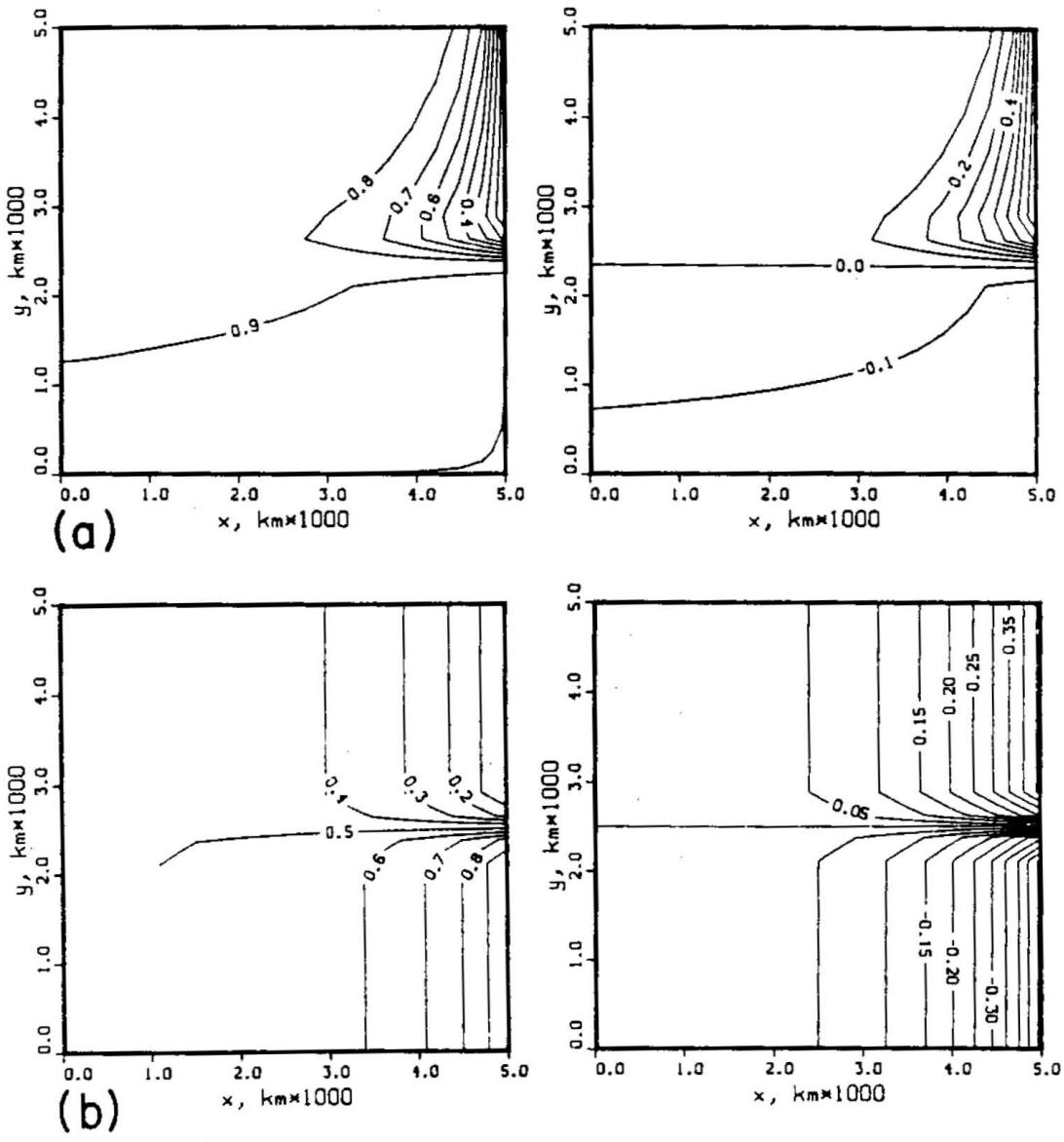

Figure 12: The circulation in the diffusive one moving layer case when the mass flux of the inflow into layer is not balanced by cross isopycnal mass flux out of this layer in the interior. See text for more details. a) The pressure in layer 0 (left), and $w_{0,top} - w_{0,bottom}$ (right) with f and β functions of latitude. b) same as in (a), for the β plane case.

decreases in density, until it reaches a depth where its density is equal to that of the surrounding stratification, and it can spread horizontally. In the model presented above, the inflow from the eastern boundary represents the inflow of the *diluted* Mediterranean water, of density equal to that of the density surface it spreads on. There is no contrast in density between the water of the inflow and the interior stratification, and the scale for $\Delta_H \rho$ is calculated from the transport of the inflow, keeping ϵ not too large. It is difficult to estimate the actual transport of the diluted Mediterranean water from observations, and therefore difficult to estimate ϵ for the Mediterranean outflow. As stated before, we have not tried to use 'realistic' values for the problem, and preferred concentrating on the understanding of the physics of the problem.

To summarize, the tendency of the inflow to turn northward is a fairly robust feature of the model, which also has some support in observations of the Mediterranean water circulation in the North Atlantic. For a more quantitative comparison of model and observations one needs to obtain estimates of the magnitude of the mixing coefficient, the transport of the Mediterranean water after it entrains North Atlantic water and starts spreading horizontally, and of how much of the Mediterranean water is transformed to other density ranges by interior mixing.

b. *Eastern boundary currents:* After turning northward, the inflow in the solutions presented above becomes narrower and flows as a broad eastern boundary current (figure 3). The Rossby wave argument in section 4 indicates the possible existence of such broad boundary currents in a stratified ocean. The physical balance in these boundary currents is between the β effect, and vertical diffusion of density (i.e. heat and salt). As explained in section 4, the diffusion traps long westward propagating Rossby waves near the eastern boundary. The trapping distance (the width of the boundary current) depends on the vertical scale of the current; currents with small vertical scales also have smaller width. The width of the current is proportional by (4.22) to the fourth power of the vertical scale.

The above physical mechanism is, perhaps, a possible explanation for the deep flow calculated by Saunders (1982) at a depth of 850-1200m in the eastern north Atlantic. But whether these eastern boundary currents exist or not, it is interesting to note that the addition of stratification and density diffusion to the physics, allows the existence of eastern boundary currents which are otherwise impossible.

8. Conclusions.

Deep buoyancy driven flows are more likely forced by interior mixing (turbulent diffusion) than by direct atmospheric heating or cooling. The interior diffusive fluxes depend on the stratification as in the parameterization $\mathbf{u} \cdot \nabla \rho = [\kappa(z)\rho_z]_z$. They result in cross–isopycnal (near vertical) velocities, and therefore force a horizontal circulation. The interior circulation is indirectly forced by the injection of water masses from formation regions into the interior. The interior stratification and circulation must adjust to balance the injection of water mass into a given density range by interior cross–isopycnal velocities.

The model presented above demonstrates the coupling of the remote forcing by water masses flowing into the interior, the basic vertical stratification, the local diffusive forcing, and the horizontal structure of the stratification and circulation. It emphasizes the need to include all these factors and their interaction in a complete model of a deep buoyancy driven circulation.

Chapter 3

Calculating mixing coefficients and time–mean circulation from hydrographic data

1. Introduction

In the previous chapters we have tried to understand the importance of diapycnal mixing in the physics of the general circulation. We found that although numerically small relative to other physical processes, cross isopycnal mixing is crucial to the determination of the basic stratification and of the deep circulation. In the present chapter, the role of mixing in general circulation dynamics is examined from the point of view of understanding and explaining observations. This is done through the analysis of a hydrographic data set from the eastern Mediterranean sea, by inverse methods.

In addition to calculating the horizontal circulation of the region, the inverse machinery will be used to try and resolve second order physical processes such as mixing and vertical velocities. We would like to test whether the addition of mixing to the physics is necessary for explaining the temperature and salinity distributions, and whether one can calculate mixing coefficients and vertical velocities from the hydrographic data. Having a data set which covers the region in both time and space, we will also try to examine the problem of estimating time average circulation —and the appropriate mixing coefficients parameterizing the time dependent eddies— from hydrographic data. Although the circulation of the eastern Mediterranean is of a different scale from the flows considered in the general circulation models of the previous chapters, we examine several points which are, we hope, relevant to the understanding of the circulation in larger ocean basins as well.

The eastern Mediterranean sea is an area of general interest to physical oceanography for several reasons. It is the source of the Intermediate Levantine water, produced mostly south of Turkey (Özsoy, 1981), which is believed to be an important component

of the high salinity Gibraltar outflow (Wüst, 1960). [Although other possible sources for the outflow were suggested by Bryden and Stommel, 1982)]. Being reasonably accessible, the eastern Mediterranean can also be used to study water mass formation processes which are difficult to observe in polar formation regions. Presently, knowledge of the region is based on the analysis of historic hydrographic data (Wüst, 1960). This data gives some idea of the water masses distribution but is less useful for dynamic calculations and inferring the velocity field (see El Gindy, (1982) for an extensive analysis of historic hydrographic data and dynamic calculations for yearly and seasonally averaged data). The recent observational program Physical Oceanography of the Eastern Mediterranean (POEM, 1985) will be a source of very useful data from this region.

The seasonal signal in the eastern Mediterranean is very strong, and the energy in the seasonal signal is probably larger than that in the yearly average. The wind forcing changes on a time scale of 3–4 months (May, 1982), and the air–sea heat fluxes, evaporation and precipitation — all presumed to be important driving mechanism in the region — are seasonally variable and therefore drive a seasonally variable circulation. The spatial scales for the circulation in the region are also different from those in major ocean basins. The Rossby radius of deformation is about 15km (Feliks, 1984), while the basin size is of the order of a few hundred kilometers. The 'general circulation' of the eastern Mediterranean can therefore be characterized by spatial scales of 150–200 km, and time scales of a few months. These scales, although small relative those of the circulation in major ocean basins, are still well separated from those of the small mesoscale eddies of the region.

During the winter months, the water of the region is homogenized by strong mixing to a depth of two to three hundred meters. In the summer, however, one can clearly observe several different water masses as the Intermediate Levantine salinity maximum at about 300m, and the Atlantic water salinity minimum at 50–100m. The inverse

model presented below uses advection–diffusion equations for the temperature and salinity to calculate the reference geostrophic velocities. These equations are probably not valid in the presence of very strong winter mixing and catastrophic sinking events. We have chosen, therefore, to use data from summer season only, in order to try and calculate the summer circulation of the region.

The following sections describe the data set (2), formulate and refine the inverse model (3, 4), describe the inversion results for six summer cruises (5), and discuss the problem of calculating the time–average circulation from hydrographic data (6).

2. The data set and preliminary data treatment

The data used for the inverse calculation is part of an extensive data set acquired by Israeli Oceanographic and Limnological Research (IOLR) in the eastern Levantine basin of the Mediterranean Sea from 1979 to 1984 (figure 1 and table 1). The data were collected on 17 cruises, each about ten days long, separated by 3–4 months periods. During each cruise the 27 CTD stations shown in figure 1 were occupied. The stations were arranged in a 5 by 6 regular grid, with half a degree spacing in latitude and longitude. Initial quality control, bin averaging over 1 decibar intervals, and calculations of salinity, density, potential temperature etc. were all done at IOLR (Hecht, 1986).

We have chosen to use the vertical salinity profile as a criterion for choosing cruises representing the summer circulation of the region. The typical summer profile of salinity (figure 2) is destroyed by winter mixing and convection, and is normally found in June/July to November/December. Out of the cruises available at that period, one or two with possible data problems were removed. Profiles of temperature and salinity for each of the remaining cruises were examined, to remove cruises in which the summer profile was not fully developed due to a particularly severe preceding winter. At the end of this filtering process, six summer cruises were left, and were used in the inverse model: MC13, MC14, MC15, MC18, MC19 and MC24 (see table 1 for dates).

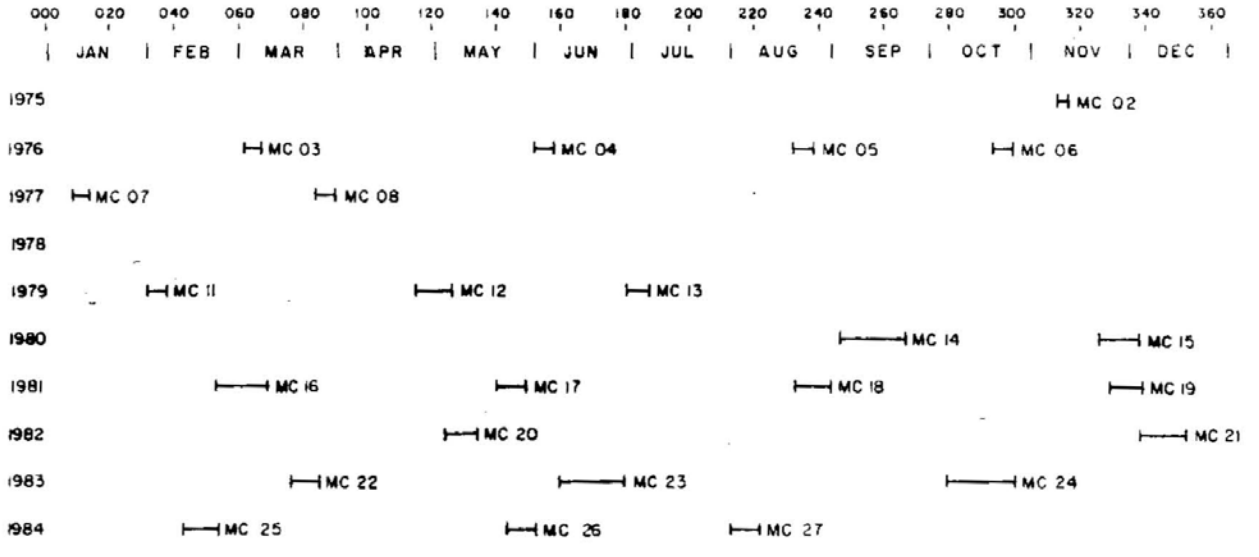

Table 1: Time table for the MC cruises.

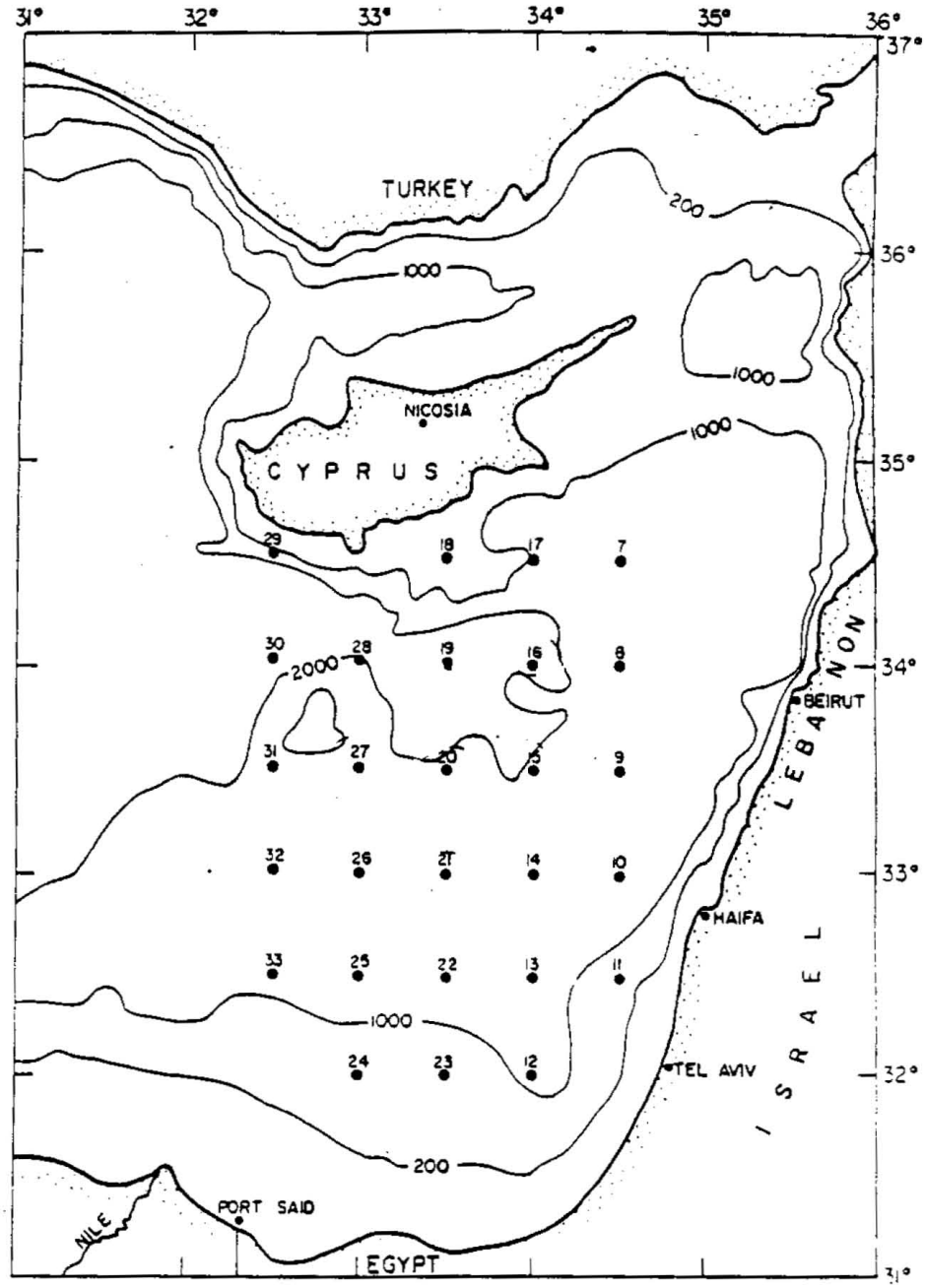

Figure 1: Location of CTD stations taken in each of the cruises, and bottom topography of the region.

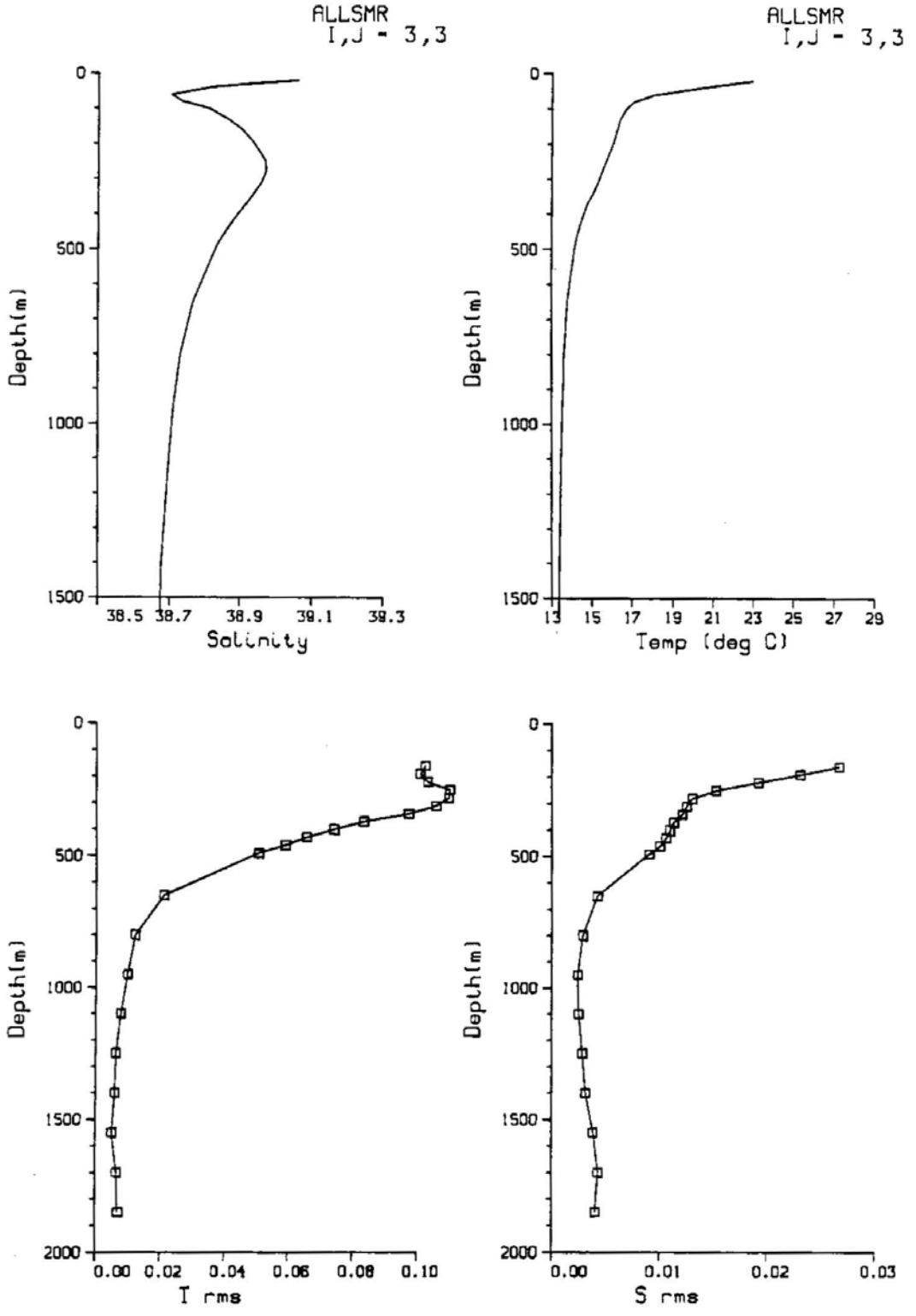

Figure 2: (a,b) Average summer salinity and temperature profiles for the eastern Levantine basin. (The average is over six summer cruises). (c,d) Root mean square (rms) T, S profiles, indicating the natural variability around the average summer profiles (see section 3).

To prepare the data for the inverse calculation, the vertical coordinate was transformed from pressure to depth using the algorithm given by Saunders and Fofonoff (1976), profiles were smoothed by a 20 meter running average to remove small scale structure, and were sub-sampled in the vertical to obtain potential temperature, salinity and density at 30 standard depths specified by the model grid (see next section).

3. The inverse model

The model chosen to describe the data includes the geostrophic equations, mass conservation, and advection diffusion equations for the temperature and salinity fields. Mixing of salt and heat is parameterized with horizontal and vertical eddy mixing coefficients which are possibly functions of depth. Because the area covered by the data is small (250km by 200km), it did not seem necessary to allow for horizontal variation of the mixing coefficients.

In a stably stratified ocean, mixing along isopycnals by meso-scale eddies is much stronger than cross–isopycnal mixing due to small scale turbulence, salt fingers etc. It is possible to use tensor diffusivities to parameterize the long and cross isopycnal mixing (Redi, 1982, Olbers et. al., 1985). But as long as the isopycnal slope is not too large, vertical and horizontal mixing coefficients may be used to replace the cross– and long–isopycnal mixing coefficients without introducing large errors. As will be seen below, the mixing coefficients are, in any case, not very well resolved by the model. The uncertainty in their values due to resolution problems is probably much larger than errors due to the simplified parameterization used.

The use of a steady model requires, perhaps, some justification in view of the strong seasonal variability of the region. The typical summer salinity profile (figure 2) is maintained for about six months. During the summer, the strong local evaporation slowly builds high surface salinity values, but these do not penetrate below about 50m, while in the inversions described below we use data from below 160m only. The

destruction of the summer profile below the surface water by winter cooling and mixing occurs in 'catastrophic' events, rather than by continuous cooling during the fall and early winter. In short, the summer structure of water properties below the surface waters appears, to a good approximation, to be in a steady state during the months of June to December. Furthermore, although the wind forcing changes on a 3–4 months time scale, we may expect the deep circulation to have longer time scales due to the much slower baroclinic adjustment process.

The model equations are

$$\begin{aligned} fu &= -(1/\rho_0)p_y \\ fv &= (1/\rho_0)p_x \\ p_z &= -g\rho \\ u_x + v_y + w_z &= 0 \\ uT_x + vT_y + wT_z &= [\lambda_V(z)T_z]_z + \lambda_H(z)\nabla_H{}^2 T \\ uS_x + vS_y + wS_z &= [\lambda_V(z)S_z]_z + \lambda_H(z)\nabla_H{}^2 S. \end{aligned} \tag{1}$$

From the geostrophic and continuity equations we obtain the thermal wind equations

$$\begin{aligned} fu_z &= \frac{g}{\rho_0}\rho_y \\ fv_z &= -\frac{g}{\rho_0}\rho_x. \end{aligned} \tag{2}$$

Integrating these equations in z, from a reference level, we obtain the vertical structure of the horizontal circulation in terms of the known density field. The velocities at the reference level are calculated later by the inverse.

To obtain the vertical profile of the vertical velocity, w, we need to form a vorticity equation. From (1, a,b,d) we have

$$\beta v = f w_z. \tag{3}$$

Substituting v from (2) and integrating this equation in z, we can obtain the vertical velocity profile in terms of the density field and the reference velocities. This, in

fact, is the approach used in the β-spiral calculations (Stommel and Schott, 1977, or Olbers et al, 1985). One can add vorticity mixing terms to (3), to account for the small viscous terms neglected in the momentum equations (Olbers et al, 1985). After some experimentation, using the linear vorticity equation (3) to calculate the vertical velocity profile, we have decided to abandon this approach, and to simplify the model by using a depth independent vertical velocity. The main reasons for this choice are the difficulties in using an appropriate vorticity equation for the region, and the inability of the model to resolve the small vertical velocities. These are discussed below by scaling and examining the physical balances in the vorticity and tracer equations.

Consider first the vorticity equation, including the advection of relative vorticity (Pedlosky, 1979)

$$(u\partial_x + v\partial_y)\{[v_x - u_y] + \beta y\} = f w_z.$$

Nondimensionalizing all variables, using $(x, y) \sim L$, $z \sim D$, $(u, v) \sim U$, $w \sim W = UD/L$, we have

$$Ro(u'\partial_{x'} + v'\partial_{y'})[v'_{x'} - u'_{y'}] + \frac{L}{R}\beta' v' = f' w'_{z'}, \tag{4}$$

where primed quantities are nondimensional, $Ro = U/f_0 L$ is the Rossby number, $f' = \sin(\theta)$, $\beta' = \cos(\theta)$ and R is the radius of the earth. The internal Rossby radius of deformation, and therefore the scale of mesoscale eddies in the region, is about 15km. Using $L = L_R = 15$km, and $U = 10$cm/sec, we find

$$Ro = 1/15; \qquad \frac{L}{R} = 1/400.$$

The nonlinear relative vorticity advection clearly dominates the β effect at these scales. Our data, however, does not resolve the small eddies, nor can our model handle nonlinear dynamics. If we spatially average (4), and use the scales appropriate to the general circulation of the region, ($L = 200$km, $U = 10$cm/sec), the nonlinear terms would still

be important and appear as vorticity mixing terms in the vorticity equation — possibly parameterized by eddy mixing coefficients. We will see below that the parameterization of tracer mixing by eddy mixing coefficients did not prove to be very useful. Not expecting the mixing coefficients parameterization to do better in the vorticity mixing, we have decided to avoid the use of mixing terms in the vorticity equation.

In view of the above difficulties in finding as appropriate and usable vorticity equation for calculating the vertical velocity profile, and in accordance with the relatively small scales of the circulation in the region, we have chosen to use the f-plane approximation to the geostrophic equations, with $f = f_0 =$ constant. The horizontal relative geostrophic velocities are then nondivergent ($u_x + v_y = 0$), and the vertical velocity is depth independent to lowest order. (We allow non zero constant vertical velocity although a more rigorous scaling (Pedlosky, 1979) may require the constant w to vanish. We prefer to let the inverse model determine the constant w most appropriate for the explanation of the tracer fields.)

The choice of using the f-plane approximation is also consistent with the results of numerical experiments for the eastern Mediterranean (Bergamasco and Malanotte-Rizzoli, 1986), showing the β effect not to be important in the dynamics of the region.

The full velocity field can now be written as

$$\begin{aligned} u(x,y,z) &= u_0(x,y) + \int_{z_0}^{z} \frac{g}{\rho_0 f_0} \rho_y \, dz' \\ v(x,y,z) &= v_0(x,y) + \int_{z_0}^{z} \frac{g}{\rho_0 f_0} \rho_x \, dz' \\ w(x,y,z) &= w_0(x,y), \end{aligned} \tag{5}$$

where $u_0(x,y) = u(x,y,z_0)$, v_0 and w_0 are the velocities at the reference level.

Substituting the velocity field (5) in the advection diffusion equations for the temperature and salinity (1e,f), we obtain

$$\begin{aligned} &u_0(x,y)T_x(x,y,z) + v_0(x,y)T_y(x,y,z) + w_0(x,y)T_z(x,y,z) \\ &\quad - (\lambda_v(z)T_z)_z - \lambda_H(z)\nabla_H{}^2 T = \Gamma(x,y,z), \end{aligned} \tag{6}$$

where Γ contains the advection terms of temperature by the known relative velocities in (5). Evaluating T_x, T_y and T_z, as well as the geostrophic velocities relative to the reference level, in terms of the known temperature and density fields, and forming a similar equation for the salinity, we obtain linear equations for the unknown reference velocities and mixing coefficients. These equations can be formed at any depth where data is available, to obtain many equations for the problem's unknowns — reference velocities and mixing coefficients.

We have already explained the difficulties in using a vorticity equation to obtain the vertical structure of the vertical velocity in the region. It is possible, in principle, to use (6) without assuming that w is depth independent, and to solve for w at each level where equations are evaluated. Olbers et al. (1985) show that the resulting w is very noisy, and we will see below that the model is not successful even in resolving the constant vertical velocity — indicating that one should probably not try and complicate the model by allowing a vertically variable vertical velocity. We will come back to the problem of resolving the vertical velocities using the tracer equations later in this section.

a. *Finite difference formulation*

The derivatives and integrals in (6) are approximated by their finite difference forms. The finite difference grid follows the stations location in the horizontal—a five by six grid, with half a degree spacing in latitude and longitude. In the vertical, there are 30 levels, with high resolution in the upper water, and lower in the deep water. With $z = 0$ at the surface, the levels are at depths of

$$z_k = 20,\ 40, \ldots, 100,\ 130,\ 160, \ldots, 490,\ 650,\ 800,\ 950, \ldots, 2300\text{meters}. \qquad (7)$$

Potential temperature, salinity, and density are calculated (where data is available) at each of the grid points, as explained in the previous section. Derivatives of these fields

are calculated using center differences,

$$T_x(x_i, y_j, z_k) \approx \frac{T(x_{i+1}, y_j, z_k) - T(x_{i-1}, y_j, z_k)}{2\Delta x}, \tag{8}$$

and the integrals in (4,5) are approximated by the appropriate sums.

To represent the possible variation of the mixing coefficients with depth, it was chosen to represent their vertical structure by a series of Chebyshev polynomials instead of treating the coefficient at each level as a separate unknown. (The Chebyshev polynomials in the range $(-1, 1)$ are similar to sines and cosines)

$$\lambda_V(z) = \sum_{n=0}^{N_V} C_{V,n} T_n(1 - 2z/D), \tag{9}$$

where D is the maximum depth of data, and a similar expression for $\lambda_H(z)$. This way the unknowns of the problem [the coefficients $C_{V,n}$ in the expansion (9)] do not depend on the choice of levels where equations are evaluated. One can also impose correlation between coefficients at different depths by reducing the maximum degree of polynomials in the expansion (N_V and N_H), or allow for more structure in the solution for the coefficients by increasing N_V.

b. *The matrix equation*

Equation (6) can be evaluated only at horizontal locations where data is available on all four sides, so that centered differences can be evaluated. Forming equation (6), in all possible station locations, for temperature and salinity and at several levels, we obtain a set of linear equations which can be written in matrix form as

$$Ab = \Gamma. \tag{10}$$

The column vector b contains the unknowns

$$b = \left(u_0(\mathbf{x}_1),\, v_0(\mathbf{x}_1),\, w_0(\mathbf{x}_1), \ldots, w_0(\mathbf{x}_n) C_{V,0}, \ldots, C_{V,N_V},\, C_{H,0}, \ldots, C_{H,N_H}\right)^T, \tag{11}$$

Γ is the right hand side of (6), and A contains the coefficients of the unknowns evaluated using the temperature and salinity equations.

In addition to the set of equations, the mixing coefficients are required to be positive in levels where equations are evaluated, and this is written as a set of linear inequalities for the Chebyshev coefficients

$$Gb \geq 0. \tag{12}$$

The equations (10) are solved by Singular Value Decomposition (SVD), and the inequalities are solved using a modification of the LSI/LDP algorithm of Lawson and Hanson (1974). Details of incorporating the inequalities in the SVD solution are given in the appendix.

c. *Nondimensionalization, weighting, choosing the rank of A*

General. Before calculating the SVD of A and solving (10) and (12) for b, one normally weights the equations and unknowns (Wiggins, 1972, Wunsch, 1978). Given an estimate for the error in each equation, ε_i, we have

$$Ab = \Gamma \pm \varepsilon, \tag{13}$$

and the weighted problem can be written as

$$(S^{-1/2}AW^{1/2})(W^{-1/2}b) = S^{-1/2}\Gamma \pm S^{-1/2}\varepsilon. \tag{14}$$

In general W and S are the covariance matrices of the unknowns b and the noise ε. When the noise in different equations is uncorrelated, and there is no correlation between the unknowns, both S and W are diagonal matrices. Having no *a priori* information about the noise correlation, and no reason to specify *a priori* correlation between the unknowns, we have chosen to use diagonal weighting matrices.

The row weights, S, are chosen so that the weighted error on the rhs is the same for all equations, downweighting equations with large errors, so that they do not affect

the inversion as much as other equations. The weighting of the columns by $W^{1/2}$ is done after the row weighting, to remove artificial structure from the solution due to the arbitrary size of the coefficients in A, and to specify the expected magnitude $[b_i]$ of the unknowns b,

$$W_{ii}^{1/2} = \left(\frac{[b_i]}{\left(\sum_{j=1}^{N} a_{ij}^2 \right)^{1/2}} \right)^{1/2} . \tag{15}$$

For both row and column weighting to be effective, one needs to nondimensionalize all variables and measure them in units in which they are of order one. Otherwise, the column weights may be very large or small because of the variables having large or small expected magnitude (e.g. $[w] \sim 10^{-5}$, $[\lambda_H] \sim 10^6$ in c.g.s units). Large or small column weights may change the desired relative weights of different equations as determined previously by the row weighting.

Row weighting. Errors on the rhs (ε_i) are due in part to measurement errors, but mostly due to unresolved small scale processes like internal waves. With no information about the magnitudes of these errors, we do not have any reason to prefer the advection diffusion equation, (6), evaluated at one place over that evaluated at another, or to prefer (6) evaluated for temperature over a similar equation evaluated for the salinity. We have therefore chosen to weight the rows of A by their length,

$$S_{ii}^{1/2} = \left(\sum_{j=1}^{M} a_{ij}^2 \right)^{1/2} . \tag{16}$$

Such row weighting forces the inversion to use all equations equally to find the first eigenvalue of the matrix A. The diagonal elements of the data resolution matrix, UU^T, with only the first eigenvalue, and the first U-vector taken into account, should then all be different from zero and equal, indicating that all equations were used to calculate λ_1, V_1 and U_1 — unless some of the equations are dependent. When using a subset of CTD stations, evaluating (6) for temperature and salinity at all levels, and using (16)

for row weighting, the diagonal elements of UU^T indicated that equations evaluated deeper than about 500 meters did not contribute to λ_1 as much as those evaluated at higher levels. The uniformity of the deep water in the small area covered by the data caused the equations evaluated there to be dependent, and the inversion responded by not using the redundant equations. In the inversions shown below, we could therefore use only one or two of the deep levels, without loss of information, as indicated by the above discussion. The depths at which the equations were evaluated are

$$z_k = 160,\ 190,\ 220,\ 250,\ 310,\ 370,\ 430,\ 650,\ 950,\ 1100\text{meters}. \tag{17}$$

Choosing the rank of A. Although there are always more equations than unknowns in the present model, the matrix equation is never full rank. The number of unknowns, M, is equal to the number of stations having four horizontal neighbors (four neighbors are needed to evaluate the centered differences), times three reference velocities at each station (u_0, v_0, w_0), plus the number of degrees of Chebyshev polynomials for vertical (and horizontal) diffusion, or, typically,

$$M = 11 \times 3 + 11(+11) = 44 \text{ to } 55.$$

The number of equations, N, is equal to the number of stations having four neighbors, times the number of levels where equations are evaluated, times the number of tracer equations evaluated at each location (two, for temperature and salinity),

$$N = 11 \times 10 \times 2 \approx 200.$$

To determine the rank of A one can examine the eigenvalues of A and look for a place where there is a sudden drop in their magnitude. One can also look at the variance of the parameters and choose the rank when some maximum allowed variance

is reached which indicates that too small eigenvalues and therefore too much noise entered the solution. Another possibility is to examine the parameter

$$\sigma^2 = \frac{\|residuals\|^2}{N-k} \tag{18}$$

(Wiggins, 1972) and determine the rank of A at the minimum of σ. The criterion used here was that of maximum allowed variance, because it allows a direct control over the amount of noise in the solution. The rank was chosen so that the variance of all parameters was less then twice their expected magnitude as specified by the column weighting

$$\max\{(\mathrm{var}(b_i))^{1/2}\} \leq 2[b_i]. \tag{19}$$

The rank (k) of A, is then typically found to be about 25 to 30. One finds a sudden drop in the magnitude of the eigenvalues very close to the rank determined by (19). The rank chosen by (19) was usually one or two less than the location of the drop in magnitude of the eigenvalues λ_i. The σ parameter was less useful in determining the rank. The rank was found not to be sensitive to the exact form of (19), and replacing the factor 2 by a 3 did not change the rank in most cases. The rank was always such that the horizontal reference velocities were resolved (diagonal elements of VV^T about 0.99), vertical reference velocities were not resolved, and mixing coefficients were partly resolved (diagonal elements of VV^T about 0.3). The vertical velocities are resolved at ranks higher than that determined by (19), but with very large variance, indicating that they cannot be distinguished from zero.

Resolution of the vertical velocities: The inability of the model to resolve the vertical reference velocities, w_0, can by explained by carefully scaling the advection diffusion equation (6) used to solve for the reference velocities. Consider only the advection terms in (6)

$$u_0 T_x + v_0 T_y + w_0 T_z = \ldots \tag{20}$$

Denoting the expected magnitude of (u_0, v_0) and w_0 by U and W respectively, and applying the column weighting (15) to (20), we have

$$\left(\frac{u_0}{\sqrt{U/T_x}}\right) T_x\sqrt{U/T_x} + \left(\frac{v_0}{\sqrt{U/T_y}}\right) T_y\sqrt{U/T_y} + \left(\frac{w_0}{\sqrt{W/T_z}}\right) T_z\sqrt{W/T_z} = \ldots \quad (21)$$

or, in terms of the weighted, nondimensional reference velocities

$$u_0' T_x\sqrt{U/T_x} + v_0' T_y\sqrt{U/T_y} + w_0' T_z\sqrt{W/T_z} = \ldots \quad (22)$$

With $T_x \equiv \Delta T/L$ and $T_x \equiv \Delta T/H$, the ratio of the coefficients of (u_0', v_0') and w_0' is

$$\frac{T_x/\sqrt{UT_x}}{T_z/\sqrt{WT_z}} = \left(\frac{WL}{UH}\right)^{1/2} \quad (23)$$

Normally, one uses the continuity equation, and scales the vertical velocity by UH/L, but the important thing to note here is that UH/L is not equal to the magnitude (W) of the vertical velocity. Rather, it is an upper bound for the magnitude of the vertical velocity (Pedlosky, 1979). For quasigeostrophic motions, where $\beta L/f = O(Ro) \ll 1$, $Ro = U/Lf$, the magnitude of the vertical velocity is

$$W = Ro\frac{UH}{L} \ll \frac{UH}{L}. \quad (24)$$

For a planetary–scale geostrophic motion, where $\beta L/f = O(1)$ and $\beta v = f w_z$, one has

$$W = \frac{H}{L}\frac{UH}{L} \ll \frac{UH}{L}. \quad (25)$$

In both cases, (24), and (25), together with (23), indicate that the coefficients of w_0' in the matrix equation are much smaller then those of u_0', and v_0'. The inverse procedure prefers, therefore, to minimize the residuals $\|Ab - \Gamma\|^2$ by making small changes to u_0', and v_0' rather than large ones to w_0', which tends to be left out of the problem, unnecessary and unresolved.

Residuals. Is the model consistent with the data? With more equations than unknowns, the solution one obtains from the inverse, $\hat{b}$, does not satisfy all equations exactly, and

there are always residuals $\|Ab - \Gamma\|^2 = \|r\|^2 > 0$. When the error in each equation is known, one can write

$$Ab = \Gamma \pm \epsilon$$

and for the model to be consistent with the data, one requires $\|Ab-\Gamma\|^2 = \|r\|^2 < \|\epsilon\|^2$. Having no direct information about ϵ, we have chosen to examine the size of the residuals in the following way. Let $\hat{u}, \hat{\lambda}_V$ and $\hat{\lambda}_H$ be the total velocity field and mixing coefficients calculated by the inverse. Then,

$$\hat{u} \cdot \nabla T - (\hat{\lambda}_V(z) T_z)_z - \hat{\lambda}_H(z) \nabla_H^2 T = r(x,y,z) \neq 0. \tag{26}$$

The residuals $r(x,y,z)$ may be viewed as a time change term in the temperature equation, due to the inability of the model to satisfy the steady state advection diffusion equation: $r \sim \partial T/\partial t$. Multiplying $r(x,y,z)$ by 3 months, we obtain an equivalent temperature change one expects to occur at (x,y,z) within a 3 months period, due to the residuals. Comparing this equivalent temperature change to the natural variability around steady state, which occurs at (x,y,z), one can decide whether the model adequately describes the data. As an estimate for the natural variability, we calculate the RMS of the temperature and salinity fields as function of position, using the data from the six summer cruises (figure 2).

Another criterion for deciding if the model is consistent with the data is the structure in the residuals. If the residuals arise only from random errors present in the data, they should be random in (x,y,z). Any structure in $r(x,y,z)$ indicates some missing physics in the model. With the small area covered by the data set, we cannot say much about the horizontal structure of the residuals, but we can examine the vertical profile of $r(x,y,z)$, using the 10 levels where equations for the temperature and salinity are evaluated at each station location.

Error estimates. The SVD solution for the reference velocities and mixing coefficients also provides an estimate for the variance of each unknown (Wiggins, 1972). Because

the mixing coefficients are represented by a series of Chebyshev polynomials, we actually obtain error estimates for the Chebyshev coefficients, $C_{\nu,n}$, and not for the mixing coefficients $\lambda_\nu(z)$. We then use these estimates to calculate the expected error for the mixing coefficients. Let the expected error calculated by the SVD for the nth coefficient be $\sigma[C_{\nu,n}]$. Write

$$\hat{C}_{\nu,n} = C_{\nu,n} + \varepsilon[C_{\nu,n}] \tag{27}$$

where $\hat{C}_{\nu,n}$ and $C_{\nu,n}$ are the SVD estimate and the actual value of the nth Chebyshev coefficient, and $\varepsilon[C_{\nu,n}]$ is the error in the SVD estimate:

$$\langle(\varepsilon[C_{\nu,n}]\,\varepsilon[C_{\nu,m}])\rangle = \delta_{nm}\sigma[C_{\nu,n}]. \tag{28}$$

The expected error in the mixing coefficients, in terms of the expected error of the Chebyshev coefficients, is

$$\begin{aligned}\sigma^2[\lambda_\nu(z)] &= \left\langle \left(\hat{\lambda}_\nu(z) - \lambda_\nu(z)\right)^2 \right\rangle \\ &= \left\langle \left(\sum_{n=0}^{N_V} \hat{C}_{\nu,n} T_n(1-2z/D) - \sum_{n=0}^{N_V} C_{\nu,n} T_n(1-2z/D) \right)^2 \right\rangle .\end{aligned} \tag{29}$$

If the different Chebyshev coefficients are not correlated, (29) reduces to

$$\sigma^2[\lambda_\nu(z)] = \sum_{n=0}^{N_V} \sigma^2[C_{\nu,n}]\, T_n^2(1-2z/D), \tag{30}$$

which is the expression used to calculate the error bars for $\lambda_\nu(z)$ shown below.

The SVD estimate for the covariance of the parameter vector b is

$$\sigma^2[b] = \sigma^2 V \Lambda^{-2} V^T + \left(I - VV^T\right)\rangle bb^T \langle\left(I - VV^T\right), \tag{31}$$

where σ^2 is given by (18), and b is the true value of the parameter (which we do not know). As can be seen in (31), the error estimate is made of two parts: one due to errors in the data, and the second due to lack of resolution of the parameters. For the

horizontal velocities in the present model, which are fully resolved, the error estimate is given by the first part in (31). We can obtain a first order estimate for the full error for parameters which are not fully resolved by the model by dividing the known first part of the error in (31) by the resolution of these parameters. The error estimate for the mixing coefficients, for example, is about three times the first part of the error in (31), because they are resolved to about 30 percent.

Note that the error bars shown in the profiles for the mixing coefficients represent only the first part of the error estimate — for the noise variance only — and should therefore be multiplied by about three to obtain the full error bars for the mixing coefficients.

4. Calibrating the model

We now use the data from a single cruise (MC24, October 1983) to try and understand the physics governing the region, examine several variations of the inverse model, and choose one that explains the data reasonably well. Table 2 summarizes the different versions of the model and the figures showing the resulting circulation and residuals. Profiles of the residuals [rhs of (26)] are shown together with profiles of the different terms in the temperature and salt equations [lhs of (26)].

The simplest model ([ref-lvl]) is the starting point for the inverse calculation, of zero horizontal velocity at the reference level (460m depth), no vertical velocity, and no mixing. The only terms in the temperature and salt equations are the horizontal advection terms, and their sum gives the residuals. In the next simplest model, ([a]), we use the salt and temperature equations, without mixing, to determine the velocities at the reference level, u_0, v_0 and w_0. Allowing the model to determine the reference velocities is certainly an improvement over the initial assumption of level of no motion [compare residuals in ([ref-lvl]) and ([a])]. The residuals in ([a]) are about 50% of those in ([ref-lvl]). The dominant balance in the temperature and salt equations is between

run	mixing N_V, N_H	column weights (c.g.s) $[u_0], [v_0], [w_0], [C_{V,n}], [C_{H,n}]$	N, M, k	figure
[ref-lvl]	$-, -$	$-, -, -, -, -$	$-, -, -$	3
[a]	$-, -$	$1, 1, 10^{-5}, -, -$	$194, 33, 23$	4
[b]	$10, -$	$1, 1, 10^{-5}, 1, -$	$194, 44, 27$	5
[c]	$5, -$	$1, 1, 10^{-5}, 1, -$	$194, 39, 26$	6
[d]	$10, 10$	$1, 1, 10^{-5}, 1, 10^{6}$	$194, 55, 32$	7
[e]	$10, -$	$1, 1, 10^{-5}, 10, -$	$194, 55, 32$	-

Table 2: summary of calibration runs of the inverse model.

Figures 3–8: Results of the inverse calculation for the different calibration runs in table 2. See table for details of the different runs. **(a)** Different terms in the advection–diffusion equations for temperature and salinity. Dotted lines are the horizontal advection terms, uT_x, vT_y; The dashed line is the sum of the horizontal advection terms, $uT_x + vT_y$; The chain–dotted line is the vertical advection term wT_z and the chain–dashed line is the vertical diffusion term $[\lambda_V(z)T_z]_z$. **(b)** absolute velocity field (relative velocities plus reference velocities calculated by the inverse) at two levels. **(c)** Mixing coefficients profiles calculated by the inverse. The three solid lines are the SVD solution and error bars, and the dashed line is the value of the mixing coefficients when inequalities forcing it to be positive are applied.

the horizontal advection terms, with the vertical advection much smaller, as expected. But while the magnitude of the residuals decreases, they still have some structure at deeper levels, (a consistent slope below 400–500 meters depth for some of the stations) which may indicate, as mentioned in the previous section, some missing physics in the model. The following three runs in table 2 all include mixing terms in the T, S equations. They differ in the type of mixing (vertical, horizontal, both) and in the correlation imposed between mixing coefficients at different depths through the degree of Chebyshev polynomials in the expansion (9) of the mixing coefficients.

Although the 'ideal fluid' run, ([a]), seemed to point to some missing physics in the model, the addition of mixing parameterized by eddy diffusivities does not bring much improvement. This is true for all of the different versions ([b],[c], [d]). The mixing coefficients are not fully resolved by the model, and as can be seen in the profiles

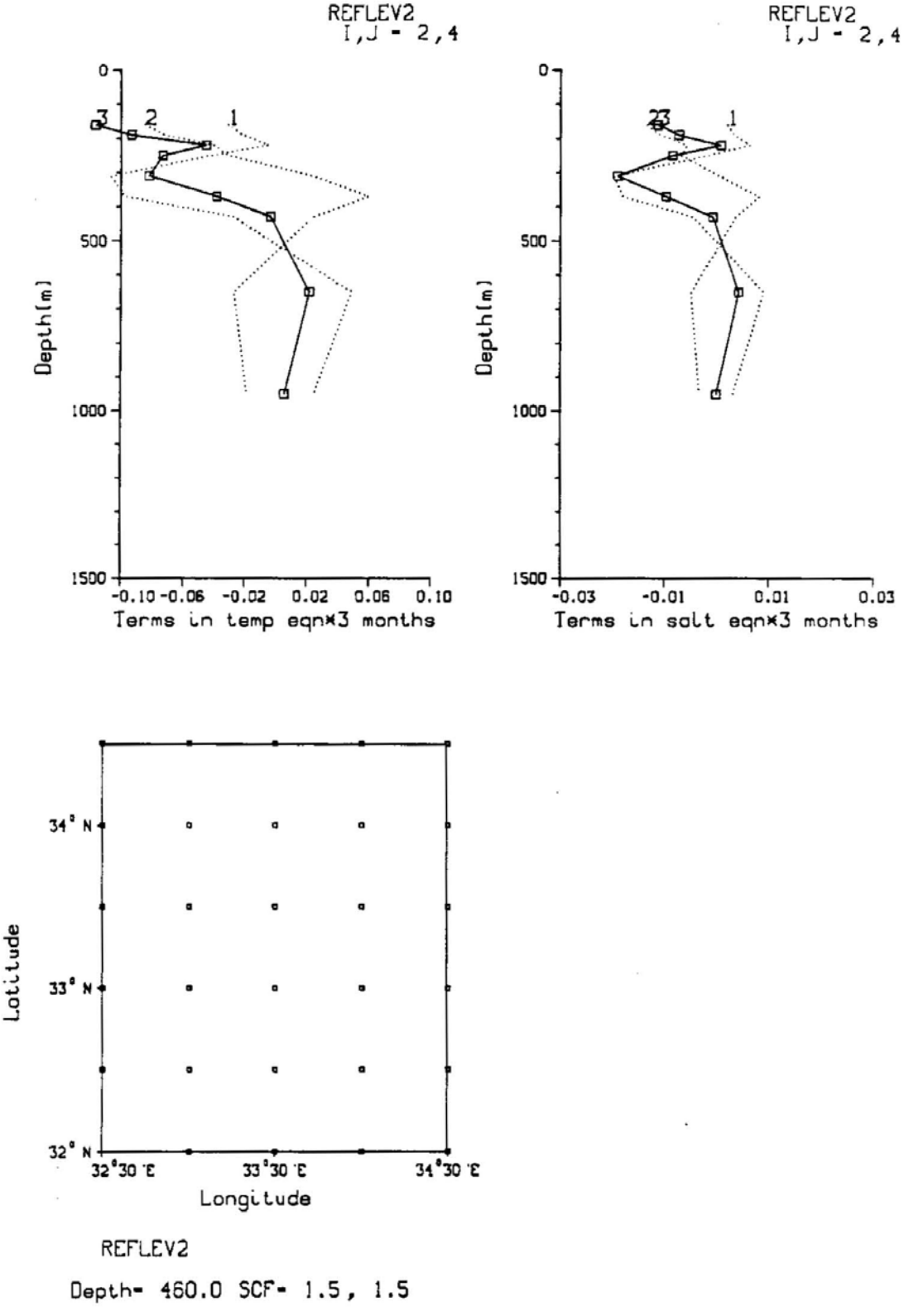

Figure 3: Initial reference level (see [ref-lvl] in table 2)

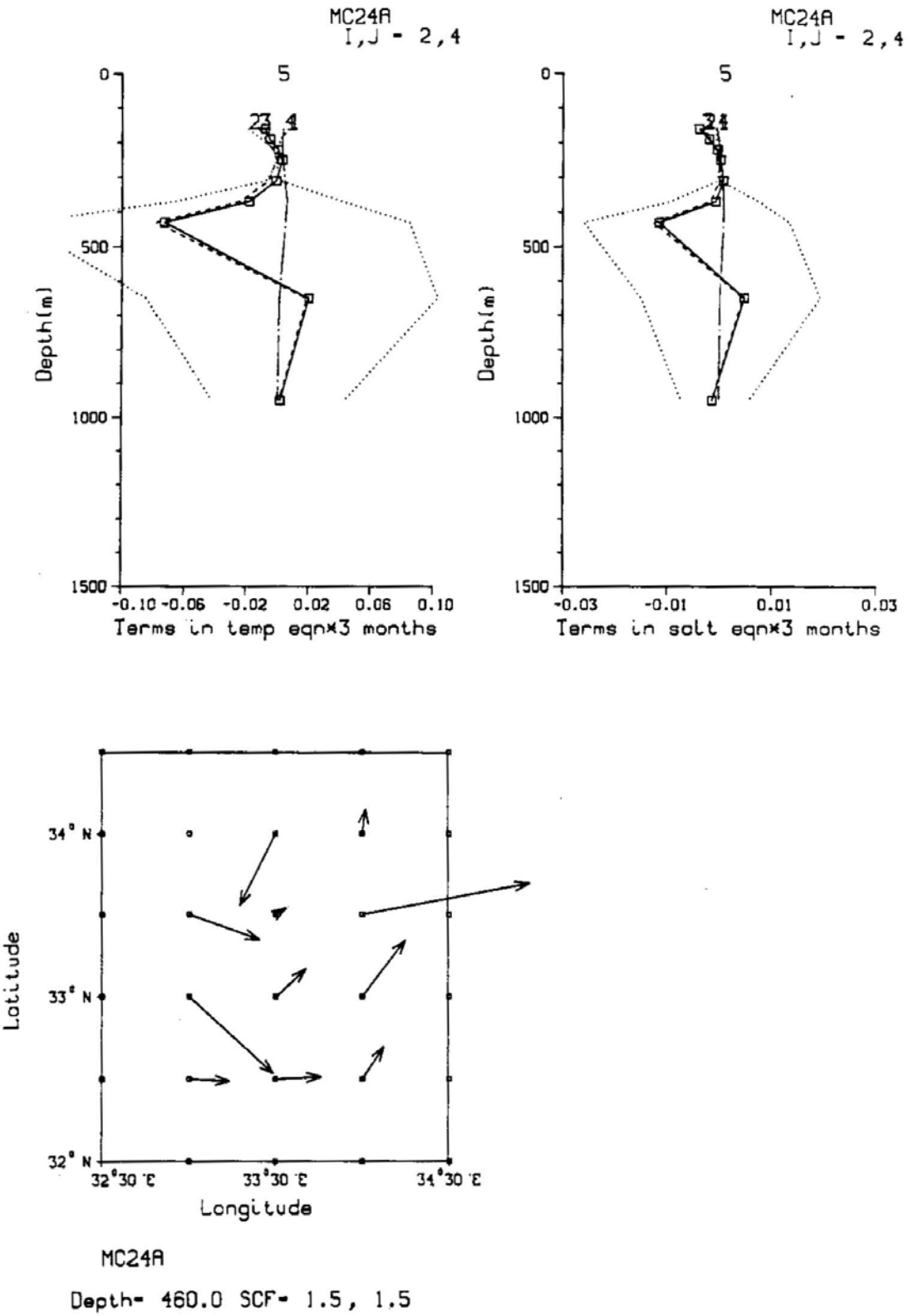

Figure 4: run [a] (see table 2).

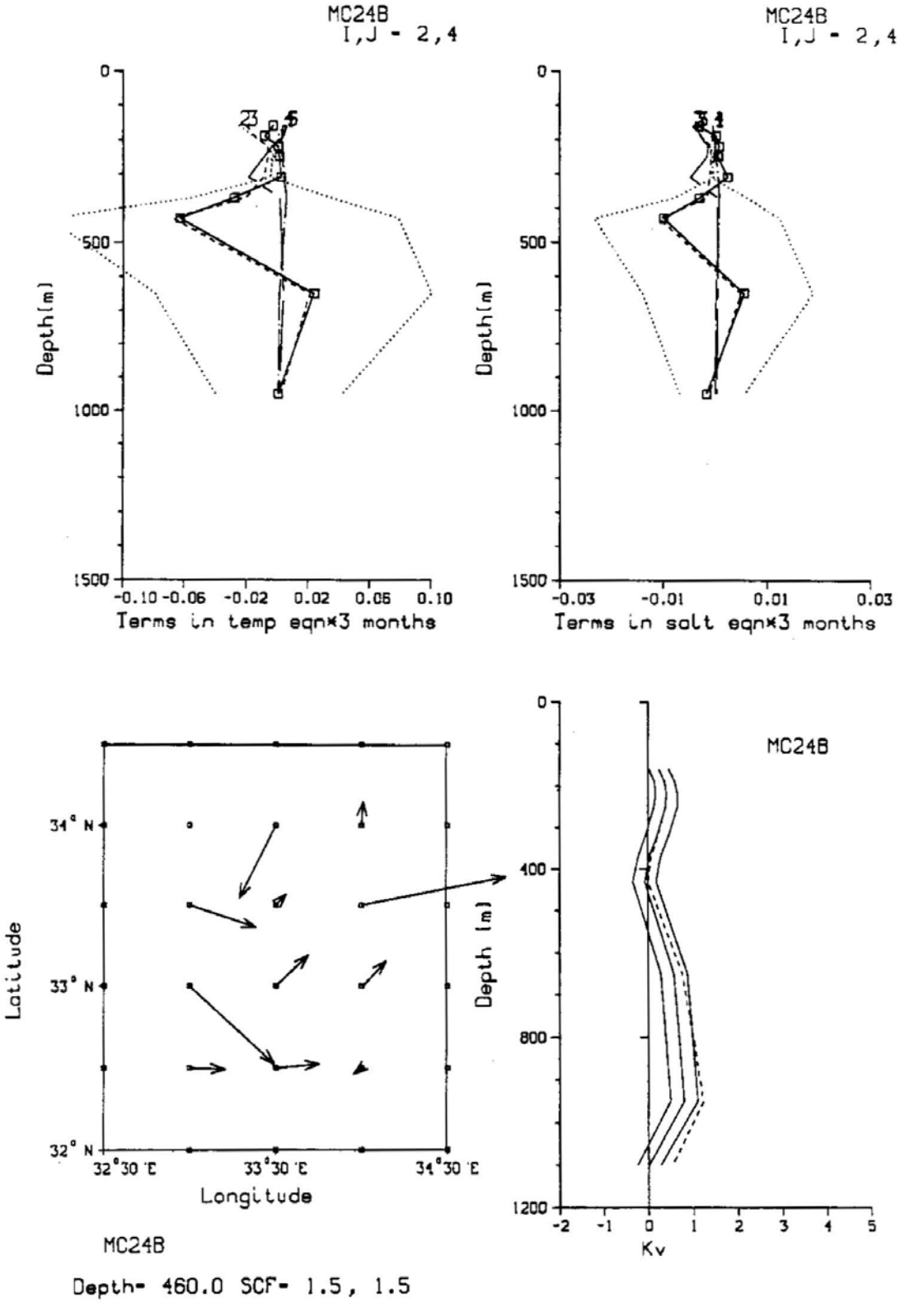

Figure 5: run [b] (see table 2).

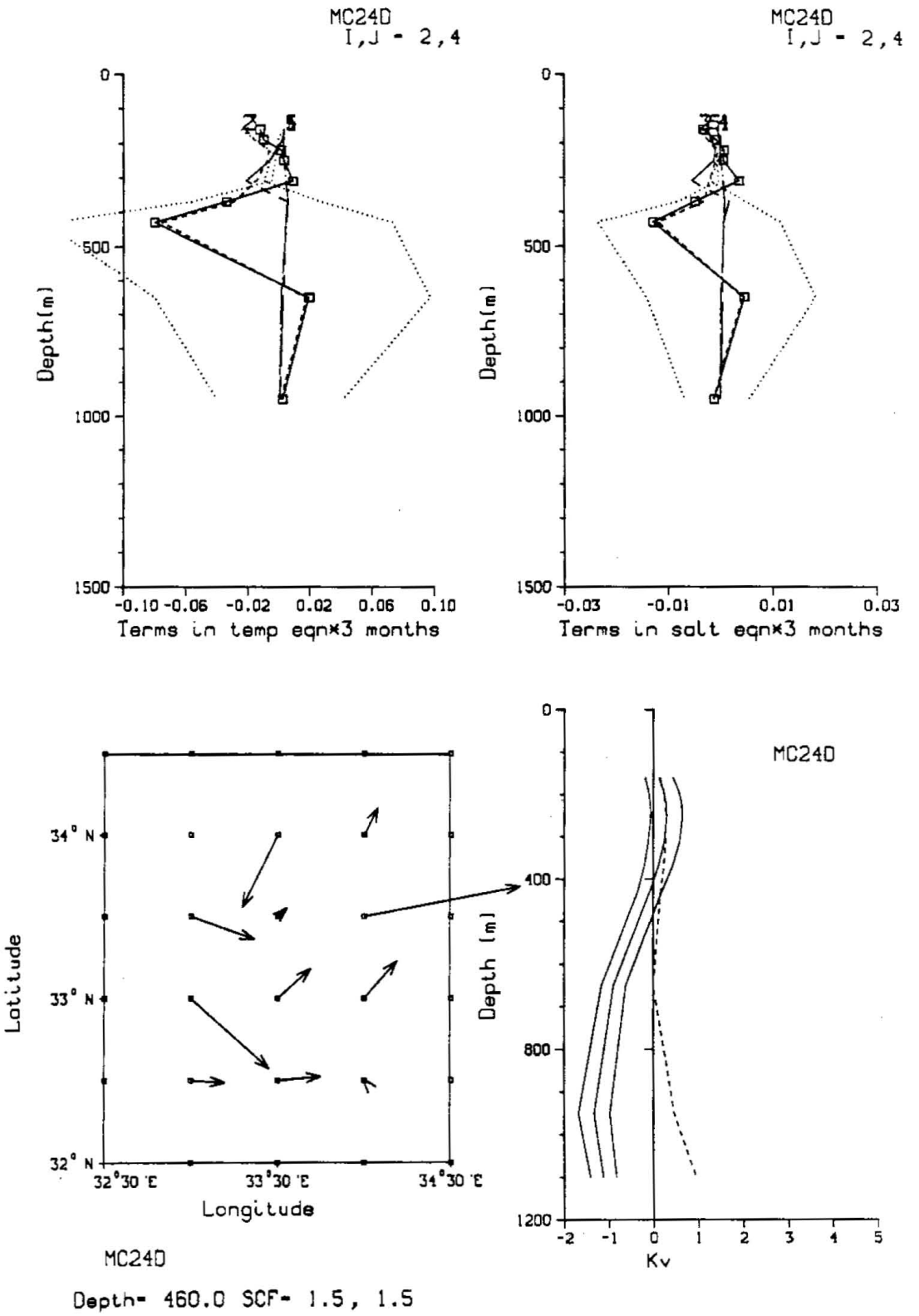

Figure 6: run [c] (see table 2).

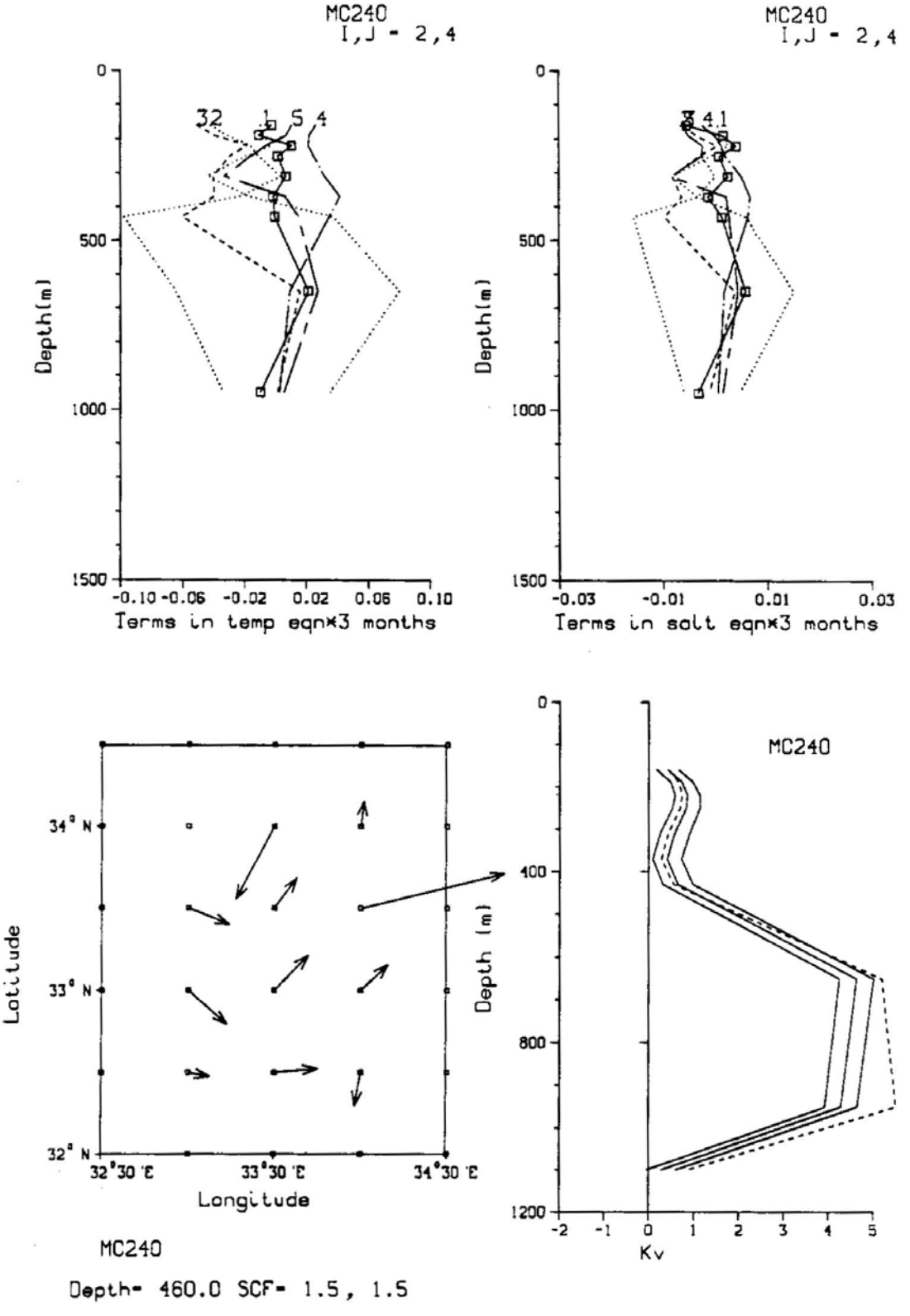

Figure 7: run [d] (see table 2).

shown, the mixing terms are always much smaller than the horizontal advection terms. The addition of mixing does not reduce the residuals significantly, and as mentioned before, the mixing coefficients cannot be completely resolved by the inverse, nor can the vertical velocities.

In the last run listed in table 2, ([e]), the vertical diffusivities were given larger weight, by specifying their expected value (column weights) to be $10\text{cm}^2/\text{sec}$, instead of only $1\text{cm}^2/\text{sec}$ chosen for the previous runs. This was done in the hope of better resolving the mixing coefficients, and the average diagonal term for the mixing coefficients in the VV^T matrix did actually increase from 0.37 to 0.54. But although they were somewhat better resolved, the mixing coefficients were still of order $1\text{cm}^2/\text{sec}$, and the mixing terms in the temperature and salt equations could still not reduce the residuals significantly.

One may conclude that the mixing terms cannot be effectively used by the model and that mixing parameterized by eddy coefficients may not be the physics perhaps missing in the ideal model. In any case, the vertical mixing coefficients are not likely to be much larger than $1\text{cm}^2/\text{sec}$ as indicated by the results of run ([e]). There are, on the other hand, several arguments in favor of keeping some form of mixing in the model. The addition of vertical diffusion did change the structure of the residuals at the deeper levels to some extent. Also, although vertical mixing coefficients are resolved to about 40% only, their vertical structure is consistent in all the six cruises analyzed, which enforces our confidence in their relevance to the physics.

In view of these arguments, and especially because one believes that some mixing does occur in the ocean, it was decided to keep in the model the vertical diffusion parameterized by a vertically varying eddy coefficient. Horizontal diffusion is not included, because while one tends to trust *vertical* derivatives of the data due to the high vertical resolution of the CTD data, calculating the second order *horizontal* derivatives is undesirable. Because the vertical scales of the features present in the data range

from about 300m (the intermediate salinity maximum) and up, we allow for variations of similar scale in the mixing coefficients, and set $N_\nu = 10$ [see (9)].

In spite of the uncertainly concerning the parameterization of the mixing processes, all the different models shown in table 2 give almost identical horizontal velocity fields. Also, although the residuals may indicate some missing physics, they are still acceptable and certainly smaller than those obtained by assuming an arbitrary level of no motion. We have also examined the sensitivity of the results to the choice of initial reference level. The well resolved horizontal reference velocities are not sensitive to the initial choice of reference level, while unknowns that are not very well resolved (vertical velocity) are more sesitive to it. We therefore conclude that the results — in particular for the horizontal velocity field — are believable, and proceed to use the final inverse model chosen here to analyze the data from all the six summer cruises.

5. Results for the six summer cruises

The model described in section 3 and refined in section 4 in now applied to the data from the six cruises chosen to represent the deep summer circulation of the region. The initial reference level for the calculation was chosen as the deepest level with data in all stations. This depth is 460m for four of the cruises, and 400m for the remaining two (MC14, MC19).

The results of the inversions, both velocity fields and mixing coefficients, are shown in figures (9–12). The velocity field is shown by both arrows indicating the velocity magnitude and direction, and by 'stream lines' calculated from the absolute velocity field found by the inverse. Note that although the relative geostrophic velocity field is horizontally non divergent, the absolute one, including the reference velocities calculated by the inverse, may not be. This is a result of the small number of horizontal CTD station in the data set. In order to require the reference velocity to be horizontally non divergent, we need to add to the model equations of the form

$$\frac{u(x_{i+1}, y_j, z_0) - u(x_{i-1}, y_j, z_0)}{\Delta x} + \frac{v(x_i, y_{j+1}, z_0) - v(x_i, y_{j-1}, z_0)}{\Delta y} = 0.$$

But this can be done only at horizontal locations (i, j) where reference velocities are calculated at all four neighboring points used in the above equation. Examining figures 9a and 10a we see that there are no more than two such horizontal locations for each cruise, and sometimes only one. We could not, therefor, require the reference velocity field to be non divergent at all horizontal grid points. We still calculate the 'stream function' from the horizontal velocity field as if it were non divergent, to help in presenting and interpreting the results.

The first obvious conclusion drawn from these results is that the steady circulation in the region is dominated by the very strong eddy activity. The velocity calculated for different cruises varies from 1–2cm/sec in MC24, to 10 cm/sec in MC13 and MC19. Even when considering cruises that are close in time (MC14 and MC15, or MC18 and

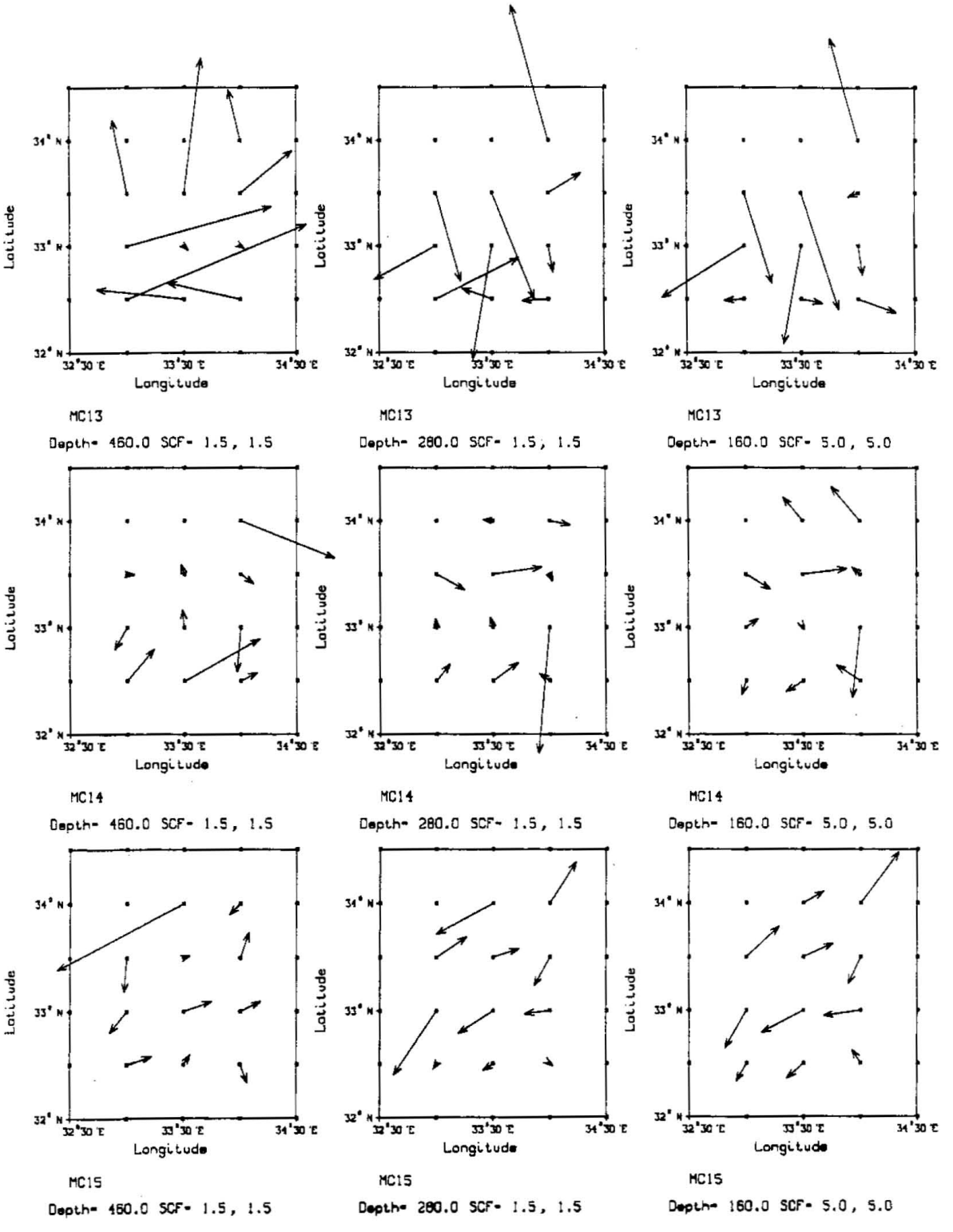

Figure 8a: The velocity field for cruises MC13, MC14, MC15, at three levels. (a) stick diagrams.

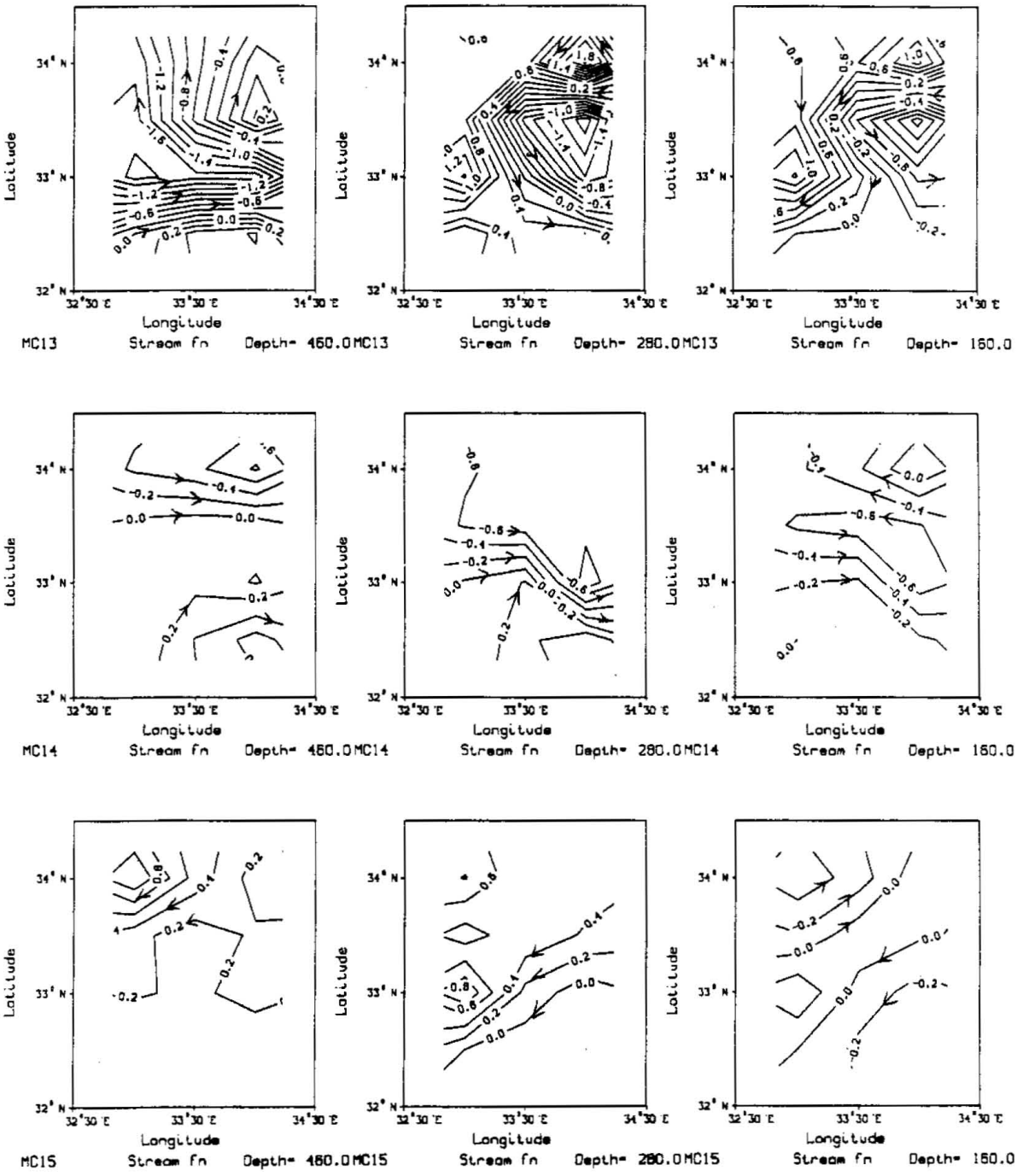

Figure 8b: The velocity field for cruises MC13, MC14, MC15, at three levels. (b) 'stream lines' drawn from the horizontal velocities.

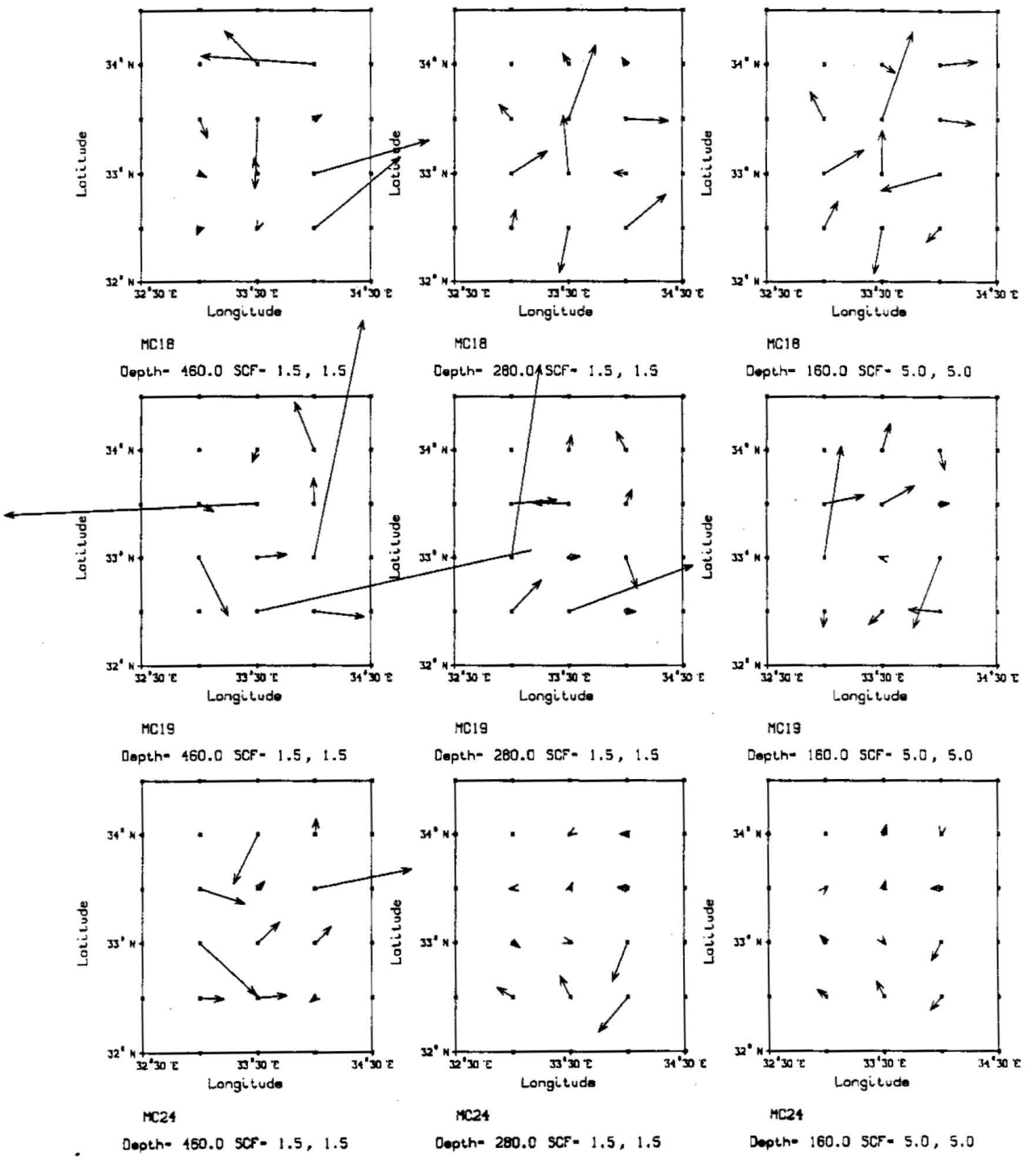

Figure 9a: Same as fig 8a, for MC18, MC19, MC24.

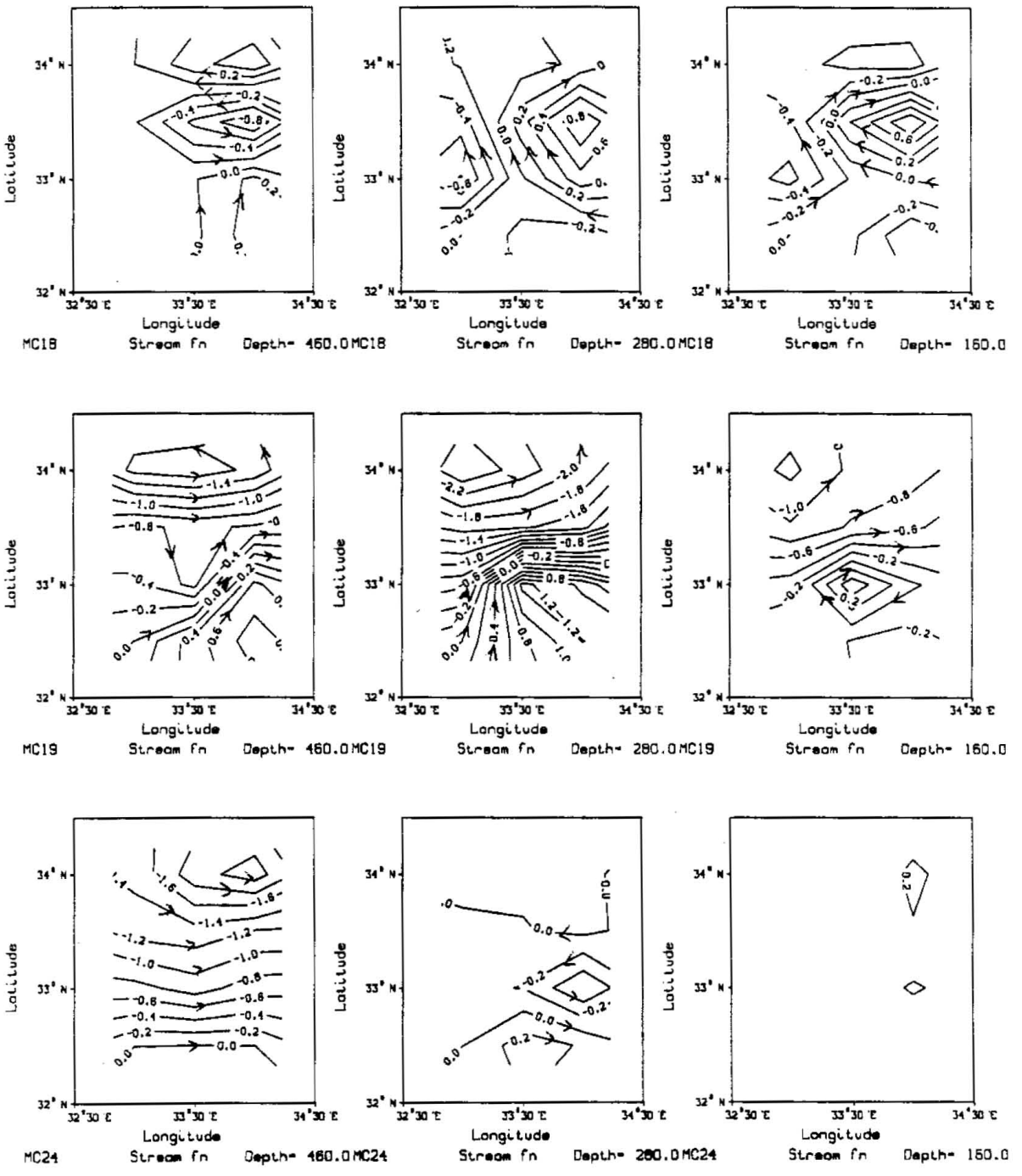

Figure 9b: Same as fig 8b, for MC18, MC19, MC24.

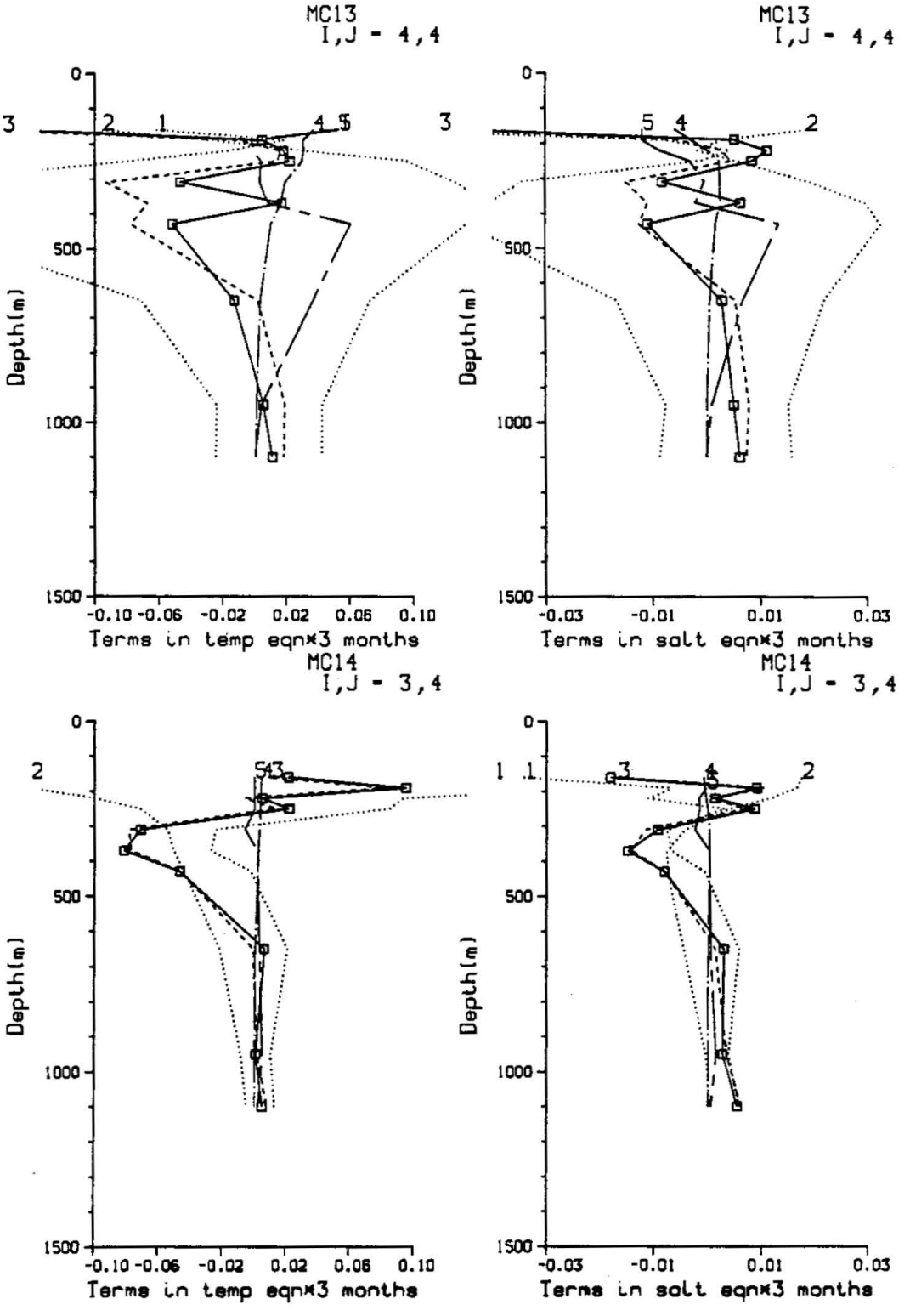

Figure 10a: The different terms in the advection diffusion equations for cruises MC13 and MC14, for one horizontal location. See caption for figures 4–7 (Table 3) for the meaning of the different lines.

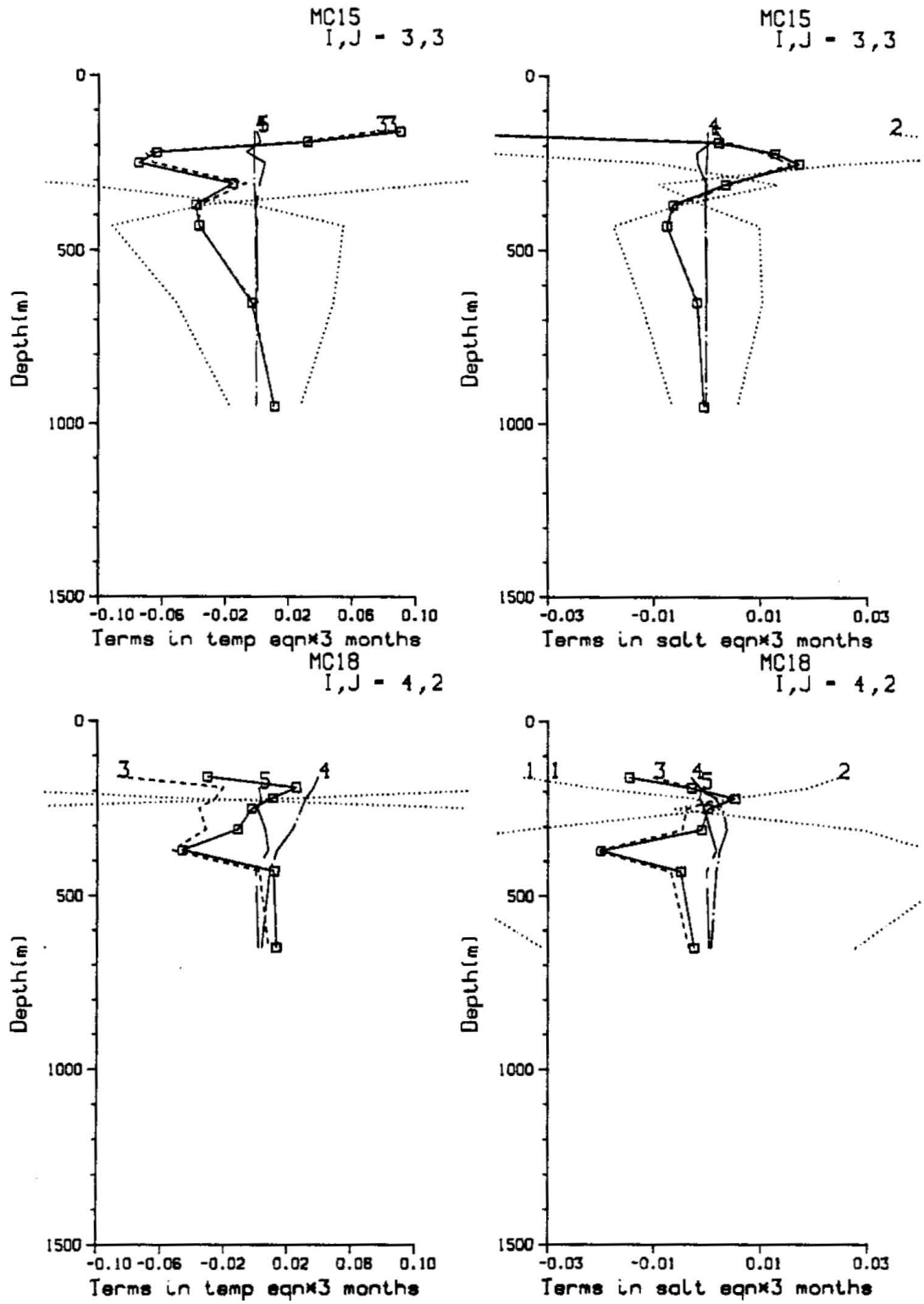

Figure 10b: Same as figure 10a, for cruises MC15 and MC18.

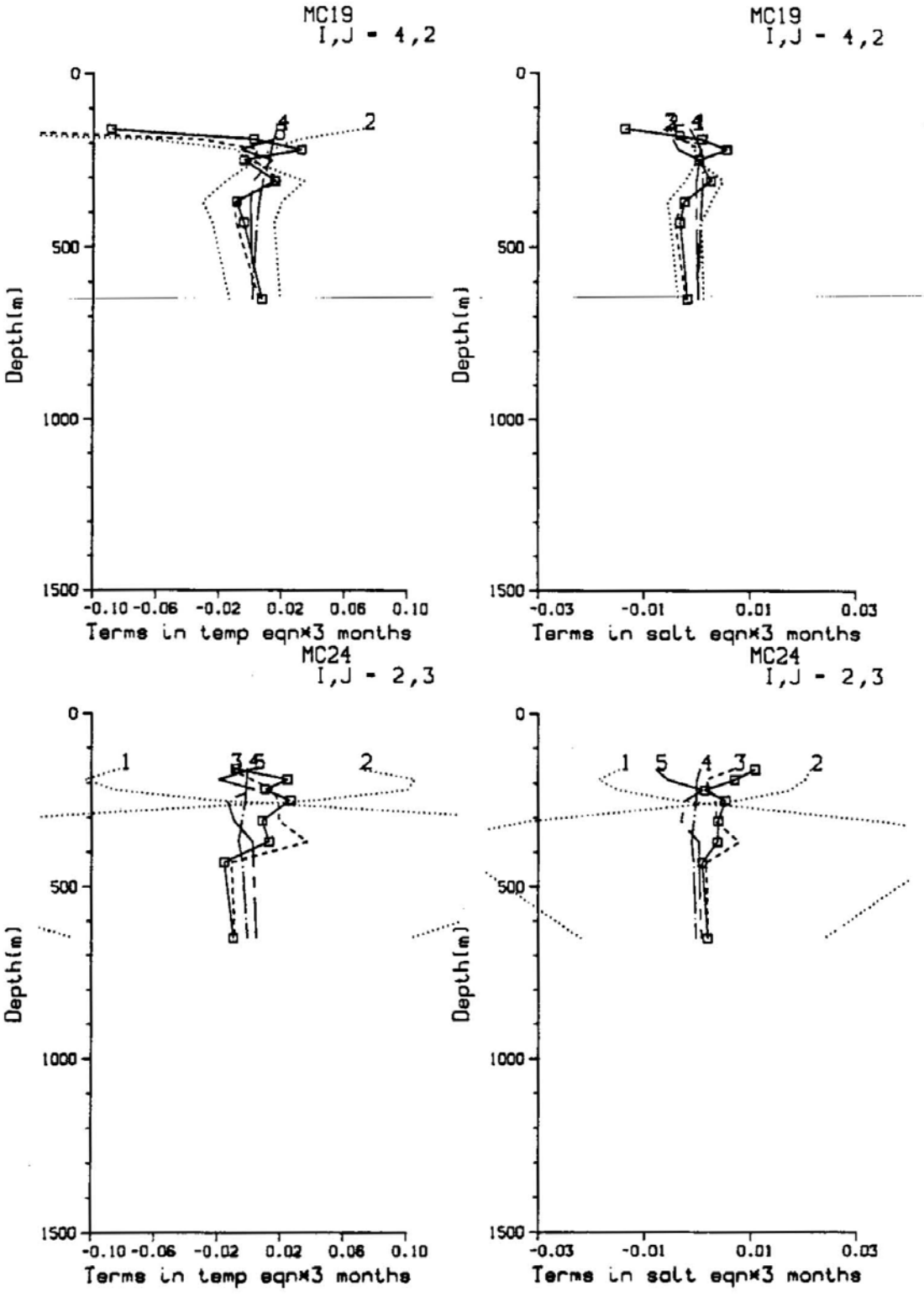

Figure 10c: Same as figure 10a, for cruises MC19 and MC24.

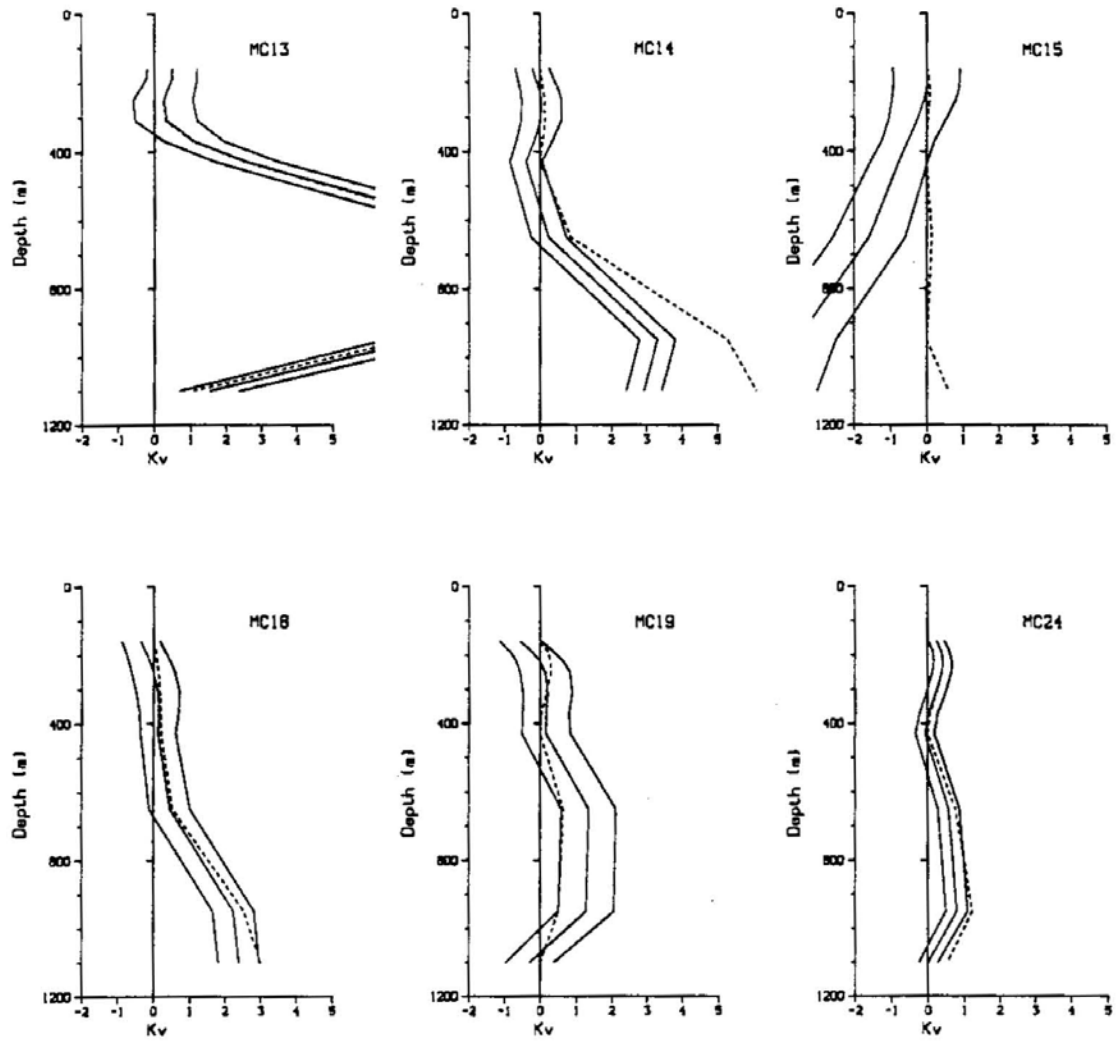

Figure 11: Profiles of the vertical mixing coefficients calculated for all of the six cruises.

MC19), it is difficult to point to similar structures in the calculated velocity fields, indicating the short time scales of the eddies.

Having calculated the velocity field for the six cruises, we can re-examine the physics used to describe the data, and try to see whether or not it is the appropriate one for the region. The residuals found for most of the cruises are acceptable according to the criteria described in the previous sections. There are problems, however, with the more energetic cruises, MC13 and MC19. The residuals of the temperature and salinity equations evaluated at some locations were larger than may be allowed due to errors in the data and the natural variability around the mean summer fields.

There are several possible sources for these somewhat large residuals. We have tried to use only deep data (below 160m) in order to avoid the direct influence of the time dependent surface processes. Still, it is possible that the effects of the variable wind forcing or of the strong surface evaporation and building of high surface salinity values during the winter did penetrate deeper that 160m, therefore violating our steady-state assumption. This assumption is also questionable to some extent when we consider the very different circulations found for the different cruises, indicating the strongly variable character the region.

Our results seem to suggest that future analysis of quasi synoptic data from this region should probably include the possibility of time change in the model. The strong variability, found even when using data from one season only, also suggests the need for very careful use of climatological data from the region. Using non–smoothed data combined from many sources and collected at many different times, may lead to a wrong circulation pattern for the region. As will be discussed in the next section, smoothing the climatological data may help in calculating the time averaged horizontal velocities, although it may cause problems with the mixing coefficients calculated by the inverse.

6. The time-mean circulation

• *Motivation:* Much of our knowledge of the oceanic general circulation comes from analyzing hydrographic data collected over many years, by many researchers, and using the dynamic method. In recent years, dynamic calculations were used together with inverse methods, to extract more information out of the available data and eliminate some of the arbitrariness in the assumption of level of no motion (Wunsch, 1978). But the data coverage of the different ocean basins is not very satisfactory, and even in the best observed regions, one has to use data from many different sources to study the large scale circulation (Worthington, 1981). We know now that the averaged large scale circulation is masked by a very energetic time dependent field of eddies and meanders. This makes it very difficult to obtain a consistent picture of the large scale, time–averaged circulation, by using many non–synoptic data sets patched together. One may encounter problems of inconsistency between different data sets—such as different locations of the Gulf Stream in hydrographic sections taken at different times (Wunsch, 1978) etc.

To try and overcome some of these problems, people have tried to combine data from different sources and different times into one averaged and smoothed data set, in the hope that it represents the time mean fields (Levitus, 1982). One can then use inverse methods or dynamic calculations, to calculate a velocity field from this smoothed data set (Olbers et al, 1985, Hogg, 1986). One hopes that the velocity field obtained from the averaged data set is actually an estimate for the time averaged velocity field. But is it?

The present data set samples the same region at many different times, each giving a quasi-synoptic picture of the circulation at the time of the measurement. This gives us an opportunity to examine the problem of calculating the averaged velocity field from hydrographic data. Although the region covered by the data is small, it is close to the scale of the general circulation for the eastern Mediterranean, and it is much larger

than the mesoscale eddies for this region. We believe, therefore, that the discussion here may be relevant to the use of hydrographic data for investigating the general circulation of larger oceans.

• *Calculating the average velocity field:* Ideally, when considering the time-mean circulation, one divides all fields into average and time dependent parts

$$\begin{aligned} u &= \overline{u}(x,y,z) + u'(x,y,z,t); \qquad \overline{u'} = 0, \\ T &= \overline{T}(x,y,z) + T'(x,y,z,t); \qquad \overline{T'} = 0. \end{aligned} \tag{1}$$

Substituting these into the temperature equation, and averaging over time, we have

$$\overline{u} \cdot \nabla \overline{T} = -\nabla \cdot (\overline{u'T'}) + \mathcal{F}. \tag{2}$$

The term $\nabla \cdot (\overline{u'T'})$ is the heat flux convergence due to mesoscale eddies and small scale turbulence, while $\mathcal{F}$ collects the molecular diffusion terms. Parameterizing the eddy fluxes by eddy mixing coefficients, and neglecting the molecular terms, we then have (Pedlosky, 1979)

$$\overline{u} \cdot \nabla \overline{T} = -\nabla \cdot (\kappa \nabla \overline{T}). \tag{3}$$

Although the division into averaged and time dependent fields cannot normally be used in the analysis of hydrographic data, it is possible to follow it to some extent using the present data set.

We will try and calculate the average circulation of the eastern Levantine basin in two ways. First, we calculate the averaged fields $(\overline{T}, \overline{S}, \overline{\rho},)$, and use the inverse model with the averaged data to calculate a velocity field. This calculation mimics those based upon average data set such as that of Levitus (1982). The inverse model used is the one described before (section 2).

The second way we calculate the average circulation is closer to the procedure outlined in equations (1) to (3) above. We invert the data from the 6 cruises to calculate

the velocity field and mixing coefficient for each cruise, and then average the 6 velocity fields to obtain the time averaged velocity field, and the average mixing coefficient.

But the average mixing coefficient is not what we are after according to (1)–(3). The mixing coefficient in (3) parameterizes the eddy mixing terms obtained by averaging the full temperature equation, and this is what we need to calculate here. Having calculated the time–averaged velocity and tracer fields, we use them to calculate the residuals left by the advection of the average temperature by the average velocity

$$\overline{u} \cdot \nabla \overline{T} = r(x, y, z) \neq 0. \tag{4}$$

These residuals come from the eddy mixing terms, $\nabla \cdot (\overline{u'T'})$, not represented in the model yet. We now assume, as in (3), that they can be parameterized by eddy mixing coefficients

$$\overline{u} \cdot \nabla \overline{T} = r(x, y, z) = -\nabla \cdot (\kappa \nabla \overline{T}). \tag{5}$$

The lhs in (5) is known from the previous calculations, and we can use (5) to obtain a set of linear equations for the mixing coefficients. Inverting for the mixing coefficients, we find the mixing coefficients consistent with the average circulation calculated before. The different ways of calculating the average circulation and the mixing coefficients are summarized in table 3.

Assuming that errors in different cruises are not correlated, the error estimate for the average fields is $\frac{1}{\sqrt{6}}$ of the average of the error estimates for the single cruises. This reduction can be seen when comparing the error bars for the mixing coefficients in ([inv{avg}]), and ([avg{inv}]).

• *discussion.* Comparing the velocity fields obtained by the two different procedures outlined above, ([inv{avg}], [avg{inv}] in table 3) we find that they are surprisingly similar — in particular the reference level velocity at 460m depth. In contrast, the mixing coefficient calculated from the average tracer fields ([inv{avg}]) is significantly

run	description	figures
[inv{avg}]	Inversion of the averaged $\overline{T}, \overline{S}, \overline{\rho}$ fields.	12,13
[avg{inv}]	Average of the velocity fields and mixing coefficients obtained by inverting each of the six cruises separately.	12,13
[mix{avg}]	Calculating the mixing coefficients by using the average velocity $\overline{u}$ from ([avg{inv}]), and average temperature and salinity fields, $\overline{T}$ and $\overline{S}$, to form the equation $\overline{u} \cdot \nabla \overline{T} = \nabla \cdot (\kappa \nabla \overline{T})$ and solve it for κ.	12,13

Table 3: Calculating the average circulation. The notation for the different runs describes their meaning: [inv{avg}] is the inverse of the averaged fields, [avg{inv}] is the average of the six inversions, [mix{avg}] is the calculation of mixing coefficients dynamically consistent with the average circulation.

different from that averaged over all cruises ([avg{inv}]), and the coefficient obtained by inverting $\overline{u} \cdot \nabla \overline{T} = (\lambda_v \overline{T}_z)_z$ ([mix{avg}]).

Off hand, at least, one would consider this similarity of the velocity fields to be somewhat surprising, because the inverse procedure is nonlinear, and is expected to give different results when the order of averaging and inversion are exchanged. The nonlinearity has two sources. The equations for the reference velocities are of the form

$$u_0 T_x + v_0 T_y + w_0 T_z - (\lambda_v T_z)_z = -(u_r T_x + v_r T_y + w_r T_z) \tag{6}$$

The relative velocities (u_r) are a function of the density field, so that the rhs depends nonlinearly on the data. Furthermore, writing the system of equations for the reference velocities and mixing coefficients as $Ab = \Gamma$, the solution is, schematically, $b = A^{-1}\Gamma$. Because Γ is $u_r \cdot \nabla T$, and A contains derivatives of the temperature and salinity fields, the solution for b is cubic in the data

$$\begin{aligned} b = A^{-1}\Gamma &\sim \left(\frac{\partial T}{\partial x_i}\right)^{-1} u_r \frac{\partial T}{\partial x_i} \\ &\sim \left(\frac{\partial T}{\partial x_i}\right)^{-1} \left(\frac{\partial \rho}{\partial x_i}\right) \left(\frac{\partial T}{\partial x_i}\right) \end{aligned} \tag{7}$$

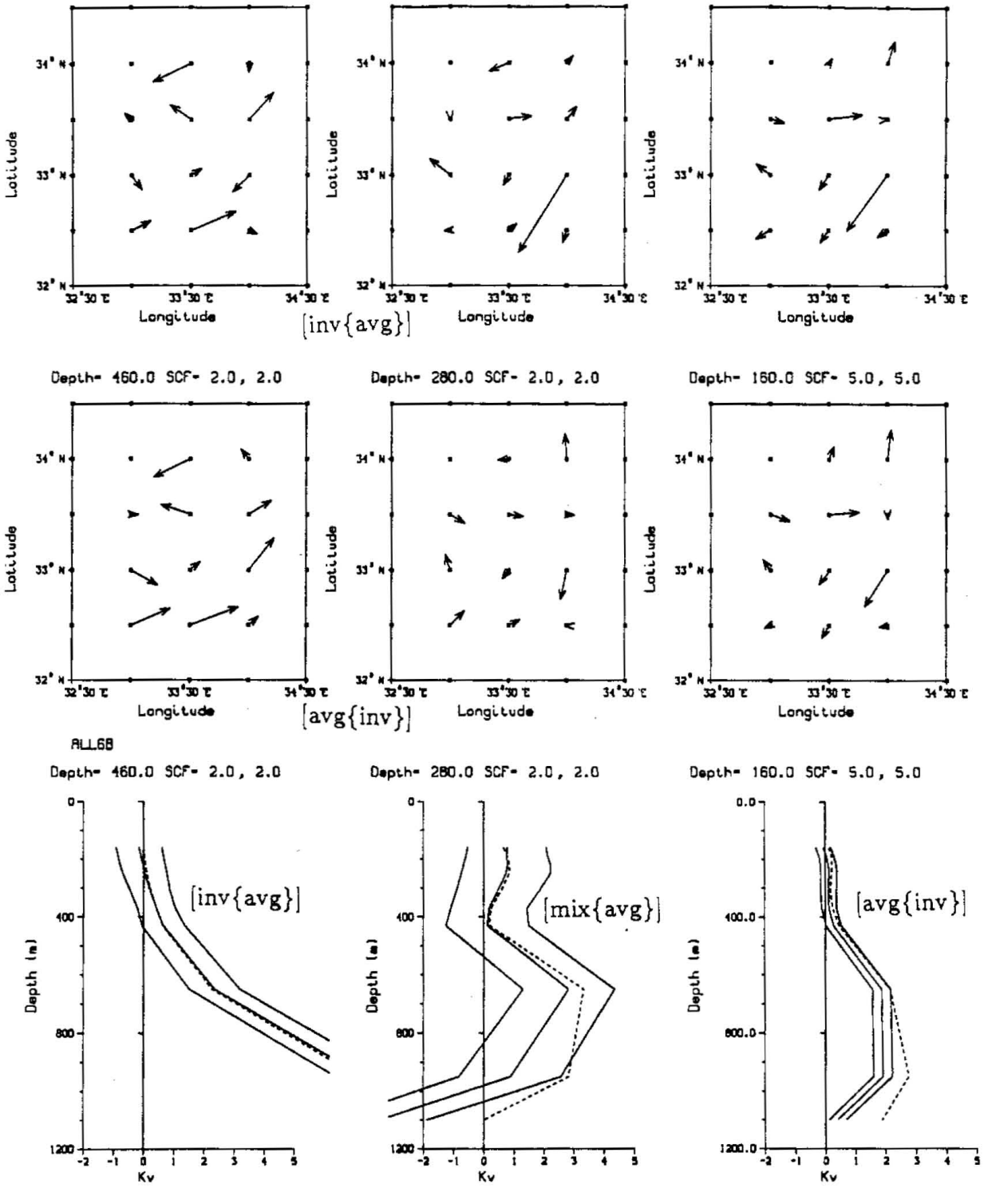

Figure 12: Calculating the average circulation (table 3): The velocity field at three levels, and the mixing coefficients calculated by the three different methods given in table 3.

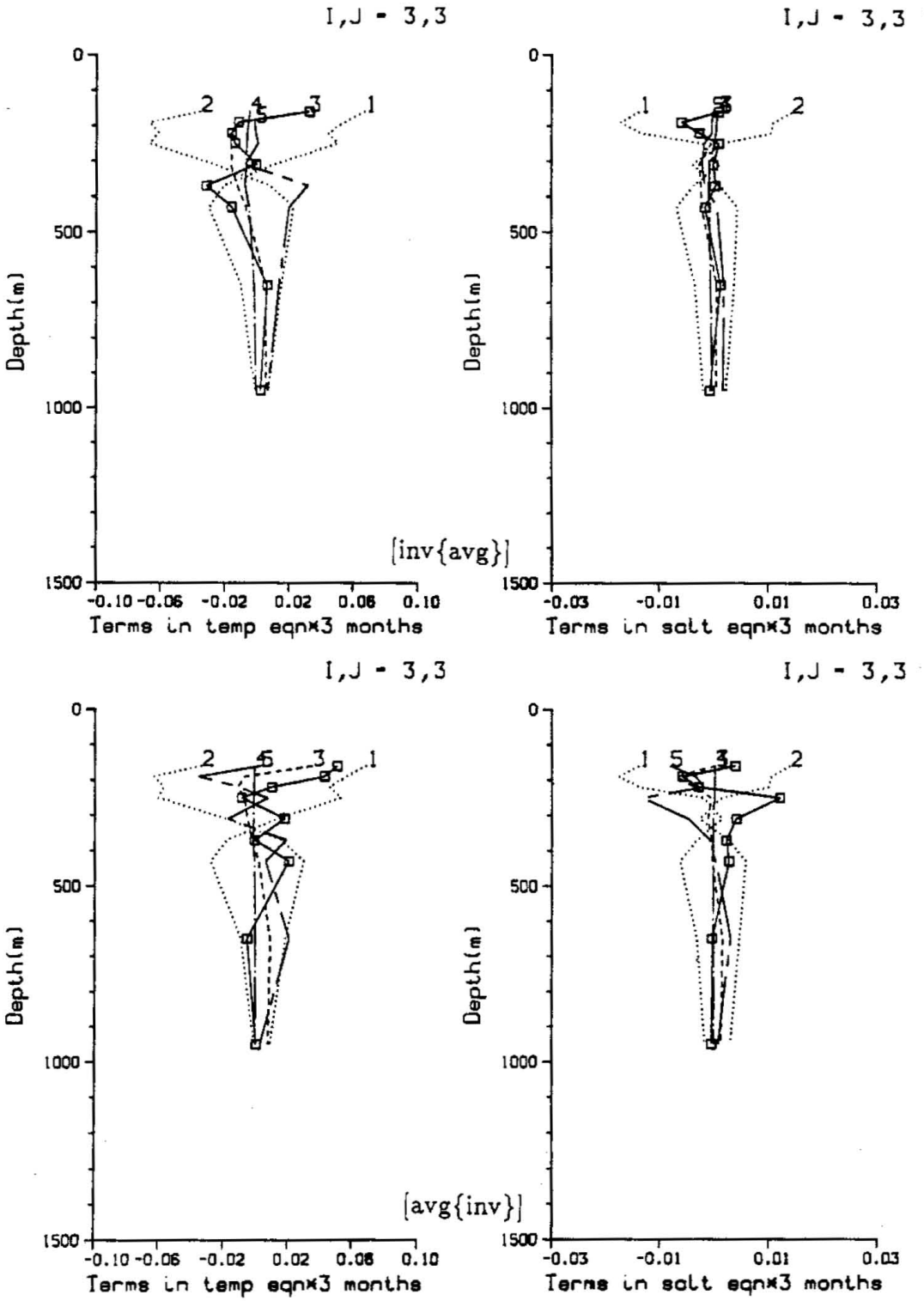

Figure 13: Calculating the average circulation: Terms in temperature and salinity equations, calculated by the inverse, as described in table 3. See captions for figures 3–7 for more details.

Let us denote the data and solution for the reference velocity and mixing coefficients of the ith cruise by $T^{(i)}$, $S^{(i)}$, $\rho^{(i)}$, $b^{(i)}$, and the average fields by

$$\overline{b} = \frac{1}{6}\sum_{i=1}^{6} b^{(i)} = \frac{1}{6}\sum_{i=1}^{6} (A^{(i)})^{-1}\Gamma^{(i)}. \tag{8}$$

More generally, we can write

$$\overline{b} = \overline{A^{-1}u_r \cdot \nabla T} \tag{9}$$

where the average is over many realizations of the fields. The velocity calculated in ([inv{avg}]) can be written schematically as

$$\text{“}\overline{b}\text{”} = (\overline{A})^{-1}\overline{u}_r \cdot \nabla\overline{T}. \tag{10}$$

The two solution $\overline{b}$ and $\text{“}\overline{b}\text{”}$ are clearly different:

$$\begin{aligned}
\overline{b} - \text{“}\overline{b}\text{”} &\sim \overline{A^{-1}u_r \cdot \nabla T} - \overline{A^{-1}}\overline{u}_r \cdot \nabla\overline{T} \\
&\sim \overline{(\overline{A} + A')^{-1}(\overline{u}_r + u_r') \cdot \nabla(\overline{T} + T')} - \overline{A}^{-1}\overline{u}_r \cdot \nabla\overline{T} \\
&\sim \overline{A}^{-1}\overline{u_r' \cdot \nabla T'} + \overline{u}_r\overline{(A')^{-1}\nabla T'} + \nabla\overline{T}\overline{(A')^{-1}u_r'} + \overline{(A')^{-1}u_r' \cdot \nabla T'}.
\end{aligned} \tag{11}$$

Roughly speaking, the difference between the average velocity field (and mixing coefficients) and the velocity calculated from the average tracer fields is due to the transport of heat (salt) by the eddies. Equation (11) makes it clear why we expect the velocity and mixing coefficients calculated in the two different ways to be different. But as was pointed out before, the velocities in ([inv{avg}]) and ([avg{inv}]) are actually very similar, and it is only the mixing coefficients that are different. Before trying to explain this observation, let us stress that our averages are only over 6 realizations — hardly an ensemble average — and that it may therefore be somewhat speculative to draw any definitive conclusions concerning the runs in table 3. Assuming, however, that the difference between the results obtained for the velocities and mixing coefficients is real, we will try to explain it in terms of the physical processes involved.

We have mentioned above that the difference between $\overline{b}$ and "$\overline{b}$" is due to the effects of the time dependent eddy field on the temperature and salinity fields. Considering for example the first term on the rhs of (11), we see that the difference between $\overline{b}$ and "$\overline{b}$" may be assumed small if the transport of heat by the eddies $\nabla \cdot (\overline{u'T'})$ is much smaller than the advection by the mean circulation $\overline{u} \cdot \nabla \overline{T}$. The dominant physical process affecting the temperature and salinity fields in the ocean is the advection by the horizontal velocity field. The transport of water properties by the eddy field is a second order effect, and therefore the eddy terms in the expression (11) for $\overline{b} -$ "$\overline{b}$" may be assumed to be small. As a result, we expect the dominant horizontal advection terms in the T and S equations to be similar in the two estimates $\overline{b}$ and "$\overline{b}$" for the average circulation. And, in fact, the horizontal flow fields in ([inv{avg}]) and ([avg{inv}]) are quite similar.

The situation is very different for the estimates of second order physical processes like mixing or advection by the vertical velocity. As we have seen, the inverse procedure reduces the larger part of the residuals by determining the horizontal velocity field. The remaining small residuals are then reduced, if possible, by adjusting the vertical velocity and mixing coefficients. Now, the (very) small difference between the actual average horizontal velocity in $\overline{b}$ and the horizontal velocities in "$\overline{b}$" may completely change the small residuals left after the calculation of the horizontal velocities. A few percent change in uT_x and vT_y may change both the structure and the magnitude of the small residuals. The difference in the residuals left by the horizontal velocities in $\overline{b}$ and "$\overline{b}$" is therefore small in absolute terms, but large relative to the size of the already small residuals, and relative to the magnitude of the diffusive terms, $\nabla \cdot (\kappa \nabla T)$.

We can now try to understand why the mixing coefficients calculated in the different ways described in table 3 ([inv{avg}], [avg{inv}] and [mix{avg}]) are so different. The mixing coefficients are calculated by the inverse in a way that minimizes the small residuals left by the horizontal advection. Because these residuals may be so different

in the three different runs in table 3, the resulting mixing coefficients will also be very different. In other words, the results for the second order physical processes (mixing coefficients, w) are very sensitive to small changes in the dominant processes (u, v).

One can summarize the difference between the actual time-mean circulation obtained by averaging instantaneous velocities and then solving for the dynamically relevant mixing coefficients ([avg{inv}], [mix{avg}]) and the circulation obtained from the average ($\overline{\rho}$, $\overline{T}$ and $\overline{S}$) fields ([inv{avg}]) as follows. The dominant horizontal velocities may be expected to be similar, but the second order mixing coefficients obtained from the averaged fields are, in principle, completely different from the correct ones calculated by actually parameterizing $\nabla \cdot (\overline{u'T'})$.

Note that according to the above argument, even the average *horizontal* velocities may not be calculated correctly from the mean tracer fields if the horizontal advection is not the dominant physics in the tracer equations. The small difference in the horizontal velocities in $\overline{b}$ and "$\overline{b}$" may be of the magnitude of the horizontal circulation at deep levels, and then the circulation calculated at these levels from the mean fields is not a good estimate for the actual time-mean circulation there.

Let us assume for a minute that we have data from many realizations of the instantaneous fields, and try to find out how accurate this data should be for us to be able to follow the procedure outlined in table 3 ([avg{inv}], [mix{avg}]), and obtain *reliable* estimates for both the average circulation and the appropriate mixing coefficients. Let $\varepsilon[\overline{u}\overline{T}_x + \overline{v}\overline{T}_y]$ be the total error in the estimate for the horizontal average advection terms, including measurements errors in T, and in the absolute averaged velocity field obtain from the instantaneous data. To overcome the 'sensitivity' of the estimates for mixing coefficients to errors in the horizontal advection terms, we want according to the above discussion

$$\varepsilon[\overline{u}\overline{T}_x + \overline{v}\overline{T}_y] \ll \nabla \cdot (\overline{u'T'}) \sim \nabla \cdot (\kappa \nabla \overline{T}). \tag{12}$$

This condition assures that the structure and magnitude of the residuals which are parameterized by the mixing coefficients [see (4)–(5)] cannot be radically changed by the errors in $\overline{u}\overline{T}_x + \overline{v}\overline{T}_y$. A careful examination of the errors in $\overline{u}\overline{T}_x + \overline{v}\overline{T}_y$ for the data we have used above (table 3) indicates that (12) is not satisfied, so that we are not able to confidently calculate the mixing coefficients parameterizing the time dependent motions.

It is worth mentioning at this point that evaluating the *instantaneous* velocities from quasi–synoptic hydrographic data poses some problems as well. Tracer distributions measured at any time are a result of both the instantaneous velocities, and of mixing by time dependent motions over long periods preceding the time of the measurement. Even if one's data resolves the mesoscale eddies at some time, (which is not normally the case) it is impossible to explain the large scale tracer distribution as being a result of the instantaneous advection only, ignoring the mixing effects. A correct parameterization of the long term mixing by eddies is necessary even for the calculation of the instantaneous velocity field. Also, as indicated by the results of the six inversions in section 5, it is not clear whether one may ignore the time change terms in the tracer equations when using instantaneous data to calculate an instantaneous velocity field. However, as in the calculation of the average velocity field, the first order instantaneous horizontal velocities can probably be calculated correctly even when neglecting time change terms, and without a good parameterization of the mixing. It is only the second order instantaneous fields (e.g. vertical velocity) that will suffer in the absence of a good estimate for the effects of long term mixing by eddies.

• *Conclusions.* We have considered the problem of estimating the time averaged general circulation, and the appropriate mixing coefficients from hydrographic data. The above calculations and discussion seem to indicate that one can safely calculate the time–averaged horizontal velocity field from an estimate of the averaged density and tracer fields (such as the Levitus (1982) data set). It does not seem feasible, however, to obtain

reliable estimates for the mixing coefficients parameterizing the time dependent eddy terms $\nabla \cdot (\overline{u'T'})$, by using only the average density and tracer fields. Furthermore, even with quasi–synoptic data *from many different realizations* available, it is difficult to reliably calculate the mixing coefficients parameterizing the time dependent eddy field. Such a calculation requires the data to be very accurate, and the model to correctly include second order physics such as mixing or time variability.

The difference between the mixing coefficients calculated by actually parameterizing the eddy fluxes $(\nabla \cdot \overline{u'T'})$, and those calculated directly from the mean averaged tracer fields, raises the question of what is actually calculated in the second way. One can regard the procedure used to obtain the coefficients from the averaged fields as an operational definition of what they represent. But then — are the results meaningful outside of the calculation?

In fact, the difficulties in calculating physically meaningful mixing coefficients from data are only one part of the problem. One wonders whether the whole concept of parameterizing the eddy fields by mixing coefficients is a useful one. The results of the calibration runs in the previous sections suggest that the inverse model could not effectively use the mixing coefficients to reduce the residuals and better explain the data. Olbers et al. (1985) calculated long and cross isopycnal mixing coefficients for both vorticity and tracers, but found that they were not distinguishable from zero in most cases. One would like to be able to use models — whether numerical models, inverse methods, or data assimilation techniques — that do not rely too heavily on eddy coefficient parameterization.

Clearly, the numerical values of the mixing coefficients is not what one is actually after. The value of these coefficients lies in helping to answer questions about the ocean circulation, such as what is the effect of ocean heat transport on climate changes, or

what is the role of the oceans in the global CO_2 cycle, etc. Such questions should probably be answered using methods which do not depend on sub grid parameterization, at least as far as the information we are interested in is concerned.

Appendix to chapter 3: including inequalities in the SVD solution

Lawson and Hanson (1974, p. 168) gave an algorithm (LSI/LDP, which stands for Least Squares with Inequality constraints, and Least Distance Programming) for incorporating linear inequalities in the SVD solution of a linear system of equations. Given an equations matrix $A_{n\times m}$ of rank m, a right hand side $\Gamma_{n\times 1}$, inequalities matrix and rhs $G_{n_1\times m}$ and $h_{n_1\times 1}$, the algorithm finds the vector solution b which minimizes $\|Ab-\Gamma\|^2$ subject to $Gb \geq h$. The algorithm cannot be applied to under determined problems ($n < m$) or to formally over determined system ($n > m$) where the rank of A is less than m, as happens in the model presented in chapter 3. This appendix presents an extension of the LSI/LDP algorithm, to allow for rank deficient A matrices.

Fu (1981) incorporated inequalities in the SVD solution of an under determined system by looking for the smallest vector from the null space of the equations matrix A that will satisfy the inequalities. This method can satisfy only the null space part of the inequalities, and it may give an unphysically large solution when the null space is too small (i.e. when the problem is not very under determined). These problems are demonstrated below by simple examples.

A different approach was taken by Olbers et al (1985) who used a tapered cutoff modification to the LSI/LDP algorithm to eliminate the effects of very small eigenvalues on the parameter variance. The advantages and disadvantages of tapered cutoff vs. sharp cutoff were discussed in detail by Wiggins (1972).

Example

Before going into the details of the mathematical formalism, consider the following simple example (shown also in figure A.1) demonstrating the difference between the approach here and in Fu (1981), and the difficulties with LSI/LDP when the system of equations is not full rank:

$$\text{Equation:} \qquad x + y = 3$$

$$\text{Inequalities:} \qquad y \geq 1, \qquad x + y \leq 2.$$

Fu's approach here is to find the SVD solution to the equation ($(3/\sqrt{2}, 3/\sqrt{2})$, dashed arrow in figure A.1) and then to look for the smallest null space vector which brings the solution into the feasible space determined by the inequalities (shaded area in figure A.1). The null space vector in this example, $(1/\sqrt{2}, -1/\sqrt{2})$, lies along the line $x + y = 3$), and therefore cannot bring the solution into the feasible space. More generally, the method is not able to satisfy the inequalities when one of the rows of G belongs to the range part of A.

The LSI/LDP algorithm would try to minimize $\|Ab - \Gamma\|^2$ (here $\|x + y - 3\|^2$), subject to the inequalities. The solution must therefore lie in the feasible space, as close as possible to the line $x + y = 3$. It is clear from figure A.1 that every point in the shaded region, along the line $x + y = 2$ is a possible solution to the problem posed by LSI/LDP, and the solution is not unique.

To make sure that the solution is unique even when the equations matrix is not full rank, one must add more constraints. The procedure outlined below requires the solution to have the smallest possible null space vector in addition to minimizing the residuals of the equations. The solution for the above example is then the point (1,1).

The formalism:

Given a system of equations $Ab = \Gamma$, and inequalities $Gb \geq h$, where A is an $n \times m$ matrix of rank k, Γ is a $n \times 1$ column vector, G is as $n_1 \times m$ matrix, and h an $n_1 \times 1$ column vector, the SVD of A is

$$A = U_{n\times k}\Lambda_{k\times k}{V^T}_{k\times m}. \tag{1}$$

The solution to the system of equations, without the inequalities, may be written (Wunsch, 1978) as

$$b = b_{SVD} + b_{null} = \sum_{i=1}^{k} \alpha_i V_i + \sum_{j=k+1}^{m} \beta_j V_j. \tag{2}$$

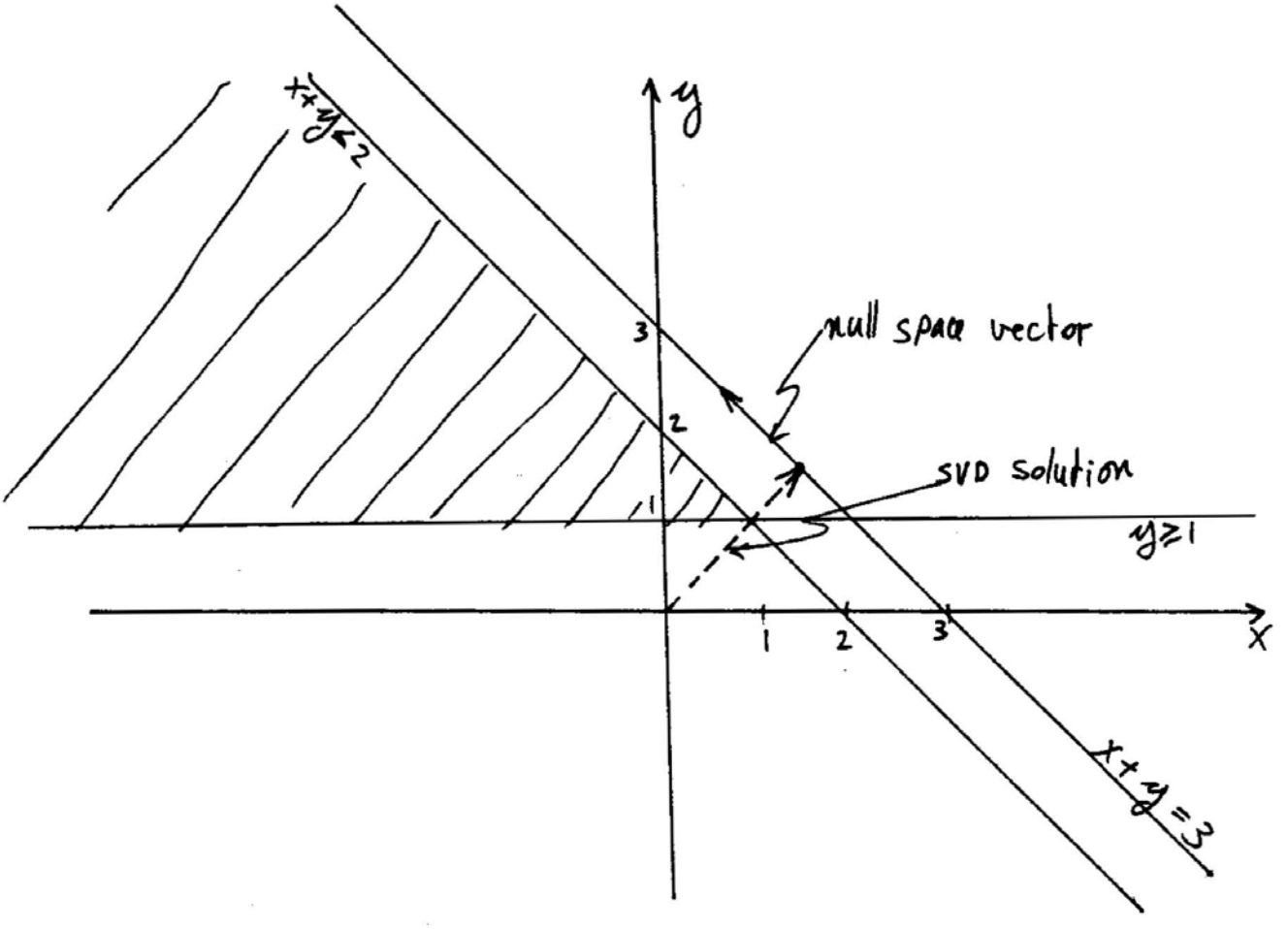

Figure A.1: Trying to solve non full rank system with LSI/LDP, Fu's method, and using the present approach. See text for details.

The first k V-vectors are the columns of the V matrix from the SVD of the equations matrix A. The other $m-k$ are orthonormal vectors spanning the null space part of A. Fu (1981) described a way of calculating these null space V-vectors.

We look for the solution vector b which solves the problem

$$\begin{aligned} &\text{minimize} && \|(U_{n\times k}\Lambda_{k\times k}V^T{}_{k\times m})b-\Gamma\|^2+\epsilon^2\|b_{null}\|^2 \\ &\text{subject to} && Gb\geq h. \end{aligned} \tag{3}$$

The small constant ϵ is discussed below. The solution to this problem is unique, because both the range and the null parts of b are constrained by the minimization. This is not the case when using LSI/LDP with a singular matrix A, as demonstrated by the example above. It is important to note that only the range part of the matrix A (the first k eigenvalues) is taken into account when the algorithm given below minimizes $\|Ab-\Gamma\|^2$ in (3). The solution to problem (3) is now found by transforming it to an equivalent LSI/LDP problem, and then using the Lawson and Hanson algorithm to solve it.

Let us now append $m-k$ equations to A, and form a modified set of equations

$$\hat{A}_{(n+m-k)\times m}b=\begin{pmatrix} A_{n\times m} \\ \epsilon V^T_{(m-k)\times m}\end{pmatrix}b=\begin{pmatrix}\Gamma_{n\times 1}\\ 0_{(m-k)\times 1}\end{pmatrix}=\hat{\Gamma}. \tag{4}$$

The rows of the matrix $V^T_{(m-k)\times m}$ are the null space V-vectors. The rank of this matrix is $m-k$, and because its rows are orthogonal to those of A, the rank of the modified equation matrix, $\hat{A}$, is $k+(m-k)=m$.

We may now use the LSI/LDP algorithm to solve the modified problem, with the full rank $\hat{A}$. The LSI/LDP problem is now

$$\begin{aligned} &\text{minimize} && \|\hat{A}b-\hat{\Gamma}\|^2 \\ &\text{subject to} && Gb\geq h. \end{aligned} \tag{5}$$

But

$$\begin{aligned}\|\hat{A}b - \hat{\Gamma}\|^2 &= \left\| \begin{pmatrix} A_{n\times m} \\ \epsilon V^T_{(m-k)\times m} \end{pmatrix} b - \begin{pmatrix} \Gamma_{n\times 1} \\ 0_{(m-k)\times 1} \end{pmatrix} \right\|^2 \\ &= \|Ab - \Gamma\|^2 + \epsilon^2 \|V^T_{(m-k)\times m} b\|^2 \\ &= \|Ab - \Gamma\|^2 + \epsilon^2 \|b_{null}\|^2 \end{aligned} \tag{6}$$

so that the modified problem (5) with the full rank equations matrix $\hat{A}$ is equivalent to the problem (3) which we want to solve.

The LSI/LDP algorithm requires that we know the SVD of the $\hat{A}$ matrix. This can be written in terms of the already known SVD of the smaller original equations matrix $A_{n\times m}$, and there is no need to recalculate the SVD for the larger matrix. Defining

$$\begin{aligned}\hat{U}_{(n+m-k)\times m} &= \begin{pmatrix} U_{n\times k} & 0_{n\times(m-k)} \\ 0_{(m-k)\times k} & I_{(m-k)\times(m-k)} \end{pmatrix}, \\ \hat{\Lambda}_{m\times m} &= \begin{pmatrix} \Lambda_{k\times k} & 0_{(m-k)\times(m-k)} \\ 0_{(m-k)\times(m-k)} & \epsilon I_{(m-k)\times(m-k)} \end{pmatrix}, \\ \hat{V}_{m\times m} &= \begin{pmatrix} V_{k\times m} \\ V_{(m-k)\times m} \end{pmatrix}, \end{aligned} \tag{7}$$

it is not difficult to see that

$$\hat{A} = \hat{U}\hat{\Lambda}\hat{V}^T.$$

Choosing ϵ

Figure (A.2) shows a simple example which demonstrates the effect of varying the magnitude of ϵ. The example is of two unknowns, one equation (the line a'–b), and one inequality (shaded area). The solution to problem (3) in this case must lie on the line a–b, in the feasible space, but its exact location is determined by ϵ. When ϵ is very small, minimizing $\|Ab - \Gamma\|^2 + \epsilon^2\|b_{null}\|^2$ is equivalent to minimizing $\|Ab - \Gamma\|^2$ only. There is a weak constraint only on the size of the null space vector, and the solution approaches the point b. If, on the other hand, ϵ is chosen larger, then the

algorithm tries to minimize the null space vector while staying in the feasible space, and the solution moves towards the point a.

There are two factors which help in choosing a 'good' ϵ for a given problem. In the model presented above, using a very small ϵ, (or using null space vectors only to satisfy the inequalities) leads to large null space vectors, which made the vertical velocities unphysically large ($O(10^{-3})$cm/sec). One would like to make sure that the magnitude of the parameters (unknowns) stays within some *a priori* limits, and this may be controlled by varying ϵ.

A second factor is the size of the residuals $\|Ab-\Gamma\|$. When determining the rank of A, one must usually truncate the eigenvalues at some value which is very small, but not zero, to avoid increase of noise level in the solution due to very small eigenvalues. The null space part of A contains, therefore, non zero eigenvalues. One may want to name this part of A the physical null space , to distinguish it from the mathematical null space which contains only strictly zero eigenvalues. With this in mind, let us calculate the residuals and determine their dependency on the magnitude of ϵ.

Let us assume that the rank of A was chosen to be k. The SVD of the matrix A, including the very small eigenvalues, is

$$\begin{aligned} A = U\Lambda V^T &= U \begin{pmatrix} \lambda_1 & & 0 \\ & \ddots & \\ 0 & & \lambda_n \end{pmatrix} V^T \\ &= U(\Lambda_k + \Lambda_{m-k})V^T, \end{aligned} \tag{8}$$

where

$$\Lambda_k = \begin{pmatrix} \lambda_1 & & & & & 0 \\ & \ddots & & & & \\ & & \lambda_k & & & \\ & & & 0 & & \\ & & & & \ddots & \\ 0 & & & & & 0 \end{pmatrix}, \tag{9}$$

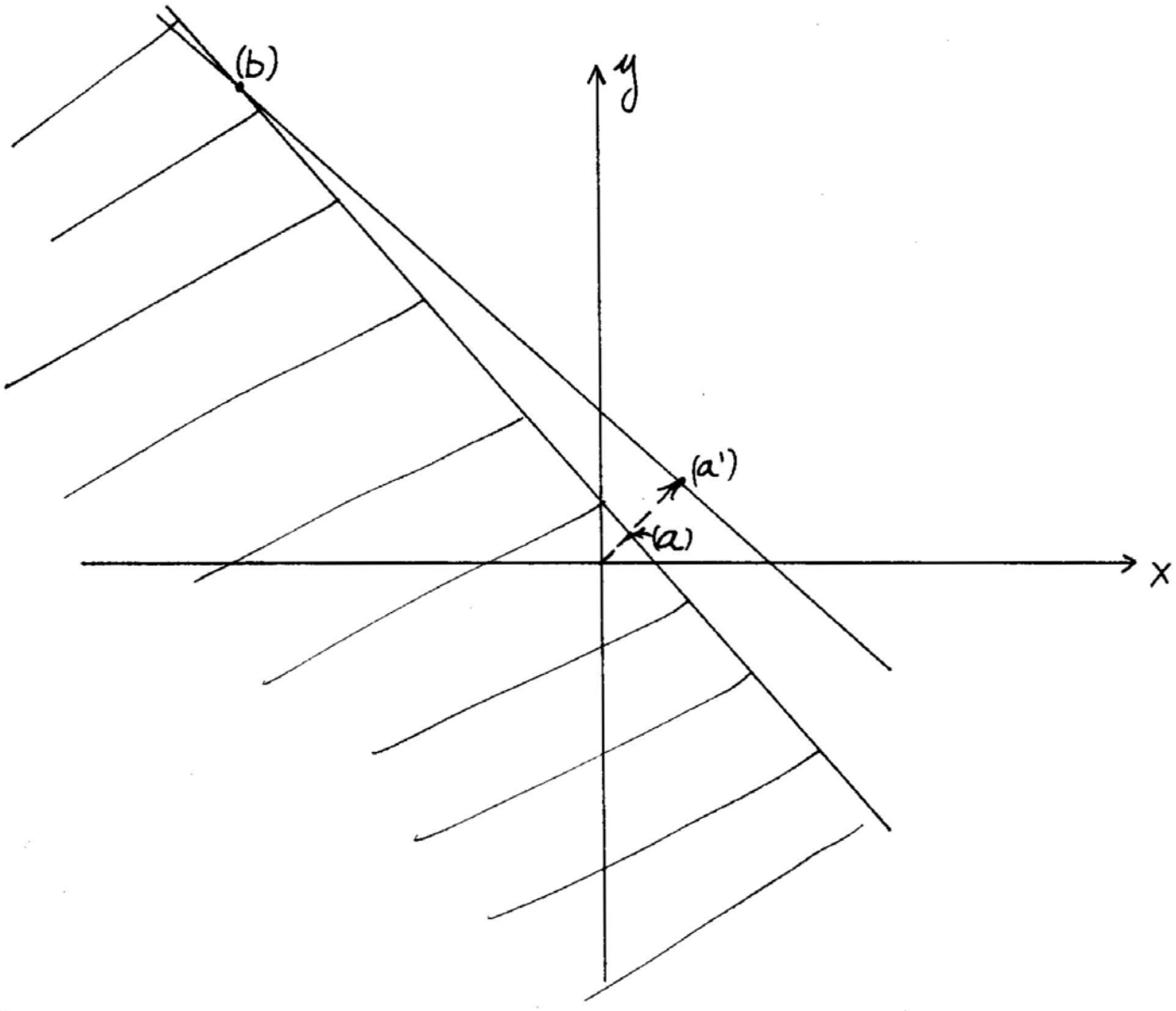

Figure A.2: Effects of changing ϵ in (2), on the solution b, see text.

and Λ_{m-k} is a similar matrix containing the rest of the eigenvalues. The solution to problem (1) may be written as

$$b = V(\alpha + \alpha' + \beta) \tag{10}$$

where

$$\alpha = \begin{pmatrix} \alpha_1 \\ \vdots \\ \alpha_k \\ 0 \\ \vdots \\ 0 \end{pmatrix}, \qquad \alpha' = \begin{pmatrix} \alpha'_1 \\ \vdots \\ \alpha'_k \\ 0 \\ \vdots \\ 0 \end{pmatrix}, \qquad \beta = \begin{pmatrix} 0 \\ \vdots \\ 0 \\ \beta_{k+1} \\ \vdots \\ \beta_m \end{pmatrix}. \tag{11}$$

The vector α is the SVD solution: $\alpha = \Lambda_k^{-1} U^T \Gamma$, while α' and β are the range and null space additions to the SVD solution necessary to satisfy the inequalities. The residuals are

$$\begin{aligned} \|Ab - \Gamma\|^2 &= \| \left[U(\Lambda_k + \Lambda_{m-k})V^T\right] \left[V(\alpha + \alpha' + \beta)\right] - \Gamma\|^2 \\ &= \|(UU^T - I)\Gamma + U(\Lambda_k \alpha' + \Lambda_{m-k}\beta)\|^2 \end{aligned} \tag{12}$$

Ignoring the term $(UU^T - I)\Gamma$ and the factor U which do not depend on the magnitude of ϵ, we have

$$\begin{aligned} \|Ab - \Gamma\|^2 &\leq \|\Lambda_k \alpha'\|^2 + \|\Lambda_{m-k}\beta\|^2 \\ &\leq \lambda_1^2 \|\alpha'\|^2 + \lambda_{k+1}^2 \|\beta\|^2. \end{aligned} \tag{13}$$

The relative size of $\|\alpha'\|^2$ and $\|\beta\|^2$ is determined by ϵ. Minimizing $\|Ab - \Gamma\|^2 + \epsilon^2 \|b_{null}\|^2$ may be thought of as minimizing the range and null space additions to the SVD solution, $\|\alpha'\|^2 + \epsilon^2 \|\beta\|^2$, subject to the inequalities. One expects, as a result, that the relative magnitudes of $\|\alpha'\|$ and $\|\beta\|$ are

$$\frac{\|\alpha'\|^2}{\|\beta\|^2} = O(\epsilon^2). \tag{14}$$

In the simple example of figure A.2 $\|\alpha'\|^2$ goes to zero as epsilon becomes smaller, and $\|\beta\|^2$ vanishes for very large values of ϵ. Assuming more generally, that

$$\|\alpha'\|^2 \sim \epsilon, \qquad \|\beta\|^2 \sim \frac{1}{\epsilon}, \tag{15}$$

we have from (13) and (14)

$$\|Ab - \Gamma\|^2 \leq \lambda_1^2 \epsilon + \frac{\lambda_{k+1}^2}{\epsilon}. \tag{16}$$

Choosing

$$\epsilon = \frac{\lambda_{k+1}}{\lambda_1} \tag{17}$$

gives, therefore, the minimum residuals $\|Ab - \Gamma\|^2$, of the full (range and null parts included) A matrix.

The above discussion of choosing the magnitude of ϵ is far from rigorous, and some experimentation can show that (17) does not always produce a minimum residuals solution. Still, we have used (17) to determine the magnitude of ϵ, simply on the basis that it produces physically reasonable solutions. The important thing to remember from the above discussion, is that when the rank of the equations matrix A is chosen so that the (physical) null space eigenvalues are not identically zero, adding null space vectors does add to the residuals. This is further demonstrated by the following simple example.

Example. Consider the system of two equations, one inequality, and two unknowns, shown in figure (A.3). The equations are

$$\begin{pmatrix} 5.5 & 5 \\ 5 & 6 \end{pmatrix} \begin{pmatrix} x \\ y \end{pmatrix} = \begin{pmatrix} 5.5 \\ 5 \end{pmatrix},$$

and the inequalities

$$\begin{pmatrix} 1 & 1 \end{pmatrix} \begin{pmatrix} x \\ y \end{pmatrix} \leq 0.$$

The two lines in figure (A.3) representing the two equations have almost the same slope. Consequently, the eigenvalues of A are (11,0.74), with one much larger than the other, and we may chose the rank of A to be $k = 1$.

The SVD solution lies at the point (a), where $(x, y) = (0.48, 0.5)$. The null space vector lies along the line (a)–(b). Starting from the SVD solution, and adding a null

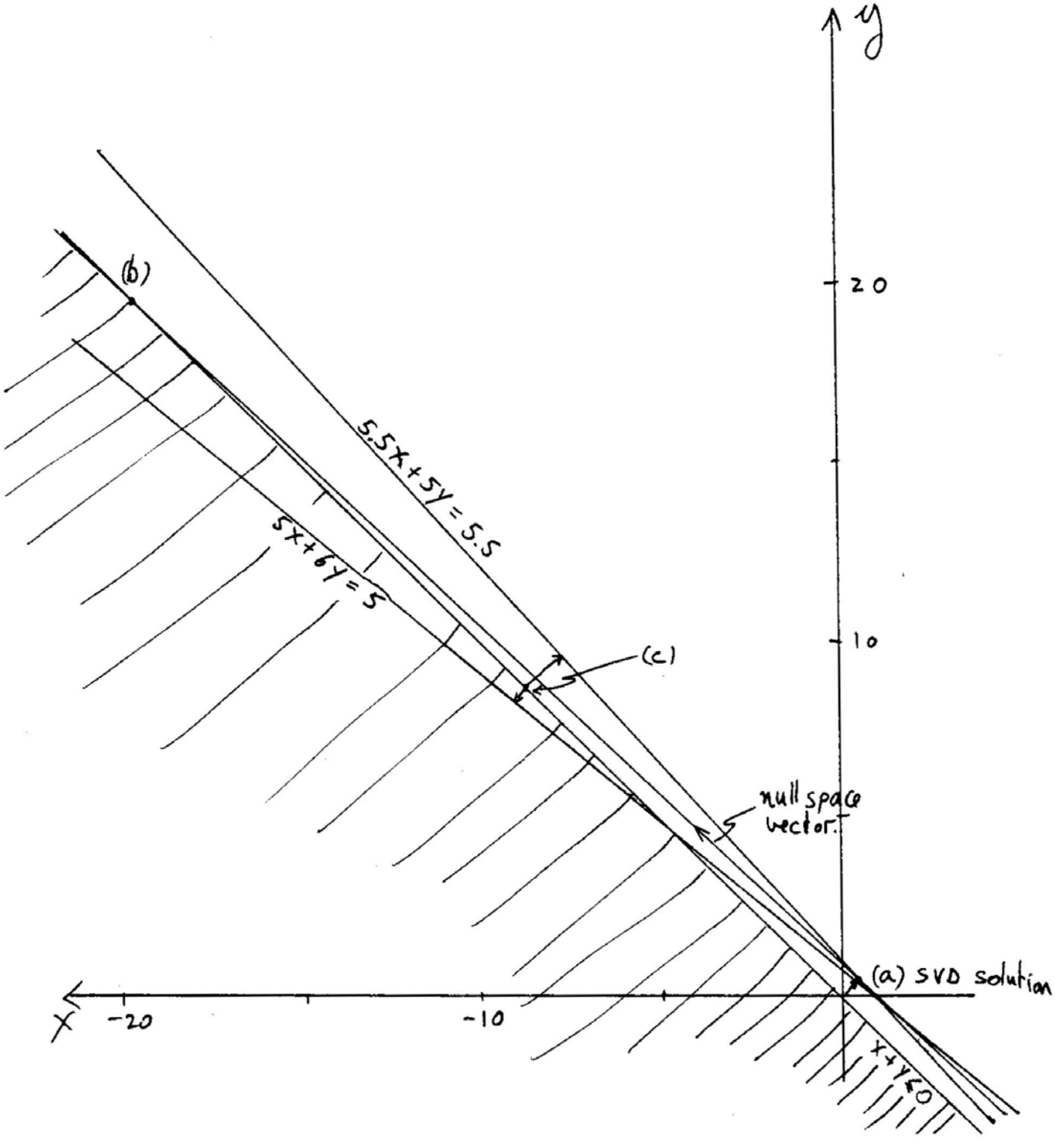

Figure A.3: An example of increased residuals due to the addition of (physical) null space vectors to the solution.

space vector to get into the feasible space and satisfy the inequalities, the solution is at the point (b), with $(x, y) = (-19.5, 19.5)$. On the other hand, using the procedure outlined above, [problem (2)] the solution is at the point (c), with $(x, y) = (-8.5, 8.5)$. The residuals in the first case $(-15, 15)$, are larger than in the second $(-9.8, 3.7)$, which can also be seen in figure (A.3), where the distance between the solution and the equation lines is larger in point (c) than in point (b). Clearly, using only vectors from the physical null space in order to satisfy the inequalities resulted in a large amplitude solution, with large residuals. This is typically what happens in the model when we try to satisfy the inequalities on the mixing coefficients with the null space vectors only: the vertical velocities and the coefficients in the Chebyshev expansion of the mixing coefficients become unphysically large, and so do the residuals.

Concluding remarks

In the previous three chapters we have tried to understand some theoretical and observational aspects of the mixing processes in the oceans. We now examine, as a whole, the different results found before.

Considering the many different processes and scales involved in mixing the oceans, one may probably safely assume that it will be impossible in the near future to resolve all these processes within any one model. Some kind of parameterization of the unresolved mixing processes would therefore be necessary in any model of the large scale ocean circulation.

We have shown in the first two chapters that if the cross–isopycnal mixing is related to the interior stratification, it is of a major importance to the physics of the circulation. Although we have used a simple constant eddy mixing coefficient in the models of the first two chapters, it should be clear that as long as the interior mixing (or even boundary mixing) is somehow related to the interior stratification, it would play a major role in determining the circulation and stratification of the oceans.

The effort to calculate mixing coefficients from data, however, was not very successful. We found that the mixing processes are difficult to resolve from (normally) noisy hydrographic data. Furthermore, the concept of mixing coefficients itself, whether constant coefficients or not, did not prove to be very useful in explaining temperature and salinity distribution in the ocean. Finally, the calculation of mixing coefficients which actually parameterize the time dependent eddy field was shown to require very high quality data, providing both temporal and spatial sampling of the circulation.

The effects of mixing on the large scale circulation were investigated in the first two chapters using integral constraints over large ocean volumes, while in the third chapter we have used the local advection diffusion equations for heat and salt to calculate mixing coefficients from data in a small oceanic region. We have seen in the first two chapters that the stratification is not sensitive to the exact form of cross–isopycnal

mixing, but that the accumulating efects of the mixing over large regions affect the buoyancy–driven circulation, through the integral constraints on the whole basin.

It might be possible, therefore, to obtain more information concerning the mixing effects on the large scale circulation using integral relations over large basin, perhaps together with direct velocity measurements in addition to the hydrographic data. In any event, integral relations are preferable to differential forms when dealing with data because they introduce less noise into the calculations.

Combining the above theoretical and observational results, one realizes that there is a need for both a better understanding of the mixing processes, and a better data, perhaps of a different source from the mostly hydrographic data available today. With a better data, and a deeper understanding of the mixing processes, one may hope to improve the parameterization of the mixing processes, which would prove to be useful in further investigations of the oceanic circulation.

References

Arhan, Michel., 1986. On the large scale dynamics of the Mediterranean outflow. A manuscript.

Bunker, A. F., 1976. Computation of surface energy flux and annual air–sea interaction cycles of the North Atlantic Ocean. *Mon. Wea. Rev.*, *104*, 1122–1139.

Bergamasco, A. and Malanotte-Rizzoli, P., 1986. personal communication.

Bryden, H. L., and H. Stommel, 1982. Origin of the Mediterranean outflow. *J. Mar. Res.*, *40(Suppl.)*, 55–71.

El Gindy, A. A. H., 1982. Physical and dynamical structure of the Eastern Mediterranean. Ph.D. Thesis, University of Alexandria, 206 pp.

Fu, Lee-Lueng, 1981. The general circulation and Meridional heat transport of the subtropical south atlantic determined by inverse methods. *J. Phys. Oceanogr.*, *11*, 1171–1193.

Gargett, A. E. , 1984. Vertical eddy diffusivity in the ocean interior. *J. Mar. Res.*, *42*, 359–393.

Gill, A. E., 1985. An explicit solution of the linear thermocline equations. *Tellus*, *37A*, 276–285.

Hecht, A., 1986. Description of the Israeli data set. An unpublished manuscript, Harvard University, CEPP.

Käse R.H.,W. Zenk and L. Armi, 1985. Reconstructed Mediterranean salt lens trajectories. submitted.

Lawson, C. L., and R. J. Hanson, *Solving least squares problems*, 340 pp., Prentice-Hall, Englewood Cliffs, N. J., 1974.

Levitus, S., 1982. Climatological atlas of the world ocean, *NOAA Tech. pap.*, *3*, 173 pp. Thermocline. *J. Phys. Oceanogr.*, *13*, 292–309.

Luyten, J. L. , J. Pedlosky and H. Stommel, 1983. The ventilated Thermocline. *J. Phys. Oceanogr.*, *13*, 292–309.

Luyten, J. L. and H. Stommel, 1986. Gyres driven by combined wind and buoyancy flux. *J. Phys. Oceanogr.*, *16*, 1551–1560.

Maillard C., 1986. Atlas hydrologique de l'Atlantique Nord–Est. Publications IFREMER, 133 planches.

MATHLAB Group , Laboratory for computer science, MIT. 1983. *MACSYMA Reference Manual*, 2 vol.

May, W. P. , 1982. Climatological flux estimates in the Mediterranean sea: Part I. Wind and wind stress. *NORDA report 54*.

Munk, W. H. , 1966. Abyssal recipes. *Deep Sea Res.*, *13* , 707–730.

Needler, G. , 1967. A model for the thermohaline circulation in an ocean of finite depth. *J. Mar. Res.*, *25*, 329–342.

Olbers, D. J., M. Wenzel, and J. Willebrand, 1985. The inference of North Atlantic circulation Patterns from climatological hydrographic data. *Rev. Geophys.*, *23*, 313–356.

Olson, D.B., 1985. Oceanic gyres forced by the wind and surface density fluxes. *J. Geophys. Res.*, *90*, 3284–3292.

Özsoy, E. , 1981. On the atmospheric factors affecting the Levantine sea. *European Center for Medium Range Weather Forecasting*, Technical report No. 25,

Pedlosky, J. , 1979. *Geophysical Fluid Dynamics.* Springer–Verlag, 624 pages.

Pedlosky, J. , 1983. Eastern boundary ventilation and the structure of the thermocline. *J. Phys. Oceanogr.*, *13*, 2038–2044.

Pedlosky, J., 1986. The buoyancy and wind-driven ventilated thermocline. *J. Phys. Oceanogr.*, *16*, 1077–1087.

Pedlosky, J. , and W. R. Young, 1983. Ventilation, potential vorticity homogenization, and the structure of the ocean circulation. *J. Phys. Oceanogr.*, *13*, 2020–2037.

POEM steering committee meeting, Paris, June 1985. unpublished manuscript.

Redi, M. H., Oceanic isopycnal mixing by coordinate rotation, *J. Phys. Oceanogr.*, *12*, 1154–1158.

Rhines, P.B., 1986. Experiments with buoyancy driven ocean circulation. NCAR technical note NCAR/TN-260+STR.

Rhines, P. B. , and W. R. Young, 1982a. A theory of the wind–driven circulation. I. Mid–Ocean gyres. *J. Mar. Res.*, *40(Suppl.)*, 559–596.

Rhines, P. B. , and W. R. Young, 1982b. Homogenization of potential vorticity in planetary gyres. *J. Fluid Mech.*, *122*, 347–367.

Reid, J. L. , 1981. On the mid–depth circulation of the world ocean. In *Evolution of Physical Oceanography*, B. A. Warren and C. Wunsch, editors. The MIT Press. 70–111.

Saunders, P. M., 1982. Circulation in the eastern North Atlantic. *J. Mar. Res.*, *40(Suppl.)*, 641–657.

Stommel, H. , 1958. The abyssal circulation. *Deep Sea Res.*, *5*, 80–82.

Stommel, H. , and A. B. Arons, 1959a. On the abyssal circulation of the World ocean–I. Stationary planetary flow patterns on a sphere. *Deep Sea Res.*, *6*, 140–154.

Stommel, H. , and A. B. Arons, 1959b. On the abyssal circulation of the World ocean–II. An idealized model of the circulation pattern and amplitude in oceanic basins. *Deep Sea Res.*, *6*, 217–233.

Stommel, H. , and F. Schott, 1977. The beta spiral and the determination of the absolute velocity field from hydrographic station data. *Deep Sea Res.*, *24*, 325–329.

Tziperman, E., 1986. On the role of interior mixing and air–sea fluxes in determining the stratification and circulation of the oceans. *J. Phys. Oceanogr.*, *16*, 680–693.

Veronis, G. , 1969. On theoretical models of the thermocline circulation. *Deep Sea Res.*, *16(supple.)*, 559–596.

Veronis, G. , 1981. Dynamics of the large–scale ocean circulation. In *Evolution of Physical Oceanography*, B. A. Warren and C. Wunsch, editors. The MIT Press. 140–183.

Walin, G. , 1982. On the relation between sea–surface heat flow and thermal circulation in the ocean. *Tellus*, *34*, 187–195.

Warren, B. A., 1977. Shapes of deep density-depth curves. *J. Phys. Oceanogr.*, *7*, 338–344.

Welander, P. , 1971. Some exact solutions to the equations describing an ideal fluid thermocline. *J. Mar. Res.*, *29*, 60–68.

Wiggins, R. A., 1972. The general linear inverse problem: Implication to surface waves and free oscillations on earth structure, *Rev. Geophys. 10*, 251–285.

Worthington, L. V., 1981. The water masses of the world ocean: some results of a fine-scale census. In *Evolution of Physical Oceanography*, B. A. Warren and C. Wunsch, editors. The MIT Press. 140–183.

Wunsch, C. , 1970. On oceanic Boundary mixing. *Deep Sea Res.*, *17*, 293–301.

Wunsch, C. , 1978. The general circulation of the North Atlantic west of 50°W determined from inverse methods, *Rev. Geophys. 16*, 583–620.

Wüst, G. , 1960. On the vertical circulation of the Mediterranean sea. *J. Geophys. Res.*, *66*, 3261–3271.

Young W. R. and G. R. Ierley, 1986. Eastern boundary conditions and weak solutions of the ideal thermocline equations. of the thermocline. *J. Phys. Oceanogr.*, Vol. *16*, No. 11.

Acknowledgments

I would like to thank Carl Wunsch for his guidance and help as well as the independence he allowed me, for careful readings of many preliminary versions of this thesis, and for patiently correcting my English. Exposure to Carl's work changed my initial dislike of dealing with data to an appreciation of the interesting and challenging aspects of data analysis. I am especially glad to have been Carl's student for this reason.

The many very useful comments from my thesis committee members, Joe Pedlosky, Paola Malanotte-Rizzoli, Bill Young and Glenn Flierl, helped me to both better understand my results, and improve their presentation. Artur Hecht generously provided the MC cruises data, his valuable help, and his knowledge of the Mediterranean sea. The long discussions with Haim Nelken, although often not about oceanography, were the source of many of the ideas in this work.

I would probably not have gotten very far with the data analysis without the help of Charmaine King who reduced five magnetic tapes full of data into something I could handle, and wrote a friendly plotting program to present the inverse results. Bud Brown drew several of the nicer looking figures in the first two chapters. Niecie's exercise class (especially the rope jumping!) and the daily tea hour with all the other kids were a necessary and important part of my day. And, of course: thanks, Nava!

NSF grants OCE-8521685 and OCE-8017791 supported me during my studies in the joint program.

I would like to dedicate this thesis to my parents.